PART I

TOTAL YIELD MEASUREMENTS FOR THE
$^{21}Ne(\alpha,n)^{24}Mg$ REACTION

PART II

A STUDY OF THE $^{12}C(\ He,p)^{14}N$ REACTION

Thesis by

Hay Boon Mak

In Partial Fulfillment of the Requirements
for the Degree of
Doctor of Philosophy

California Institute of Technology
Pasadena, California

1972

(Submitted November 12, 1971)

TO MY MOTHER AND FATHER

ACKNOWLEDGMENTS

It has been a great pleasure to work in the Kellogg Radiation Laboratory and I wish to express my sincere gratitude to all those who create the stimulating and enjoyable atmosphere there. I particularly wish to thank Professor C. A. Barnes for his helpful guidance throughout this work, and Professor William A. Fowler for his enlightening discussions. The $^{21}Ne(\alpha,n)^{24}Mg$ experiment was carried out in collaboration with Dr. D. Ashery, and the $^{12}C(^{3}He,p)^{14}N$ experiment with Dr. W. K. Lin. I am deeply indebted to them both. Dr. E. A. Adelberger and Dr. A. B. McDonald introduced the author to the experimental equipment and techniques and to them deep appreciation is due.

This work is supported in part by National Science Foundation grant GP-28027.

ABSTRACT

PART I

The total cross-section for the reaction $^{21}Ne(\alpha,n)^{24}Mg$ has been measured in the energy range 1.49 Mev $\leq E_{cm} \leq$ 2.6 Mev. The cross-section factor, S(0), for this reaction has been determined, by means of an optical model calculation, to be in the range 1.52×10^{12} mb-Mev to 2.67×10^{12} mb-Mev, for interaction radii in the range 5.0 fm to 6.6 fm. With $S(0) \approx 2 \times 10^{12}$ mb-Mev, the reaction $^{21}Ne(\alpha,n)^{24}Mg$ can produce a large enough neutron flux to be a significant astrophysical source of neutrons.

PART II

The reaction $^{12}C(^{3}He,p)^{14}N$ has been studied over the energy range 12 Mev $\leq E_{lab} \leq$ 18 Mev. Angular distributions of the proton groups leading to the lowest seven levels in ^{14}N were obtained.

Distorted wave calculations, based on two-nucleon transfer theory, were performed, and were found to be reliable for obtaining the value of the orbital angular momentum transferred. The present work shows that such calculations do not yield unambiguous values for the spectroscopic factors.

TABLE OF CONTENTS

PART I

PART I (cont'd)

PART I (cont'd)

PART II

PART II (cont'd)

PART II (cont'd)

PART II (cont'd)

PART I

Total Yield Measurement for the $^{21}Ne(\alpha,n)^{24}Mg$ Reaction.

A. INTRODUCTION

Within the framework of the S- and R- processes, a rather large neutron flux is needed to synthesize nuclei with $A \geq 60$. Cameron (Cam 54) and Greenstein (Gre 54) first suggested the reaction $^{13}C + {}^{4}He \rightarrow {}^{16}O + n$ as a possible nuetron source, following the C-N-O hydrogen burning processes. However, the large relative amount of ^{14}N produced in the C-N-O cycle would absorb all the neutrons through the reaction $^{14}N + n \rightarrow {}^{14}C + p$, and thus rule out appreciable neutron production by the $^{13}C + {}^{4}He \rightarrow {}^{16}O + n$ reaction in the products of the C-N-O cycle.

Cameron (Cam 60) later suggested the following sequence as a possible neutron source.

$$^{14}N + {}^{4}He \rightarrow {}^{18}F + \gamma \qquad A1$$

$$^{18}F \rightarrow \beta^{+} + \nu + {}^{18}O \qquad A2$$

$$^{18}O + {}^{4}He \rightarrow {}^{22}Ne + \gamma \qquad A3$$

$$^{18}O + {}^{4}He \rightarrow {}^{21}Ne + n \qquad Q = -0.705 \text{ Mev} \qquad A4$$

$$^{22}Ne + {}^{4}He \rightarrow {}^{25}Mg + n \qquad Q = -0.48 \text{ Mev} \qquad A5$$

Due to the high negative Q-value of the reaction

$^{18}O(\alpha,n)^{21}Ne$, reaction A3 is expected to dominate over A4, and the $^{22}Ne(\alpha,n)^{25}Mg$ reaction is likely to be an important neutron source.

^{21}Ne can also be produced by the Ne-Na-Mg cycle in the following sequence, as suggested by Marion and Fowler (MF 57),

$$^{20}Ne + p \longrightarrow {}^{21}Na + \gamma \qquad A6$$

$$^{21}Na \longrightarrow \beta^{+} + \nu + {}^{21}Ne \qquad A7$$

In this case, ^{20}Ne present in the material from which the star was formed can be converted into ^{21}Ne in the hydrogen-burning region surrounding the helium-burning core. The helium produced in the hydrogen burning can then react with ^{21}Ne to produce neutrons by the reaction

$$^{21}Ne + {}^{4}He \longrightarrow {}^{24}Mg + n \qquad Q = 2.557 \text{ Mev} \qquad A8$$

Alternatively, turbulence at the hydrogen-helium interface could produce ^{21}Ne from ^{20}Ne, with subsequent operation of reaction A8.

Thus the $^{21}Ne(\alpha,n)^{24}Mg$ reaction may also be a significant source of neutron for further nucleo-synthesis.

The results of the present investigation can be

used to obtain the astrophysically useful quantity (cross-section factor) S(E), for the reaction $^{21}Ne(\alpha,n)^{24}Mg$. The cross-section factor is related to the total cross-section, $\sigma(E)$, through the equation

$$S(E) = E\,\sigma(E)\exp(2\pi\eta) \quad , \qquad \text{A9}$$

where

$$\eta = Z_1 Z_2 e^2/\hbar v \quad , \qquad \text{A10}$$

v = velocity of incident particle, and

E = incident channel energy in the center-of-mass system.

A theoretical estimate of the cross-section factor of this reaction had been made by Marion and Fowler (MF 57), assuming only S-waves in the incident channel and with the following additional assumptions:

1. $\Gamma_n \gg \Gamma_\alpha$,
2. the level spacing, D, between levels with the same spin and parity is approximately 100 kev, and
3. the reduced α-particle width, θ_α^2 , is 0.1.

They estimated that S(0) was in the neighbourhood of 1.6×10^{16} eV-barns.

The differential cross-section for this reaction had been measured by Tanner (Tan 65) at $\theta_{lab} = 30^\circ$, using an implanted ^{21}Ne target and a 'Hornyak counter' as

neutron detector. Unfortunately, he had considerable difficulty with carbon build-up on the target, which produces neutrons by the $^{13}C(\alpha,n)^{16}O$ reaction.

In the present experiment, a gaseous ^{21}Ne target was used. This has the following advantages:

1. The target thickness can be determined to within $\pm$ 5% by a (mercury) manometer, and
2. The amount of carbon deposited on the entrance foil and on the rear wall of the gas cell can be checked by bombarding the empty gas cell with an α-particle beam. If the carbon build-up is found to be excessive, the foil and the gas cell can be changed.

B. APPARATUS

1. Pulsed-beam System

This experiment was carried out with the pulsed-beam, time-of-flight system associated with the ONR-CIT tandem which was able to identify the ground state and the first excited state neutron groups from the reaction $^{21}Ne(\alpha,n)^{24}Mg$. Since the neutrons from the 2nd and 3rd excited states were too low in energy to be detected efficiently by the time-of-flight spectrometer, the gamma-rays emitted by the de-excitation of these states to lower levels were detected by a 12.7 cm diameter and 10.2 cm long NaI(Tl) crystal.

The pulsed-beam and the time-of-flight system have been described in detail by Dietrich (Die 64), and Adelberger (Ade 67), and, more recently, by McDonald (McD 70). Only a brief description will be given here, together with recent modifications.

A block diagram of the pulsed-beam system is shown in figure 1. The beam from the tandem accelerator is chopped by sweeping it, at a repetition rate of 3.5 megacycles per second, vertically across a pair of horizontal slits to produce beam bursts approximately 2 nanoseconds long. The ions are velocity-modulated before entering the tandem so that they arrive at the

chopping slits in bunches. The phase and amplitude of the bunching voltage can be adjusted so that the bunches arrive at the chopping slits just as the beam is being swept across the opening between the slits, thus increasing the instantaneous current. The phase of the bunches, relative to that of the chopping voltage, is very sensitive to fluctuations in the energy of the ions from the ion source. A phase stabilizer, slightly modified from the circuit designed by Adelberger (Ade 67a), automatically adjusts the phase of the bunching voltage in response to the difference of the currents collected by the upper and lower chopping slits.

A typical time-average current of approximately 150 namp of $^4He^+$ ions was used throughout this experiment. The beam current was collected inside the gas cell, and integrated by a commercially available current integrator (Eldorado Model CI-100).

2. Neutron Detection

(i) Neutron Detection

Neutrons were detected by observing the proton-recoil scintillations in a 12.7 cm diameter, 5.08 cm thick, piece of 'Pilot B' plastic scintillator, mounted on a fast 12.7 cm diameter photo-multiplier (Amperex XP1040).

The detector was surrounded by a lead cylinder 6.25 cm thick to reduce gamma ray background.

A 1.27 cm thick lead disc in front of the detector attenuated low energy gamma rays to reduce the dead time of the multi-channel analyser.

The detector and the shielding were mounted on a cart which moved along an I-beam pivoted at one end, so that the detector could be reproducibly positioned at distances from 10 cm to 200 cm from the target over the angular range from 0° to 125°.

(ii) Electronics

Figure 2 shows a block diagram of the electronic circuits used for neutron detection.

A fast negative timing signal from the anode of the photo-multiplier was clipped by a 12.2 cm long coaxial cable, inverted, and fed into the 'START' input of an Ortec (model 437) time-to-amplitude converter (called NTAC below), the input discriminator of which triggered at -250 mv. An r.f. signal picked up by a two-turns loop mounted near the beam deflecting plates was delayed through a variable delay line and amplified. This signal was then differentiated and finally inspected by a fast discriminator, one of the outputs of which was fed into the 'STOP' input of the

NTAC. The variable delay line was used to adjust the phase of the 'STOP' signal, relative to the time of arrival of the beam bursts at the target, so that the time region of interest for the neutron spectrum fell within the range of the NTAC.

A linear signal, referred to later as the slow channel, was taken from the eleventh dynode of the photo-multiplier, amplified and inspected by a single channel analyser, whose output was used to gate a multi-channel analyser. The discriminator level of the single channel analyser was set to eliminate noise from the photo-multiplier, and very small scintillation-pulses that would have poor timing due to the finite rise-time of the photo-multiplier.

(iii) Neutron Detector Efficiency

The efficiency, $\epsilon(E)$, of the neutron detector is defined to be

$$\epsilon(E) = \frac{N(E)}{N_o(E)} \quad , \qquad \text{B1}$$

where

$N_o(E)$ = number of neutrons of energy E incident on detector, and

$N(E)$ = number of neutrons of energy E detected.

The $d(d,n)^3He$ reaction was used in measuring the

efficiency of the detector for neutrons with energies between 1.95 Mev and 10.75 Mev. The needed absolute $d(d,n)^3He$ cross-sections were interpolated from the tables of Brolley and Fowler (BF 60). For low energy neutrons, the $t(p,n)^3He$ reaction was used, with a Zirconium-Tritium target. The relative cross-sections were taken from Goldberg et al (GASW 61) and the relative efficiency was then matched onto the absolute efficiency determined by the $d(d,n)^3He$ reaction in the range where the neutron energies overlapped.

Figure 3 shows the efficiency of the neutron detector as a function of neutron energy. The slow channel, with the discriminator level set at a proton-recoil energy of 450 kev, accounts for the sharp cut off below 1.0 Mev. As a matter of experimental convenience, the discriminator level was set at the mid-point of the Compton edge of the 661.6 kev gamma line from ^{137}Cs, with an 18 db attenuator inserted at the input. After the discriminator level was set, the 18 db attenuation was removed. This gave a cut-off energy of 450 kev for proton recoils and 60 kev for gamma rays.

The solid curve shown in Figure 3 is a theoretical calculation of the efficiency of the neutron detector, computed from an expression quoted by Dietrich (Die 64), in which multiple scattering and scattering from carbon

in the scintillator are neglected.

The precision of the relative efficiency of the detector above 1 Mev was taken to be ±5%, and an overall error of 10% was assumed for the absolute efficiency.

3. Gamma Ray Detection

(i) Gamma Ray Detector

The gamma rays were detected by a 12.7 cm diameter, 10.2 cm thick, NaI(Tl) crystal mounted on a fast 12.7 cm diameter photo-multiplier (RCA C70133B). The NaI(Tl) crystal was optically coupled to the photo-multiplier through a short light pipe (RCA AJ2142).

The detector was surrounded by a lead cylinder 5 cm thick to reduce background from cosmic rays and from the walls of the room.

(ii) Electronics

Figure 4 shows the block diagram of the electronic circuits used in the gamma ray detection system.

A fast, negative, timing signal from the anode of the photo-multiplier was fed into the 'START' input of an Ortec (model 437) time-to-amplitude converter (later referred to as γTAC) whose input discriminator was set at -250 mv. The 'STOP' signal for the γTAC came from

the same fast discriminator that supplied 'STOP' signals for the NTAC.

The output of the γTAC was inspected by two single channel analysers with identical window width. One of the single channel analysers was set to bracket the prompt gamma peak in the γTAC spectrum, and the other, at the flat portion of the γTAC spectrum. The outputs of these two single-channel analysers were then used to route events into the two halves of a 400 channel pulse height analyser.

A linear signal was taken from the eleventh dynode of the photo-multiplier, amplified, shaped and fed to a 400 channel pulse height analyser in such a manner that the gamma spectrum associated with the beam plus background was stored in channels 0 to 199, while the gamma spectrum associated with the background alone was stored in channels 200 to 399.

(iii) Gamma Counter Efficiency

Suppose the angular distribution of the gamma radiation is isotropic, i.e.

$$W(\theta) = a_o \quad ,$$

the photo-peak efficiency, $\epsilon_\gamma(r)$, of the NaI(Tl) crystal at a distance r away from the source is defined

to be

$$\epsilon_\gamma(r) = \frac{N(r)}{4\pi a_o} \quad , \qquad \text{B2}$$

where $N(r)$ = number of gamma rays detected within the photo-peak.

The total efficiency of the NaI(Tl) crystal can be calculated from the expression

$$\epsilon_t(E,r) = \frac{1}{2}\int_{Vol}\left[\, 1 - e^{-u(E)\ell(r,\theta)} \,\right] \sin\theta d\theta \qquad \text{B3}$$

where $u(E)$ = linear absorption coefficient of gamma rays of energy E in NaI(Tl),

$\ell(r,\theta)$ = path length of gamma ray in NaI(Tl), and the integration is done over the volume of the crystal.

The photo-peak to total ratio, R(E), of the 12.7 cm diameter x 10.2 cm NaI(Tl) crystal has been measured as a function of energy by Lin (Lin 65), and the photo-peak efficiency is then given by $R(E)\epsilon_t(E,r)$.

The photo-peak efficiency of the NaI(Tl) crystal for detecting 4.2 Mev gamma ray was measured by detecting the 4.439 Mev gamma ray in coincidence with the neutrons from the reaction $^{9}Be(\alpha,n\gamma)^{12}C$. The NaI(Tl) crystal was placed in exactly the same position as in the $^{21}Ne(\alpha,n)^{24}Mg$ experiment, and the neutron counter was

placed at 30° to the beam, at a distance of 200 cm from the gas cell. The target was a thin self-supporting ^{9}Be foil, and was placed consecutively at the entrance, middle and the rear of the gas cell. The photo-peak efficiencies measured in these three cases differed by less than 3%, and the average was then taken to be the photo-peak efficiency of the NaI(Tl) crystal for detecting 4.23 Mev gamma rays.

The photo-peak efficiency for detecting 1.37 Mev and 2.8 Mev gamma rays was obtained by means of ^{60}Co and ThC" sources. The absolute efficiencies at 20 cm, 25 cm and 28 cm distance were obtained with sources of known strength. Then, with weaker sources, the relative efficiencies over the range 2 cm to 28 cm were obtained, and normalized to the absolute efficiencies at 20cm, 25 cm and 28 cm.

Table 1 lists the photo-peak efficiencies of the NaI(Tl) crystal at 3.47 cm, together with the calculated values, which are about 20% higher than the experimental values.

The difference between the calculated values and the experimental values may be due to the following:

a. The absorption by the approximately 3/32" of MgO reflector and 1/32" of Al wall in which the crystal was packed has not been taken into account, and

this causes approximately 6% attenuation at the photo-peak,

b. The photo-peak to total ratio does, indeed, decrease by about 5% as the distance is changed from 10 cm to 2 cm, and

c. The absorption by the 0.08 cm stainless steel wall of the gas cell has not been taken into account, and this may cause another 3% attenuation.

4. Target and Gas Cell

The neon gas used in this experiment was prepared by the Mound Laboratory of the Monsanto Research Corporation, and had a gross composition of more than 99.9 mol % of neon with an isotopic composition of 19.5 mol % of ^{20}Ne, 50.9 mol % of ^{21}Ne, and 29.6 mol % of ^{22}Ne.

The gas cell, 1.59 cm long and 1.54 cm in diameter, had a 0.08 cm thick stainless steel wall and was lined with 1 mil tantalum on the inside. The gas cell was electrically insulated from ground so that it could be used as a Faraday cup for integration of the beam current. A 0.318 cm diameter collimator, at a distance of 12.7 cm before the window, was optically lined up with the gas cell, in such a way that no beam could strike the edge of the foil window and give erroneous beam

integration. The position and size of the beam spot were checked with a dummy gas cell whose end wall was replaced by a piece of quartz. Figure 5 shows the construction of the gas cell.

The thickness of the Ni foil was measured by observing the energy lost by 2.320 Mev α-particles in passing through the foil. Figure 6a shows the spectrum obtained by a magnetic spectrometer when the entrance aperture of the spectrometer was first covered by the Ni foil, and then with the foil removed. The energy loss was found to be 384 ± 10 kev, corresponding to a foil thickness of 0.584 ± 0.06 mgm/cm^2.

The thickness of the foil was further checked by observing the shift of the $^{19}F(p,\alpha\gamma)^{16}O$ resonance at 873 kev, and this gave a result of 0.578 ± 0.06 mgm/cm^2. Figure 6b shows the excitation function of the $^{19}F(p,\alpha\gamma)^{16}O$ reaction.

Each incident energy was then corrected for the energy loss in the Ni foil by assuming a foil thickness of 0.584 mgm/cm^2. The range table compiled by Williamson et al (WBP 66) was used for the calculation of energy losses.

The gas pressure inside the cell was measured by a mercury manometer, and was kept at approximately 50 mm of Hg.

The straggling of the beam in passing through the Ni foil was estimated to be 46 kev from Figure 6a. The gas introduced another 14 kev spread in beam energy, giving a total beam resolution of 48 kev.

The beam energy from the accelerator was known to within 10 kev, after it was analysed by a 90° magnetic deflection. However, the Ni foil introduced an additional uncertainty of 20 kev. Thus the center-of-mass incident energy was known to 19 kev, and had a resolution of 41 kev.

C. EXPERIMENTAL METHOD

Figure 7 shows the energy level diagram of ^{24}Mg taken from Endt and Van der Leun (EL 67).

The neutron groups feeding the ground state and first excited state of ^{24}Mg in the reaction $^{21}Ne(\alpha,n)^{24}Mg$ could be detected with the proton recoil scintillator, but the neutron groups from the second and third excited states had too low an energy to be detected efficiently this way. Moreover, the low energy neutron groups could not be resolved reliably from the neutron groups generated by the reaction $^{22}Ne(\alpha,n)^{25}Mg$ on the ^{22}Ne present in the gas target. The gamma rays emitted by the de-excitation of the second and third excited states of ^{24}Mg were used to calculate the total cross-section for these states.

1. Neutron Detection

Figure 8 shows a neutron time-of-flight spectrum at E = 2.36 Mev, with the neutron detector at 76 cm from the target and at an angle of 25°. The neutron groups from the reaction $^{21}Ne(\alpha,n)^{24}Mg$ are labelled n_o, n_1 and n_3, while the neutron groups from the reaction $^{22}Ne(\alpha,n)^{25}Mg$ are labelled with the residual nuclei. The n_o and n_1 groups cannot be resolved, but they could be separated from the neutron groups generated by the

$^{22}Ne(\alpha,n)^{25}Mg$ reaction. The distance of the neutron detector was chosen in such a way that the n_o and n_1 groups were resolved from the neutron groups from ^{25}Mg throughout the experiment.

Neutron-production differential cross-sections were measured at $\theta_{lab} = 25^o$, 55^o, 75^o, 95^o, 115^o and 135^o for each bombarding energy, and the angular distributions were fitted by Legendre Polynomials up to order 3 or 4.

$$\frac{d\sigma}{d\Omega} = \sum_{i=0}^{3} a_i P_i(\cos\theta) \qquad C1$$

$$\frac{d\sigma}{d\Omega} = \sum_{i=0}^{4} b_i P_i(\cos\theta) \qquad C2$$

The total cross-section was then obtained by integrating equation C1 or equation C2 over angle, depending on the χ^2 of the fits.

Since, in this experiment, the neutron group n_o was not resolved from the neutron group n_1, the choice of an appropriate neutron efficiency for calculating the differential cross-section became a problem. However, in the energy range of the present experiment, the contribution from n_1 was always much larger than that from n_o except at low energies as can be seen from Figure 8. Thus the neutron yield was calculated by assuming the whole peak to be produced by the n_1 group.

The n_o and n_1 groups do not differ in energy by more than 1.4 Mev. The efficiency curve of Figure 3 indicates that the maximum error which could be introduced by assuming that the observed neutron group was all n_1 is about 10% , since the efficiency does not vary by more than 10% for a 1.4 Mev change in neutron energy, in the range 2.0 Mev to 5.5 Mev. Since the n_1 group is stronger than the n_o group in this experiment, the error is estimated to be 5% or less.

2. Gamma Ray Detection

Figure 7 shows the energy level diagram of ^{24}Mg and the branching ratios of the gamma transitions from the excited states. The NaI(Tl) crystal could not resolve the 1.37 Mev and the 2.86 Mev gamma rays generated by the reaction $^{21}Ne(\alpha,n)^{24}Mg^*$ from the 1.461 Mev (^{40}K) and 2.61 Mev (ThC") gamma rays in the room background. In order to extract the yield of the 1.36 Mev and 2.86 Mev gamma rays, the pulsed beam and time-of-flight technique was used.

The gamma time-of-flight spectrum is shown in Figure 9. The background gamma rays occur at random times with respect to the 'STOP' pulses for the γTAC, and hence give a flat background in the time-of-flight spectrum, while the gamma rays associated in time with

the beam bursts yield the so-called prompt gamma peak.

Two single channel analysers, one accepting the prompt gamma peak (denoted as the 'TRUE' single channel) and the other accepting a known portion of the flat background (denoted as the 'RANDOM' single channel analyser), were used to route the linear gamma ray pulses into the two halves of a 400-channel pulse height analyser. Figure 10 shows the two sets of gamma spectra obtained.

The width of the counting windows of the two single channel analysers were set to be as nearly identical as possible with a ^{137}Cs source, which, of course, gave a flat (random) time spectrum. The linear gamma ray signals from the ^{137}Cs sources were routed by the two single channel analysers into the two halves of the multi-channel analyser, and the windows of the single channel analysers were adjusted until the number of counts within the photo peak of the 661.6 kev line in the two spectra agreed to within 1% . The width of the windows were checked frequently throughout the experiment, and were always found to be equal to within 2%.

Suppose the branching ratio of the 4.23 Mev state is BR_1 to the 1.37 Mev state and $(1-BR_1)$ to the ground state, and that of the 4.12 Mev state is BR_2 to the

1.37 Mev state and $(1-BR_2)$ to the ground state. The NaI(Tl) crystal could not resolve a 4.23 Mev gamma ray from a 4.12 Mev gamma ray (this pair later denoted by 4.2 Mev gamma ray), and a 2.86 Mev gamma ray from a 2.75 Mev gamma ray (this pair later denoted by 2.8 Mev gamma ray). If $\sigma(n_2)$ and $\sigma(n_3)$, $\sigma(2.8)$ and $\sigma(4.2)$ represent the cross-sections for producing the 4.12 Mev level, the 4.23 Mev level, a 2.8 Mev gamma ray and a 4.2 Mev gamma ray, then

$$\sigma(2.8) = BR_1\ \sigma(n_2) + BR_2\ \sigma(n_3) \quad , \text{ and}$$

$$\sigma(4.2) = (1-BR_1)\ \sigma(n_2) + (1-BR_2)\ \sigma(n_3) \ .$$

Thus $\sigma(4.2) + \sigma(2.8) = \sigma(n_2) + \sigma(n_3)$.

The 1.37 Mev gamma ray produced in the $^{21}Ne(\alpha,n)^{24}Mg$ reaction could not be resolved from the 1.36 Mev gamma ray emmited by the inelastic scattering of α-particles on ^{21}Ne. However, since $\Gamma_\alpha \ll \Gamma_n$, the 1.37 Mev gamma ray can still be used as a good check on the cross-section for producing the 1.37 Mev level obtained from the neutron detection method.

In the present experiment, all the gamma transitions were either E2 or M1, or a coherent combination of these multipolarities. It therefore follows that the angular distributions must be of the form

$$W(\theta) = a_o + a_2 P_2(\cos\theta) + a_4 P_4(\cos\theta) \quad . \qquad C3$$

For a detector of finite size, the angular distributions are then given by the equation

$$W(E,r,\theta) = b_o + b_2 \frac{J_2(E,r)}{J_o(E,r)} P_2(\cos\theta) + b_4 \frac{J_4(E,r)}{J_o(E,r)} P_4(\cos\theta) \quad , \qquad C4$$

where r = distance between the target and the front surface of the NaI(Tl) crystal,

E = energy of the gamma ray, and

$$J_L(E,r) = \int_{Vol} P_L(\cos\theta) \left\{1-e^{-u(E)\ell(r,\theta)}\right\} \sin\theta d\theta \quad , \qquad C5$$

with $P_L(\cos\theta)$ = Legendre Polynomial of order L,

$\ell(r,\theta)$ = gamma ray path in NaI(Tl) crystal, and

$u(E)$ = linear absorption coefficient for gamma rays of energy E in NaI(Tl).

In this experiment, only the photo peaks were used for calculating the gamma yield. Under these circumstances the equation for $J_L(E,r)$ should be re-defined as

$$K_L(E,r) = \int_{Vol} P_L(\cos\theta)\tau(E,r,\theta) \left\{1-e^{-u(E)\ell(r,\theta)}\right\} \sin\theta d\theta \quad , \qquad C6$$

where $\tau(E,r,\theta)$ = probability for the absorbed gamma ray to lose all its energy to the NaI(Tl) crystal.

Peak-to-total ratios have been measured for NaI(Tl) crystals of different sizes at various distances and for different gamma ray energies (MY 68). The results of such measurements indicate that to within 5%, the peak-to-total ratio is independent of distance r. Therefore, $K_L(E,r)$ can be re-written as

$$K_L(E,r) = \tau(E) \int_{Vol} P_L(\cos\theta) \left\{1-e^{-u(E)\ell(r,\theta)}\right\} \sin\theta d\theta \quad , \qquad C7$$

and the ratio K_L/K_o is the same as J_L/J_o defined by equation C3. Hence equation C2 can be used to describe the angular distributions of the gamma rays, whether the total counts or just the photo peak is used.

The angular distributions of the 1.37 Mev, 2.8 Mev and 4.2 Mev gamma rays, with the NaI(Tl) crystals 25.8 cm away from the center of the gas cell, are shown in Figures 11,12 and 13. The measured relative angular distributions were found to be fitted by the expressions

$$W(1.37,r,\theta) = 2.78 + 0.084 \frac{J_2(1.37,r)}{J_o(1.37,r)} P_2(\cos\theta)$$

$$+ 0.065 \frac{J_4(1.37,r)}{J_o(1.37,r)} P_4(\cos\theta) \qquad C8$$

$$W(2.76,r,\theta) = 7.23 + 1.83 \frac{J_2(2.76,r)}{J_o(2.76,r)} P_2(\cos\theta)$$

$$+ 0.65 \frac{J_4(2.76,r)}{J_o(2.76,r)} P_4(\cos\theta) \qquad C9$$

$$W(4.23,r,\theta) = 9.02 + 2.67 \frac{J_2(4.23,r)}{J_o(4.23,r)} P_2(\cos\theta)$$

$$+ 0.186 \frac{J_4(4.23,r)}{J_o(4.23,r)} P_4(\cos\theta) \qquad C10$$

For the 12.7 cm diameter x 10.2 cm NaI(Tl) crystal used in the present experiment, integrating equation C5 over the angle gives the following values:

$$\frac{J_4(1.37,3.5\text{cm})}{J_o(1.37,3.5\text{cm})} P_4(\cos 55^\circ) = -0.0004$$

$$\frac{J_4(2.76,3.5\text{cm})}{J_o(2.76,3.5\text{cm})} P_4(\cos 55^\circ) = -0.007$$

$$\frac{J_4(4.23,3.5\text{cm})}{J_o(4.23,3.5\text{cm})} P_4(\cos 55^\circ) = -0.008$$

Thus, to simplify calculations, the NaI(Tl) crystal was placed at 3.5 cm from the center of the gas cell and at an angle 55°. The second and third terms of equations C8, C9 and C10 are then small compared with

the first term and can be ignored.

The following equation is used in calculating the cross-section,

$$\sigma = \frac{N}{\epsilon_\gamma} \left\{ \frac{R_o T}{PL} \cdot \frac{1}{N_o} \cdot \frac{q}{Q} \cdot \frac{1}{x} \right\} ,$$

where N = total number of gamma ray detected,

ϵ_γ = efficiency of the NaI (Tl) crystal as defined by equation B2,

R_o = gas constant,

P = pressure of neon gas,

L = length of gas cell,

T = temperature of the gas,

N_o = Avogadro's number,

Q = total charge collected,

q = charge of an electron, and

x = isotopic concentration of ^{21}Ne gas.

D. RESULT

1. Neutron Angular Distribution

22 angular distributions of the unresolved n_o+n_1 group were obtained covering the energy range $1.55 \text{ Mev} \leqslant E_{cm} \leqslant 2.57 \text{ Mev}$ in 60 kev steps. For most of the angular distributions, differential cross-sections were measured at $\theta_{cm} = 27^\circ, 58^\circ, 78^\circ, 99^\circ, 119^\circ$, and 138°. At E= 1.49 Mev, because of the low cross-section, only one differential cross-section at $\theta_{cm} = 90^\circ$ was measured. Table 2 lists the angular distributions for the n_o+n_1 groups.

In most cases, the angular distributions could be fitted equally well with a sum of Legendre Polynomials of the form

$$\frac{d\sigma}{d\Omega} = a_o + a_1P_1(\cos\theta) + a_2P_2(\cos\theta) + a_3P_3(\cos\theta) \qquad \text{D1}$$

or

$$\frac{d\sigma}{d\Omega} = b_o + b_1P_1(\cos\theta) + b_2P_2(\cos\theta) + b_3P_3(\cos\theta) + b_4P_4(\cos\theta) \qquad \text{D2}$$

Figure 15 shows the angular distributions of the n_o+n_1 group, at E= 1.65 Mev, 1.82 Mev, 2.03 Mev and 2.36 Mev.

2. Neutron Cross-sections

The cross-section for producing the ground state or the first excited state of ^{24}Mg were calculated by integrating equations D1 and D2 over angles, giving

$$\sigma(n_o + n_1) = 4\pi a_o \quad , \text{ and} \qquad D3$$

$$\sigma(n_o + n_1) = 4\pi b_o \quad . \qquad D4$$

In most cases, the ratio of a_o/b_o differs from unity by less than 1%, and in no case was the ratio more than 6% different from unity. The average of a_o and b_o was therefore used to obtain the cross-section, i.e.

$$\sigma(n_o + n_1) = 2\pi(a_o + b_o) \quad . \qquad D5$$

The uncertainty in the absolute value of $\sigma(n_o + n_1)$ was estimated to be 15% for the data taken at the high energies, and 20% for the two lowest energies.

The excitation function of $\sigma(n_o + n_1)$ is listed in table 3. The yield is a very smooth function of energy, except for a sharp resonance at E $\approx$ 1.93 Mev, about 70 kev wide.

3. Gamma Ray Cross-section

The excitation function of σ(4.2 Mev), the cross-

section for producing either the 4.23 Mev or 4.02 Mev gamma rays, is listed in table 4. The function has the same general structure as that of $\sigma(n_o + n_1)$. Since the 4.12 Mev state has been shown to have a 100% decay to the 1.37 Mev state (EL 67), there should be no 4.12 Mev gamma rays. The Q-value for the reaction $^{21}Ne(\alpha,n)^{24}Mg(4.23)$ is 1.68 Mev, and this accounts for the sharp decrease in yield at the low energies.

The 4.23 Mev state has a branching ratio of 75% to the ground state and 25% to the 1.37 Mev state. Thus the excitation function of σ(4.2 Mev) can be interpreted as the excitation function of the reaction $^{21}Ne(\alpha,n)^{24}Mg(4.23)$ if the yields are multiplied by a factor of 1.333.

The main uncertainty in this measurement arises from the uncertainty in the distance between the NaI(Tl) crystal and the target, and is estimated to be 15%.

The excitation of σ(2.8 Mev), the cross-section for producing 2.75 Mev and 2.86 Mev gamma rays, is listed in table 4. This function is also quite similar to that of $\sigma(n_o + n_1)$. The contribution from the 4.23 Mev level cascading through the 1.37 Mev level can be estimated from the known branching ratio and σ(4.2 Mev), and then subtracted away to give the cross-section for the reaction $^{21}Ne(\alpha,n)^{24}Mg(4.12)$.

The uncertainty in this measurement is dominated by the large background subtraction, and the distance between the detector and the center of the gas cell. The overall error was estimated to be 20%.

The excitation function for σ(1.37 Mev), the cross-section for producing 1.37 Mev gamma rays, is listed in table 4. While both the 4.12 Mev level and the 4.23 Mev cascade through the 1.37 Mev level, their contribution to σ(1.37 Mev) is small due to the fact that $\sigma(n_3)$ and $\sigma(n_4)$ are an order of magnitude smaller than $\sigma(n_1)$.

The cross-section σ(1.37 Mev) should serve as a cross check for the relative efficiencies of the gamma detector and the neutron detector. From the discussion of the previous paragraph, σ(1.37 Mev) should be approximately equal to $\sigma(n_o + n_1)$, the difference being equal to $\sigma(n_o) - \sigma(n_2) - 0.25\sigma(n_3)$. A comparison of tables 3 and 4 indicates that $\sigma(n_1 + n_o)$ is larger than σ(1.37 Mev) by about 20%, which can be satisfactorily accounted for by $\sigma(n_o) - \sigma(n_2) - 0.25\sigma(n_3)$.

The main uncertainty in σ(1.37 Mev) arises from the distance from the detector to center of the gas cell, and is estimated to be 15%.

4. Total Cross-section

The total cross-section for the reaction $^{21}Ne(\alpha,n)^{24}Mg$ was obtained by summing $\sigma(n_o + n_1)$, $\sigma(4.2\ Mev)$ and $\sigma(2.8\ Mev)$. The combined excitation function is shown in Figure 15 and listed in table 5.

Since both $\sigma(4.2\ Mev)$ and $\sigma(2.8\ Mev)$ are small compared with $\sigma(n_o + n_1)$, the uncertainty in the total cross-section is essentially the same as that in $\sigma(n_o + n_1)$, i.e. 15%.

5. Analysis

The excitation curve can be treated as a single sharp resonance superimposed on a smooth background. The smooth background can be parametrized by an approximation used by Fowler and Hoyle (FH 64)

$$\bar{\sigma}_B = \sum_{\ell=o}^{L} \bar{\sigma}_\ell \quad , \qquad \text{D6}$$

$$\text{where } \bar{\sigma}_\ell = 2\pi\lambda\!\!\!^{-2}\,(2\ell+1)\left\{\frac{\Gamma_\alpha \Gamma_n}{D\,\Gamma}\right\}_\ell \quad , \qquad \text{D7}$$

with D = level spacing of states with same spin and parity,

Γ_α = partial width of the α-channel,

Γ_n = partial width of the n-channel,

Γ = total width of the compound nucleus state,

L = highest partial wave that contributes significantly to the reaction,

$\lambda\!\!\!^{-} = \frac{4.57}{\sqrt{(EA)}}$ fermi,

E = beam energy in center-of-mass system, in Mev,

$A = \frac{M_1 M_2}{M_1+M_2}$,

M_1 = mass of incident particle, in AMU, and

M_2 = mass of target nucleus, in AMU.

Vogt (Vog 62) derived an optical model expression for the ratio

$$\left\{\frac{\Gamma_\alpha}{D}\right\}_\ell = \frac{2}{\pi}\left\{\frac{\beta_\ell T_\ell}{(1+T_\ell)^2}\right\} \quad , \qquad \text{D8}$$

where

$$T_\ell = \frac{P_\ell}{\left\{1+ \lambda\!\!\!^{-2}/\lambda\!\!\!^{-2}_o\right\}^{\frac{1}{2}}} \quad , \qquad \text{D9}$$

P_ℓ = penetration factor as defined later in equation E1,

$$\lambda\!\!\!^{-}_o = \frac{\hbar}{(2AV_o)^{\frac{1}{2}}} \quad ,$$

V_o = depth of the real interaction potential used in the optical model, which has been chosen

to be 75 Mev in this analysis to be consistent with the analysis of Michaud, Scherk and Vogt (MSV 70), and

β = a quantity resulting from the averaging of the optical model (expected to be of order of unity).

Since $V_o \approx 75$ Mev, and $E \approx 2$ Mev, χ is much larger than χ_o, and T_ℓ can be approximated by

$$T_\ell \approx P_\ell \frac{\chi_o}{\chi} \ll 1 \quad . \qquad \text{D10}$$

Thus we obtain

$$\frac{\Gamma_\alpha}{D} \approx \frac{2}{\pi} \beta_\ell P_\ell \frac{\chi_o}{\chi} \quad . \qquad \text{D11}$$

Equation D6 can then be converted into the form

$$\bar{\sigma}_\ell = \pi\chi^2(2\ell+1)(4\frac{\chi_o}{\chi}P_\ell)(\frac{\beta_\ell\Gamma_n}{\Gamma}) \qquad \text{D12}$$

$$= 4\pi\chi_o\chi(2\ell+1)P_\ell(\frac{\beta_\ell\Gamma_n}{\Gamma}) \qquad \text{D13}$$

In fitting the data points, all the various β_ℓ's are assumed to be the same. Then, substituting $\bar{\sigma}_\ell$ into equation D5, together with all the appropriate numerical values

$$\bar{\sigma}_B = \frac{151.3}{\sqrt{E}} \left\{ \frac{\beta \Gamma_n}{\Gamma} \right\} \left\{ P_o + 3P_1 + 5P_2 + 7P_3 \right\} \text{ mb} \quad , \qquad \text{D14}$$

where E is in Mev.

To include the sharp resonance at 1.93 Mev, we add a single-resonance of the form

$$\sigma_r = (2\ell+1)\, \pi \lambda\!\!\!^{-2} \, \frac{\Gamma_{\alpha,\ell} \Gamma_{r,n}}{(E-E_r)^2 + \Gamma_r^2/4} \qquad \text{D15}$$

Assuming that:

$$\Gamma_{r,n} \approx \Gamma_r \quad ,$$

$$\Gamma_{\alpha,\ell} = \gamma_{\alpha,\ell}^2 \, P_\ell \quad ,$$

the resonance contribution can be re-written as

$$\sigma_r = (2\ell+1)\, \pi \lambda\!\!\!^{-2} \, \gamma_{\alpha,\ell}^2 \, \frac{P_\ell \, \Gamma_r}{(E-E_r)^2 + 0.25 \Gamma_r^2} \qquad \text{D16}$$

Thus the cross-section should be given by the equation

$$\bar{\sigma} = \bar{\sigma}_B + \sigma_r$$

$$= \frac{151.3}{\sqrt{E}} \left\{ \frac{\beta \Gamma_n}{\Gamma} \right\} \left\{ P_o + 3P_1 + 5P_2 + 7P_3 \right\} +$$

$$+ \frac{195.27}{E} (2\ell+1)\ \gamma^2_{\alpha,\ell}\ \frac{P_\ell\ \Gamma_r}{(E-E_r)^2 + 0.25\Gamma_r^2}\ \text{mb} \qquad \text{D17}$$

where E, $\gamma^2_{\alpha,\ell}$, Γ_r and E_r are in Mev.

The values for $(\beta\Gamma_n/\Gamma)$, Γ_r, $\gamma^2_{\alpha,\ell}$, ℓ, E_r and the nuclear radius R were varied to obtain the best fit. However, it was found that for minimum χ^2,

$$R = 4.70 \text{ fm} \qquad \text{and} \qquad \frac{\beta\Gamma_n}{\Gamma} = 3.08 \ .$$

Michaud, Scherk and Vogt (MSV 70) suggested the following equation for estimating the interaction radius between α-particles and target nuclei if a square well optical potential is to be used to calculate the penetration factors,

$$R = 1.6 + 1.25\, A_T^{1/3} + \Delta R \ , \qquad \text{D18}$$

where A_T = mass number of the target nucleus, and

ΔR = correction to R which is approximately 0.74 fm in this case.

Thus R is expected to be approximately 5.8 fm for the reaction $^{21}Ne(\alpha,n)^{24}Mg$, instead of the value 4.7 fm found by minimizing χ^2.

Fowler and Hoyle (FH 64) have estimated β to be

in the range

$$3 \geq \beta \geq 0.2, \qquad \text{D19}$$

and, since $\Gamma_n \approx \Gamma$, $(\beta\Gamma_n/\Gamma)$ was estimated to lie between 3 and 0.2. The interaction radius R was varied from 5.0 to 6.6 fm, and the value for $\beta\Gamma_n/\Gamma$ was varied to obtain best fit, while Γ_r, $\gamma^2_{\alpha,\ell}$, ℓ and E_r were kept constant.

Table 6 lists the different sets of parameters obtained together with their χ^2 (16 degrees of freedom).

E. CONCLUSION

Since the sharp resonance at 1.93 Mev does not contribute significantly at energies far away from the resonance, only the smooth background is used in extrapolating the cross section factor S(E) to low energy.

In the case of square well optical potentials, the penetration factor at low energy, $E \ll$ Coulomb energy, can be approximated by (FH 64)

$$P_\ell \approx \left\{\frac{E_c}{E}\right\}^{\frac{1}{2}} \exp\left\{-\frac{\pi}{2}\left(\frac{E_c}{E}\right)^{\frac{1}{2}} x - \frac{4E}{3E_R x} + 2x - \frac{4\ell(\ell+1)}{x}\right\} , \qquad \text{E1}$$

where $$E_R = \frac{\hbar^2}{2MR^2} , \qquad \text{E2}$$

$$E_c = \frac{Z_1 Z_2 e^2}{R} , \quad \text{and} \qquad \text{E3}$$

$$x = 2\left(\frac{E_c}{E_R}\right)^{\frac{1}{2}} . \qquad \text{E4}$$

Michaud, Scherk and Vogt (MSV 70) suggested that the penetration factor calculated from square well potentials are too small, due to the large reflection coefficients resulting from the sharp edge. They compared the absorption cross-sections for diffuse-edge potentials with those for square wells, and gave

the following prescription for constructing equivalent square wells. The radius, R, of the square well should be increased by an amount ΔR and the (square well) penetration factor calculated for $R + \Delta R$ should be increased by a factor $f > 1$. Both ΔR and f are plotted as a function of the mass number of the target nucleus and for various kinds of incident particles in their paper (MSV 70).

From the definition of S(E),

$$S(E) = E\sigma(E)\exp(2\pi\eta) \quad , \qquad \text{E5}$$

where $$2\pi\eta = \frac{2\pi Z_1 Z_2 e^2}{\hbar v} = \frac{\pi E_c}{(E_R E)^{\frac{1}{2}}} \quad . \qquad \text{E6}$$

Substituting $\sigma_B(E)$ for $\sigma(E)$, S(E) becomes

$$S(E) = 151.3\sqrt{E}\left\{\frac{\beta\Gamma_n}{\Gamma}\right\}\exp\left\{\frac{\pi E_c}{(E_R E)^{\frac{1}{2}}}\right\}$$

$$\cdot\left\{P_o + 3P_1 + 5P_2 + 7P_3\right\} \text{ mb-Mev} \quad ,$$

$$= 151.3(E_c)^{\frac{1}{2}} f\left\{\frac{\beta\Gamma_n}{\Gamma}\right\}\exp\left\{-\frac{4}{3}\frac{E}{xE_R} + 2x\right\}$$

$$\cdot\left\{1+3\exp(-\frac{8}{x}) + 5\exp(-\frac{24}{x}) + 7\exp(-\frac{48}{x})\right\} \text{ mb-Mev} \quad . \qquad \text{E7}$$

Substituting the appropriate numerical values of

E_c, E_R and x, S(E) can be expressed in the form:

$$S(E) = G(R)\ \exp(-g(R)E)\ \text{mb-Mev} \quad , \qquad \text{E8}$$

where $g(R) = 0.0498/R^{3/2}\ \text{Mev}^{-1}$ E9

$$G(R) = 8.12 \times 10^2 \exp(8.607R^{\frac{1}{2}})\left(\frac{\beta\Gamma_n}{\Gamma}\right) f \cdot \left\{1 + 3\exp\left(-\frac{1.859}{\sqrt{R}}\right) + 5\exp\left(-\frac{5.58}{\sqrt{R}}\right) + 7\exp\left(-\frac{11.5}{\sqrt{R}}\right)\right\} \quad \text{mb-Mev} \quad , \qquad \text{E10}$$

with R in fm and E in Mev.

Table 6 lists the values of G(R) and g(R) for various values of R and $(\beta\Gamma_n/\Gamma)$, and Figure 16 shows a calculated S(E) function superimposed on the data points.

Alternatively, the experimental S(E) function could also be fitted with the form

$$S(E) = A_o \exp\{A_1 E\} \quad , \qquad \text{E11}$$

where A_o and A_1 are treated as free parameters. The data points at 1.92 Mev and 1.98 Mev are not included in this fitting procedure. For a minimum χ^2, the fit gives

$$A_o = S(0) = 1.7 \times 10^{12}\ \text{mb Mev} \ , \text{ and}$$

$$A_1 = -0.597 \text{ Mev}^{-1}$$

From equation E7, the radius can be calculated from A_1 and is found to be 5.2 fm. Figure 16 shows the fit to the experimental data points.

The estimated value for S(0) does not include any effect from possible low energy resonances. The total neutron cross-section of magnesium shows strong resonance structure around $E_n \approx 2.65$ Mev (SGMW 64) which is right in the stellar thermal region of the reaction $^{21}Ne(\alpha,n)^{24}Mg$. If any of these resonances should have a large reduced α-particle width, the value for S(0) would be increased by a large factor.

The value of S(0) varies from 1.52×10^{12} mb-Mev to 2.67×10^{12} mb-Mev in the range $5.2 \text{ fm} \leqslant R + \Delta R \leqslant 6.5$ fm. Thus the cross-section factor, S(0), is determined by the experimental data to be in the neighbourhood of 2×10^{12} mb-Mev and is not too sensitive to the radius parameter. In order to obtain a more precise value for S(0), a measurement over a wider energy range, where the effects of g(R) is more pronounced, would be needed.

Reeves (Ree 66) made an optical model calculation and obtained the values

$$g(R) = 0.72 \text{ Mev}^{-1} \quad , \text{ and}$$

$$G(R) = S(0) = 2.45 \times 10^{12} \text{ mb Mev} ,$$

with a radius of 5.05 fm.

His value for S(0) agrees remarkably well with the value, $S(0) = 2.1 \times 10^{12}$ mb Mev, obtained from the present experiment for the same choice of g(R).

The S(0) predicted by Marion and Fowler is larger than the experimental value by a factor of about 7. Considering the many assumptions which were made by the estimate of Marion and Fowler, this is surprisingly close.

With the value of $S(0) \approx 2.0 \times 10^{12}$ mb-Mev, the $^{21}Ne(\alpha,n)^{24}Mg$ reaction can produce a large enough neutron flux to be a significant astrophysical source of neutrons, provided the conditions indicated by Burbridge et al (BBFH 57) are satisfied.

REFERENCES

Ade 67 E. Adelberger, Ph.D. thesis, California Institute of Technology (1967).

Ade 67a E. Adelberger, Nucl. Inst. and Meth. 47, 327 (1967).

BBFH 57 E.M. Burbridge, G.B. Burbridge, W. A. Fowler, and F. Hoyle, Rev. Mod. Phys. 29, 547 (1957).

BF 60 J. E. Brolley and J. L. Fowler, Fast Neutron Physics, ed. by J. B. Marion and J. L. Fowler, Interscience, New York, page 73 (1960).

Cam 54 A. G. W. Cameron, Phys. Rev. 93, 932 (1954).

Cam 60 A. G. W. Cameron, Astron. J. 65, 485 (1960).

Die 64 F. S. Dietrich, Ph.D. thesis, California Institute of Technology (1964).

EL 67 P. M. Endt and C. Van der Leun, Nucl. Phys. A105, 1 (1967).

FH 64 W. A. Fowler and F. Hoyle, Astrophysics J. Supplement A1, 9 (1964).

GASW 61 M. D. Goldberg, J.D. Anderson, J. P. Stoering, and C. Wong, Phys. Rev. 122, 1510 (1961).

Gre 54 J. L. Greenstein, Modern Physics for the Engineer (L. N. Ridenour, ed.) McGraw-Hill Book Co. New York (1954).

Lin 65 W. K. Lin, California Institute of Technology, Private communication. (1965)

MF 57 J. B. Marion and W. A. Fowler, Astrophysics J. 125, 221 (1957).

MSV 70 G. Michaud, L. Scherk and E. Vogt, Phys. Rev. C1, 864 (1970).

MY 68 J. B. Marion and F. C. Young, 'Nucler Reaction Analysis, Graphs and Tables', John Wiley & Sons, Inc. New York, page 53 (1968).

McD 70 A. B. McDonald, Ph.D. thesis, California Institute of Technology (1970).

Ree 66 H. Reeves, Astrophysics J. 146, 447 (1966).

SGMW 64 J. R. Stehn, D. M. Goldberg, B. A. Maguno and R. Wiener-Chasman. 'Neutron Cross-sections', BNL 325, second edition, Supplement No.2, Brookhaven National Laboratory, Associated Universities, INC. New York (1964).

Tan 65 N. W. Tanner, Nucl. Phys. 61, 297 (1965).

Vog 62 E. Vogt, Rev. Mod. Phys. 34, 723 (1962).

WBP 66 C. F. Williamson, J. P. Boujot and J. Picard, 'Tables of Range and Stopping Power of Chemical Elements for Charged Particles of Energy 0.05 to 500 Mev', Report CEA-R3042, Centre D'Études Nucléaires De Saclay (1966).

Table 1

Photo-peak efficiency at 3.5 cm of the 12.7 cm diameter x 10.2 cm NaI(Tl) crystal. The total efficiency values are obtained from the expression

$$\epsilon_t(E,r) = \tfrac{1}{2} \int_{Vol} \left\{1 - e^{-u(E)\ell(r,\theta)}\right\} \sin\theta d\theta$$

The photo-peak to total ratios for the NaI(Tl) crystal used in this experiment had been measured earlier by Lin (Lin 65), and the uncertainty in the ratios are about 10%.

The main source of error in the determination of the gamma-ray yield is the distance, r, and it is estimated to introduce an uncertainty of 15% in the efficiency measurement.

E_γ in Mev	Total eff. ϵ_t	peak-to-total ratio	calculated photo-peak eff.	experimental photo-peak eff.
1.37	0.152	0.40 ± 10%	0.061 ± 10%	0.050 ± 15%
2.8	0.130	0.26 ± 10%	0.034 ± 10%	0.029 ± 15%
4.2	0.125	0.22 ± 10%	0.027 ± 10%	0.020 ± 15%

Table 2

Angular distributions of $n_o + n_1$.

The differential cross-sections were calculated by assuming that the whole peak was contributed by the n_1 group. This introduced an error of about 5% in the relative magnitudes. The absolute values were estimated to have an uncertainty of 15%. However, for the differential cross-sections at 1.49 Mev and 1.55 Mev, the uncertainty is estimated to be 20% due to low count rate and large background.

E_{cm}	$\frac{d\sigma}{d\Omega}(\theta_{cm})$ x 10^{-3} mb/st.				
Mev	32°	58°	90°	93°	128°
1.49			2.96		
1.55	7.8	8.5		8.5	14.0

E_{cm}	$\frac{d\sigma}{d\Omega}(\theta_{cm})$ x 10^{-2} mb/st.					
Mev	27°	58°	78°	99°	119°	138°
1.60	1.51	1.00	1.39	1.12	1.65	2.01
1.65	1.67	1.34	1.15	1.60	1.89	2.67
1.71	4.47	2.94	2.46	2.41	2.73	2.70
1.76	7.30	5.54	5.16	4.60	4.70	4.61
1.82	6.11	5.16	4.61	4.99	5.44	5.62
1.88	7.43	7.65	7.96	8.50	10.21	9.36
1.88	4.47	5.70	6.01	5.60	6.20	6.20
1.92	23.9	24.9	25.8	24.6	24.3	23.7
1.98	22.7	18.2	20.8	22.5	23.4	24.1
2.03	6.97	8.36	8.96	9.48	11.6	13.2
2.09	12.8	15.6	13.4	13.0	13.6	13.5
2.15	18.2	15.8	19.4		17.5	16.5
2.20	18.9	23.0	23.2	24.1	26.7	28.0
2.26	45.4	40.2	43.5	37.7	37.8	35.3
2.32	75.9	64.7	59.3	55.2	45.4	41.6
2.36	87.9	80.8	81.7	75.0	70.5	63.5
2.41	142.	126.	132.	121.	115.	103.
2.46	95.6	81.2	85.7	73.3	60.5	56.2
2.52	160.	149.	124.	109.	91.0	88.0
2.57	179.	201.	210.	189.	158.	129.

Table 3

Excitation function of $\sigma(n_o + n_1)$, the summed cross-sections for producing groups n_o and n_1.

E_{cm} in Mev	$\sigma(n_o + n_1)$ in mb
1.49	0.037 ± 15%
1.55	0.10 ± 15%
1.60	0.18 ± 15%
1.65	0.22 ± 15%
1.71	0.36 ± 15%
1.76	0.68 ± 15%
1.82	0.66 ± 15%
1.88	1.06 ± 15%
1.89	1.28 ± 15%
1.92	5.51 ± 15%
1.96	5.62 ± 15%
1.98	4.84 ± 15%
2.03	2.24 ± 15%
2.09	2.44 ± 15%
2.15	3.07 ± 15%
2.20	2.96 ± 15%
2.26	4.97 ± 15%
2.32	7.07 ± 15%
2.36	9.37 ± 15%
2.37	10.10 ± 15%
2.41	15.30 ± 15%
2.46	9.41 ± 15%
2.52	15.0 ± 15%
2.57	22.1 ± 15%

Table 4

Excitation functions for gamma rays production

$\sigma(1.37)$ = cross-section for producing 1.37 Mev gamma rays. The error is estimated to be 15%.

$\sigma(2.8)$ = cross-section for producing 2.86 Mev and 2.75 Mev gamma rays. The error is estimated to be 20%.

$\sigma(4.2)$ = cross-section for producing 4.12 Mev and 4.23 Mev gamma rays. The error is estimated to be 15%.

E_{cm} Mev	σ(2.8) mb	σ(4.2) mb	σ(1.37) mb
1.55			0.058
1.60	0.0010		0.132
1.65	0.0039		0.146
1.71	0.0057	0.0034	0.218
1.76	0.0240	0.0230	0.439
1.82	0.0310	0.0330	0.506
1.88	0.0183	0.0374	0.582
1.88	0.0236	0.0462	0.626
1.92	0.206	0.551	1.94
1.96		0.506	
1.98	0.164	0.456	2.07
2.03	0.063	0.117	1.33
2.09	0.140	0.176	1.21
2.15	0.175	0.435	1.84
2.20	0.175	0.586	1.59
2.26	0.271	0.596	3.59
2.32	0.320	0.500	4.59
2.36	0.401	0.844	6.58
2.37		1.100	
2.41	1.02	2.022	10.6
2.46	0.92	1.835	6.32
2.52	1.99	1.903	10.3
2.57	2.04	1.640	14.9

Table 5

Excitation function for the reaction

$^{21}Ne(\alpha,n)^{24}Mg$

E_{cm} in Mev	σ_t in mb
1.49	0.037 ± 15%
1.55	0.100 ± 15%
1.60	0.181 ± 15%
1.65	0.224 ± 15%
1.71	0.369 ± 15%
1.76	0.727 ± 15%
1.82	0.724 ± 15%
1.88	1.12 ± 15%
1.88	1.35 ± 15%
1.92	6.27 ± 15%
1.98	5.46 ± 15%
2.03	2.42 ± 15%
2.09	2.76 ± 15%
2.15	3.68 ± 15%
2.20	3.72 ± 15%
2.26	5.84 ± 15%
2.32	7.89 ± 15%
2.36	10.6 ± 15%
2.41	18.3 ± 15%
2.46	12.2 ± 15%
2.52	18.9 ± 15%
2.57	25.8 ± 15%

Table 6

Lists of parameters used to fit the cross-section data. The parameters are defined in equations D14 and D13. $\beta\Gamma_n/\Gamma$ was constrained to lie in the range, $3 > \beta\Gamma_n/\Gamma > 0.2$, and R in the range $5.0 \text{ fm} < R < 6.6 \text{ fm}$.

V_o in Mev	L	$\frac{\beta\Gamma_n}{\Gamma}$	R in fm	χ^2	G(R) = S(0) in mb-Mev	g(R) in Mev^{-1}
75 Mev	3	1.91	5.0	42.3	1.52×10^{12}	0.557
"	"	1.64	5.1	42.5	1.56×10^{12}	0.574
"	"	1.98	5.2	42.8	1.62×10^{12}	0.591
"	"	1.20	5.3	43.1	1.66×10^{12}	0.608
"	"	1.04	5.4	43.6	1.74×10^{12}	0.625
"	"	0.91	5.5	44.0	1.80×10^{12}	0.642
"	"	0.77	5.6	44.6	1.86×10^{12}	0.660
"	"	0.66	5.7	45.0	1.93×10^{12}	0.678
"	"	0.58	5.8	46.0	2.00×10^{12}	0.696
"	"	0.50	5.9	46.7	2.07×10^{12}	0.714
"	"	0.44	6.0	47.5	2.15×10^{12}	0.732
"	"	0.38	6.1	48.4	2.25×10^{12}	0.750
"	"	0.33	6.2	49.4	2.31×10^{12}	0.769
"	"	0.29	6.3	50.5	2.39×10^{12}	0.788
"	"	0.25	6.4	51.7	2.40×10^{12}	0.806
"	"	0.22	6.5	52.9	2.56×10^{12}	0.825
"	"	0.20	6.6	54.3	2.67×10^{12}	0.845

$$E_r = 1.94 \text{ Mev}$$

$$\Gamma_r = 0.07 \text{ Mev}$$

$$\ell = 1$$

$$\gamma^2_{\alpha,\ell} = 0.046 \text{ Mev}$$

Figure 1

Schematic diagram of the beam pulsing system for the ONR-CIT tandem. The chopping slits are shown as vertical slits for clarity only; the beam is actually swept vertically across a horizontal pair of slits. The controls enclosed by the dashed lines are located with the main control for the accelerator.

BEAM PULSING SYSTEM FOR CIT/ONR TANDEM

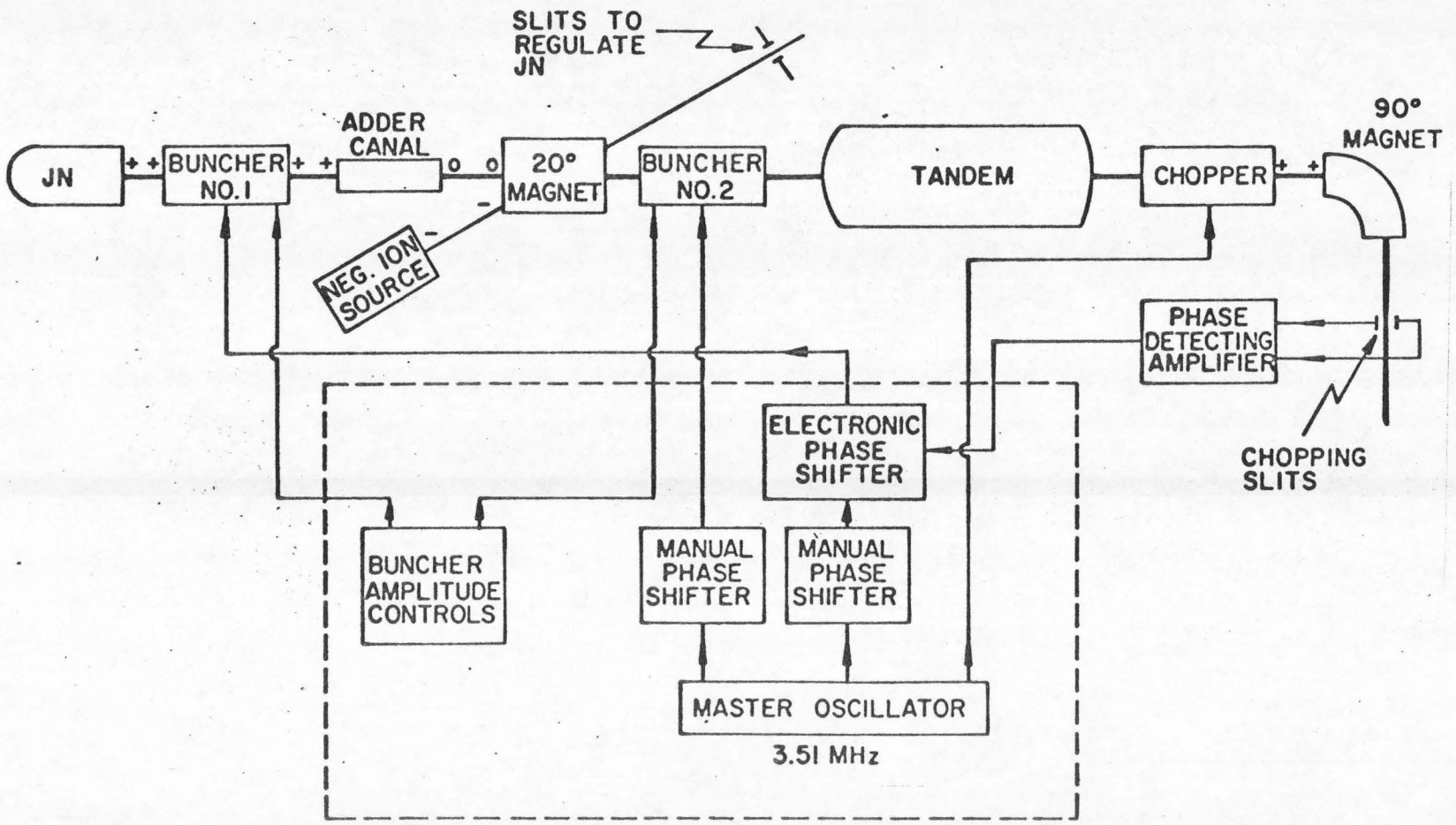

Figure 2

Block diagram of the electronics used to measure neutron flight time. The commercially available instruments symbolized by the blocks are:

1) Time-to-pulse height converter (Ortec model 437)
2) Amplifier and discriminator (Ortec models 410 and 420)
3) Fast amplifier no. 1 (Hewlett-Packard model 460 BR)
4) Fast amplifier no. 2 (Nanosecond System model 281)
5) Fast discriminator (Nanosecond System model 205 FC)
6) Multichannel pulse-height analyser (RIDL model 34-27)

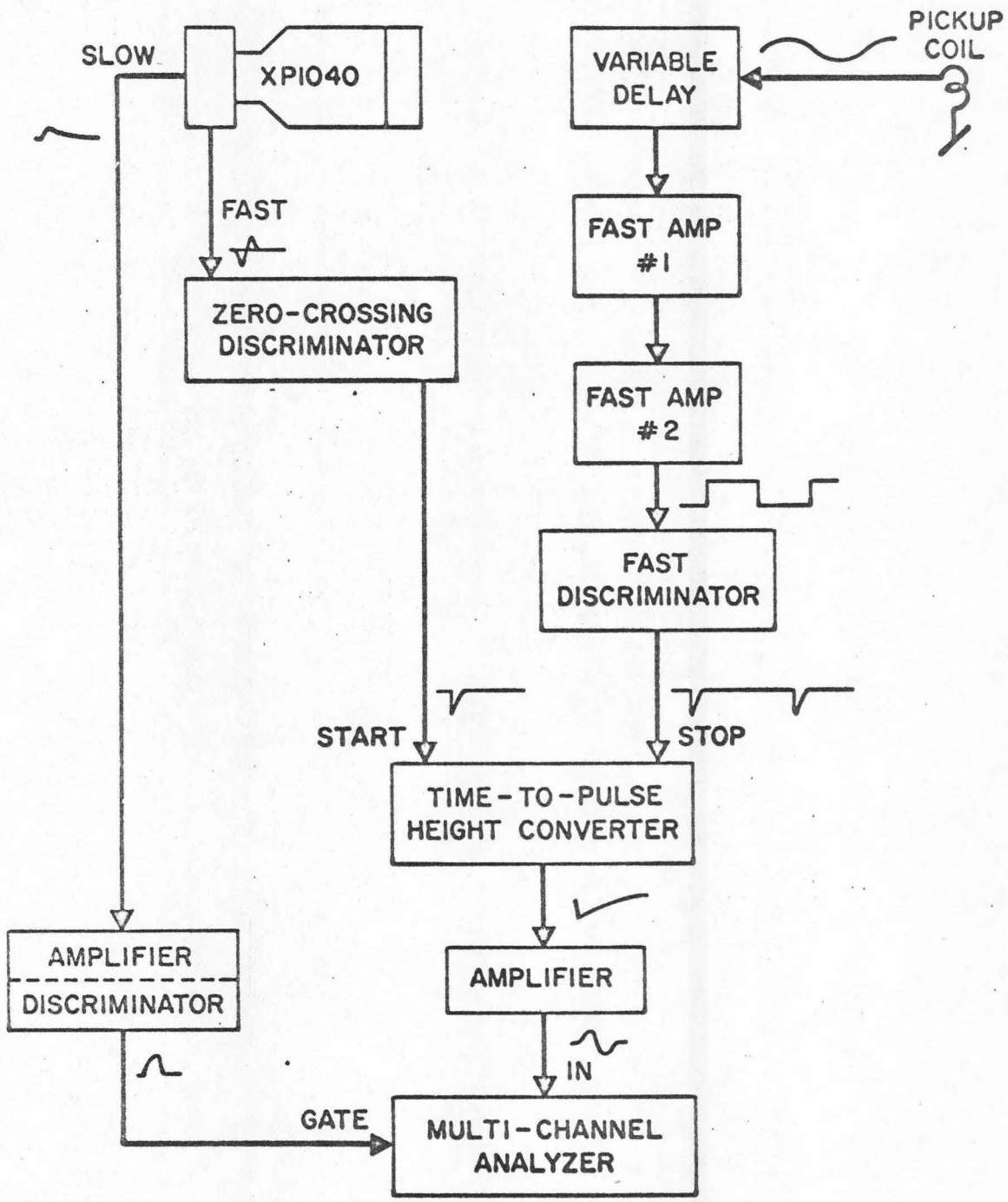
SLOW
XP1040
FAST
ZERO-CROSSING DISCRIMINATOR
VARIABLE DELAY
PICKUP COIL
FAST AMP #1
FAST AMP #2
FAST DISCRIMINATOR
START
STOP
TIME-TO-PULSE HEIGHT CONVERTER
AMPLIFIER
DISCRIMINATOR
AMPLIFIER
IN
GATE
MULTI-CHANNEL ANALYZER

Figure 3

Neutron detector efficiency curve. The solid dots are data from the $d(d,n)^3He$ reaction and the open triangles are data from the $T(p,n)^3He$ reaction. The solid curve has been computed from an expression quoted by Dietrich (Die 64) which neglects multiple scattering, scattering by the carbon in the scintillator and absorption by material between plastic scintillator and target.

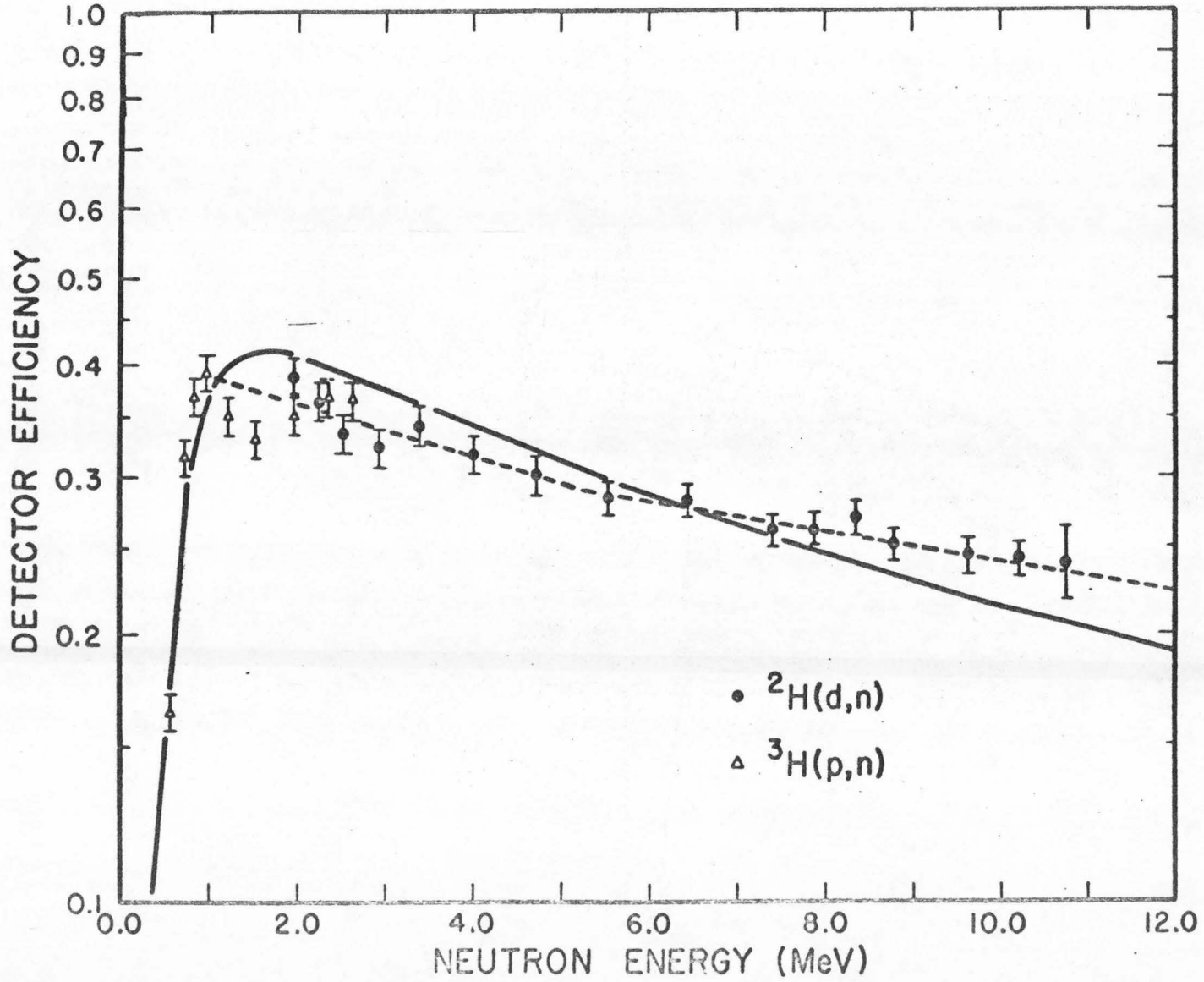
DETECTOR EFFICIENCY
1.0
0.9
0.8
0.7
0.6
0.5
0.4
0.3
0.2
0.1
0.0
2.0
4.0
6.0
8.0
10.0
12.0
NEUTRON ENERGY (MeV)
• $^{2}H(d,n)$
△ $^{3}H(p,n)$

Figure 4

Block diagram of the electronics used to measure gamma ray intensities and energies. The commercially available instruments symbolized by the blocks are

1) Amplifier (Ortec model 410)
2) Time-to-pulse height converter (Ortec model 437)
3) Single channel analysers #1 and #2 (Ortec model 420)
4) Routing system (RIDL model 30-35)
5) Multi-channel analyser (RIDL model 23-4)

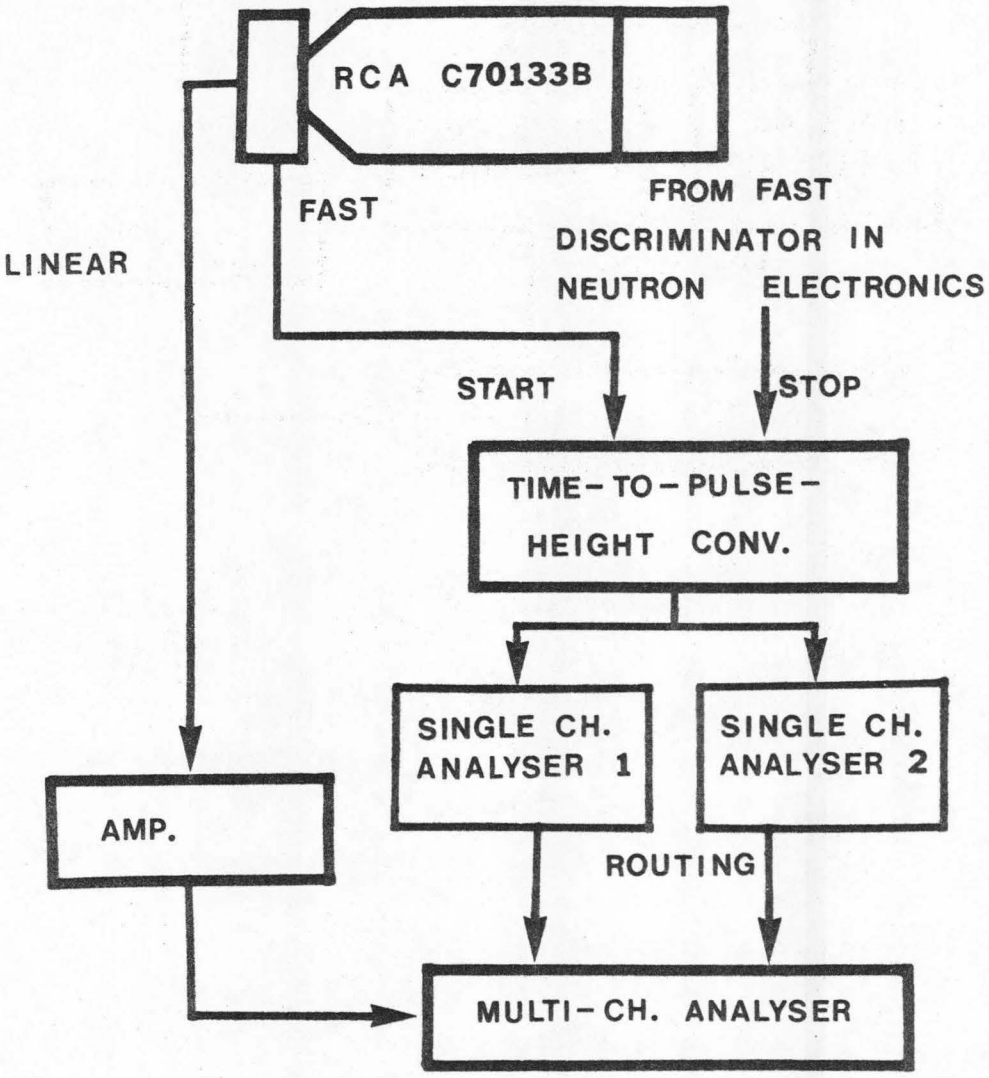
RCA C70133B
FAST
FROM FAST
DISCRIMINATOR IN
NEUTRON ELECTRONICS
LINEAR
START
STOP
TIME-TO-PULSE-
HEIGHT CONV.
SINGLE CH.
ANALYSER 1
SINGLE CH.
ANALYSER 2
AMP.
ROUTING
MULTI-CH. ANALYSER

Figure 5

Schematic drawing of the gas cell. The gas cell is electrically insulated from the beam pipe and the gas supply bottle by means of glass and teflon, respectively, and can be used as a Faraday cup for beam current integration. The nickel foil entrance window is 0.584 mgm/cm^2 thick. The tantalum collimator, together with a 2.54 cm diameter canal further up the beam pipe ensure that the beam is incident only on the entrance foil.

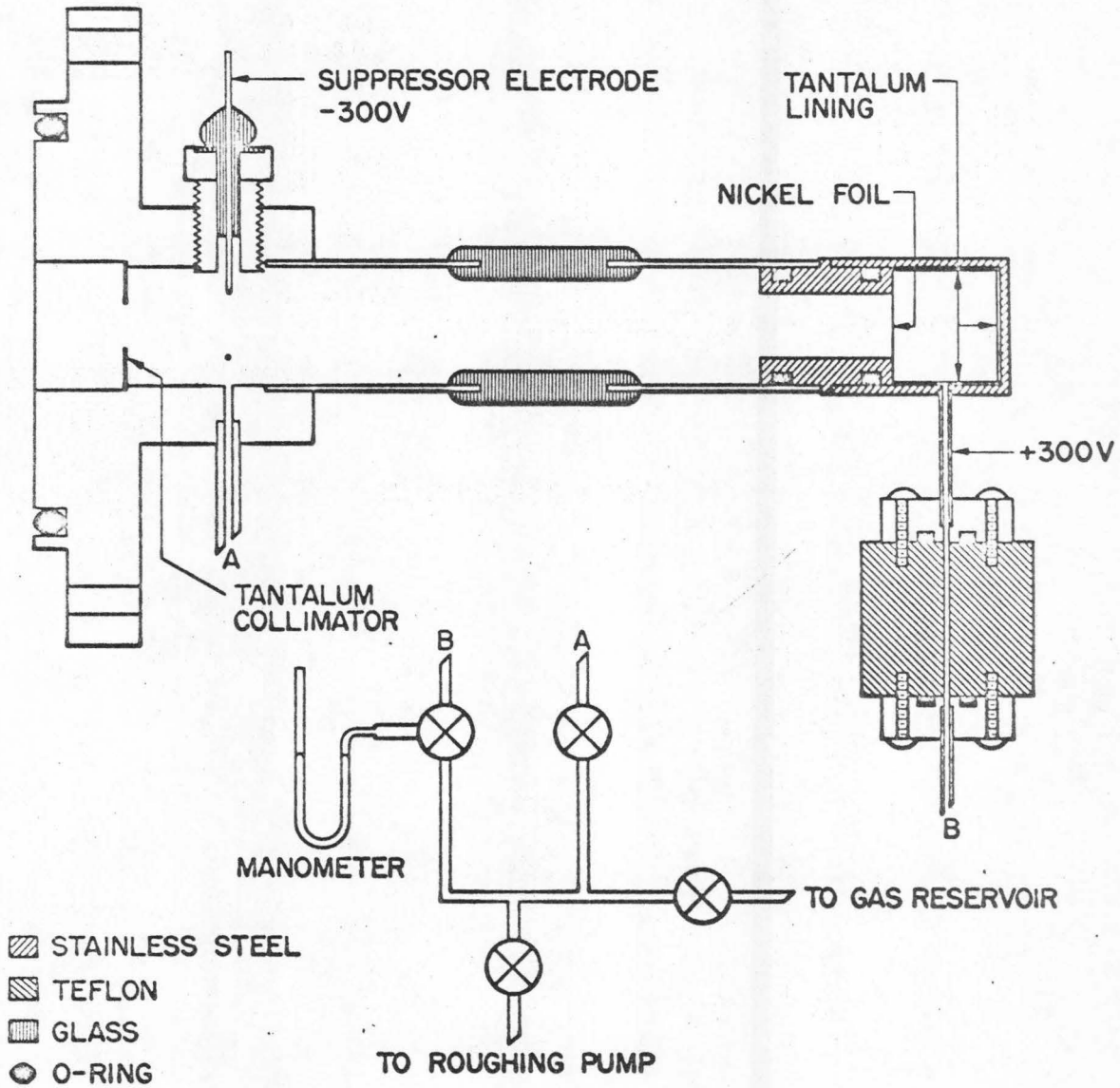
SUPPRESSOR ELECTRODE
-300V
TANTALUM
LINING
NICKEL FOIL
+300V
A
TANTALUM
COLLIMATOR
B
A
B
MANOMETER
TO GAS RESERVOIR
TO ROUGHING PUMP
STAINLESS STEEL
TEFLON
GLASS
O-RING

Figure 6a

Alpha particle spectra for determination of the Ni foil thickness and the straggling of the transmitted alpha particle. The peak on the right corresponds to 2.320 Mev α-particles while the one on the left corresponds to the 1.936 Mev α-particles which have passed through the Ni foil, placed in front of the entrance slits of the magnetic spectrometer. The 0.384 Mev energy loss corresponds to a foil thickness of 0.584 ± 0.06 mgm/cm^2.

Figure 6b

Excitation functions of the reaction $^{19}F(p,\alpha\gamma)^{16}O$ used for an alternative determination of the Ni foil thickness. The curve on the left is an excitation function without the Ni foil, while the one on the right is an excitation function with the Ni foil inserted between the target and the beam. The energy loss for 0.947 Mev protons was found to be 0.072 Mev, which gives a foil thickness of 0.578 ± 0.06 mgm/cm^2.

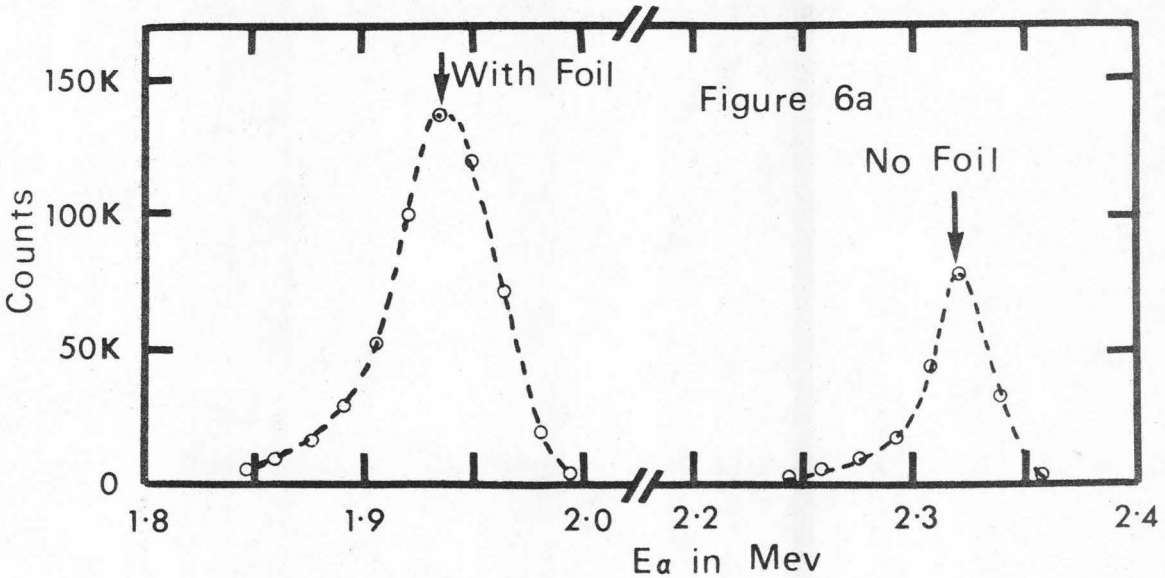
With Foil
Figure 6a
No Foil
150K
100K
50K
0
Counts
1·8
1·9
2·0
2·2
2·3
2·4
Eα in Mev

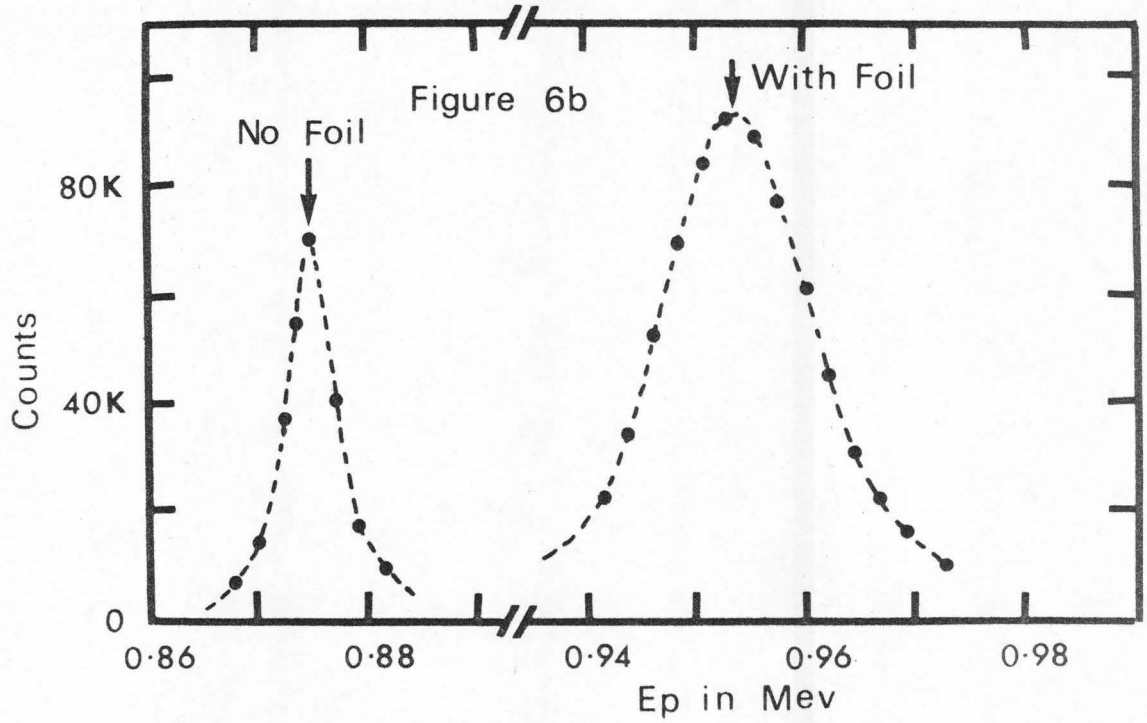
Figure 6b
With Foil
No Foil
80K
40K
0
Counts
0·86
0·88
0·94
0·96
0·98
Ep in Mev

Figure 7

Energy level diagram of ^{24}Mg (EL 67)

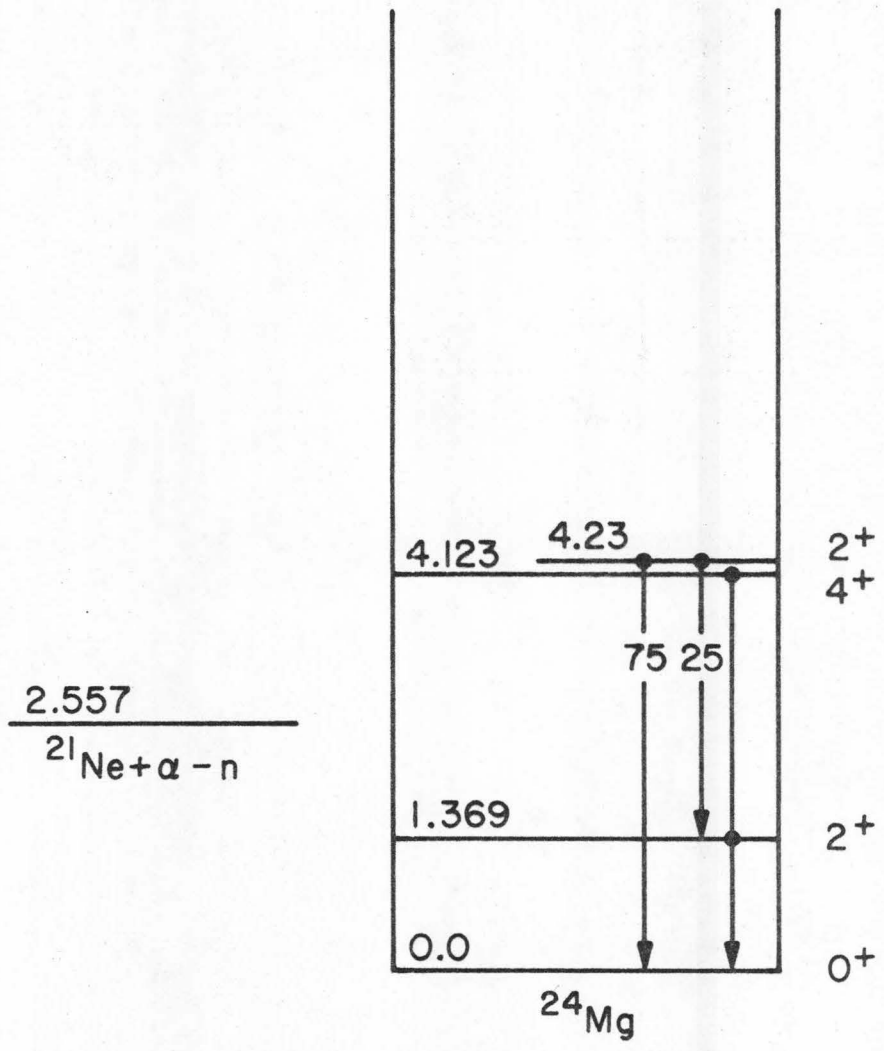
2.557
21Ne+α−n
4.123
4.23
2+
4+
75
25
1.369
2+
0.0
0+
24Mg

Figure 8

Neutron time-of-flight spectrum at E = 2.36 Mev, with the detector 76 cm away from the target and at an angle of 25^{o}. The time calibration is about 1 nanosecond per channel. The n_o and n_1 groups cannot be resolved any more, but they can still be separated from the neutron groups from $^{22}Ne(\alpha,n)^{25}Mg$.

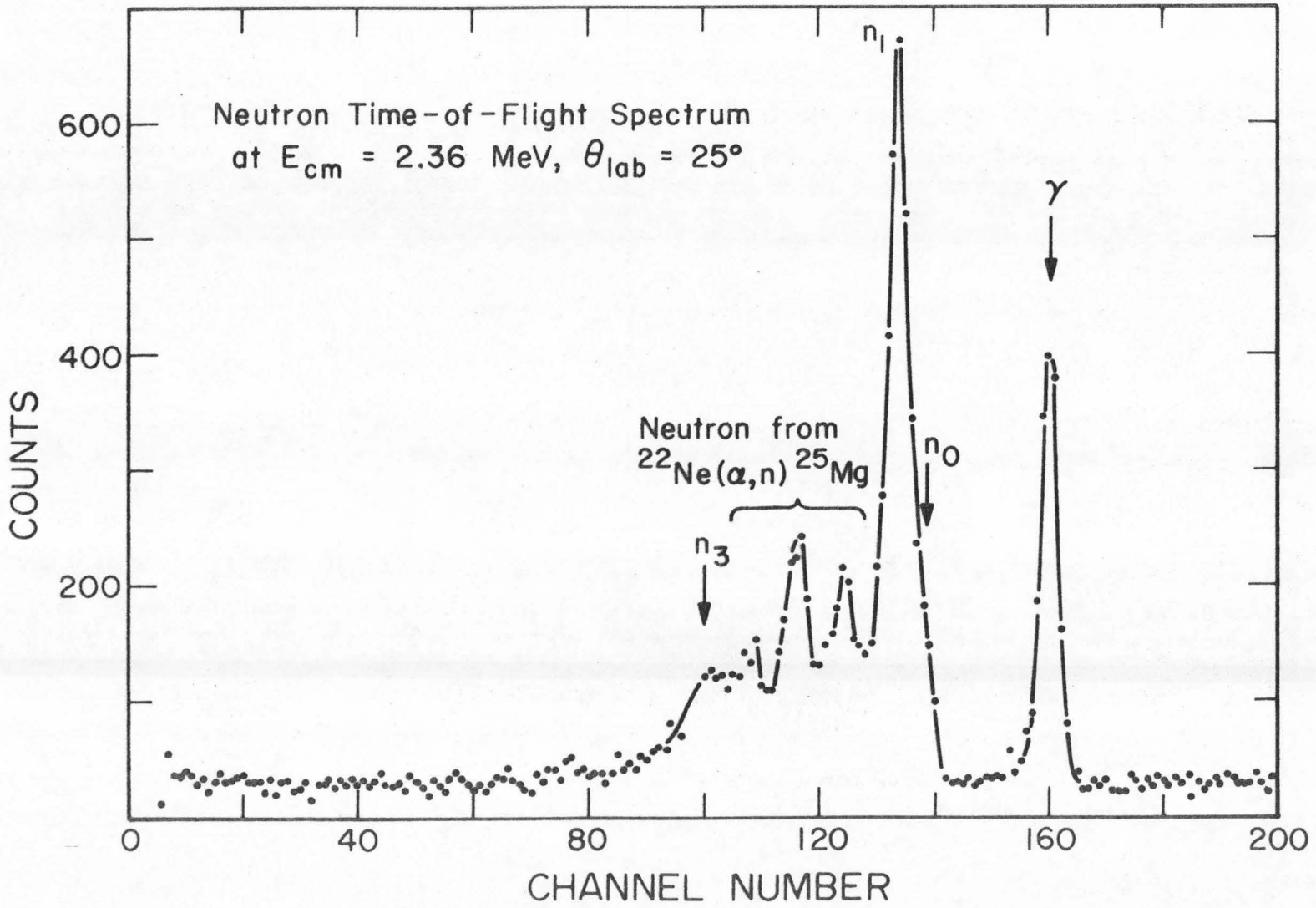
Neutron Time-of-Flight Spectrum
at E_{cm} = 2.36 MeV, θ_{lab} = 25°
n_1
γ
Neutron from
$^{22}Ne(\alpha,n)^{25}Mg$
n_0
n_3
COUNTS
600
400
200
0
40
80
120
160
200
CHANNEL NUMBER

Figure 9

Gamma ray time-of-flight spectrum with the NaI(Tl) crystal at a distance of 3.5 cm from the center of the gas cell, and at an angle of 55^{o}. Gamma rays from the walls of the room and from cosmic radiation give the flat background, while gamma rays associated with the beam bursts constitute the prompt gamma peak. The region between the 2 arrows on the left indicates the window of the 'TRUE' single channel analyser, while the region between the 2 arrows on the right indicates the window of the 'RANDOM' single channel analyser.

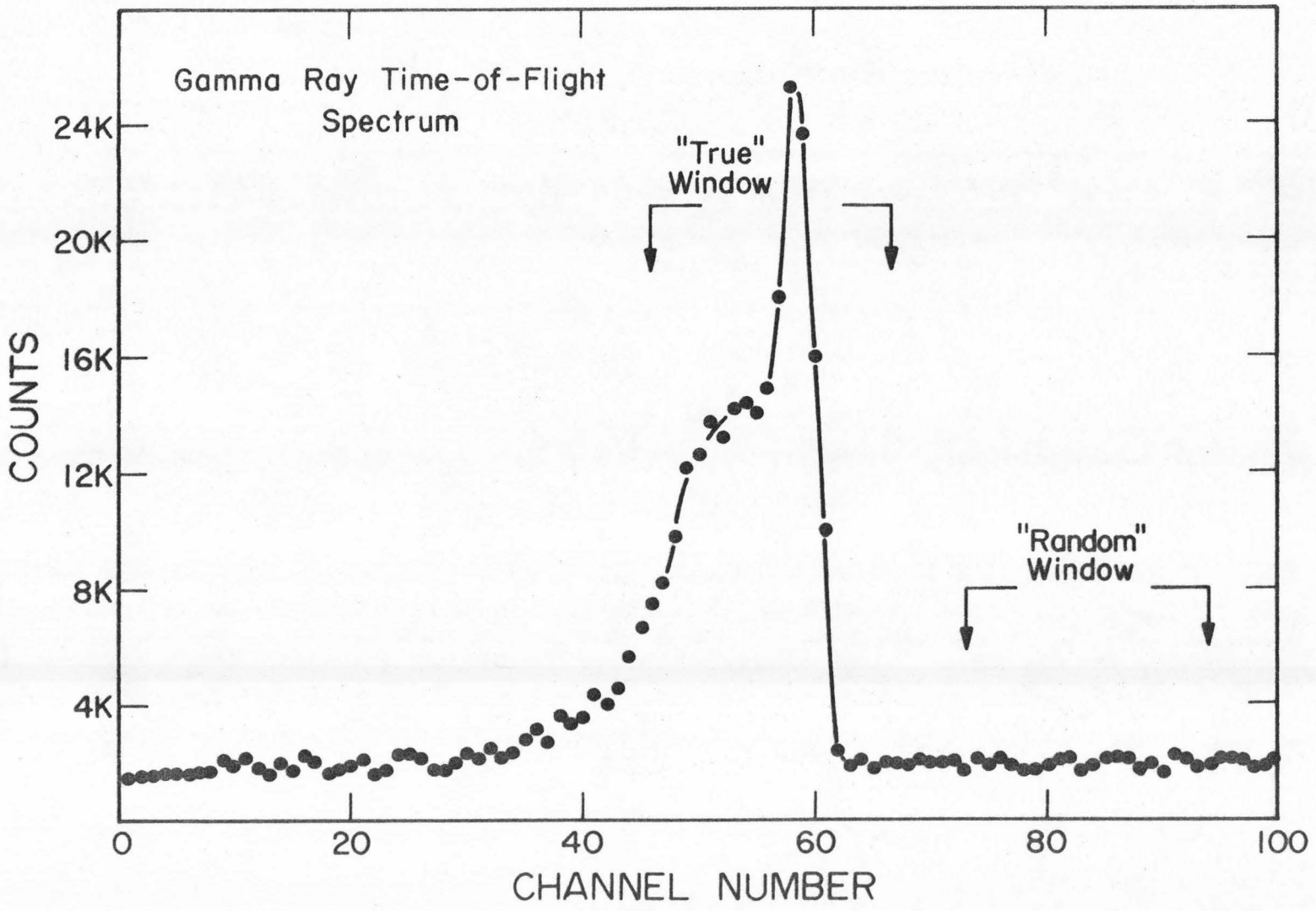
Gamma Ray Time-of-Flight
Spectrum
"True"
Window
"Random"
Window
24K
20K
16K
12K
8K
4K
COUNTS
0
20
40
60
80
100
CHANNEL NUMBER

Figure 10

Gamma ray spectra obtained at E_{cm} = 2.1 Mev, $\theta = 55^{o}$ and 3.5 cm from the target.

a) Gamma ray spectrum gated by the routing pulses from the 'TRUE' single channel analyser. The gamma rays arising from the decay of excited states of $^{21}Ne^{*}$ are labelled by their energies, while the positions of room background gamma rays are indicated by underlined energies.

b) Gamma ray spectra gated on by the routing pulses from the 'RANDOM' single channel analyser. The 1.461 Mev line is from ^{40}K and the 2.61 Mev line is from ThC" in the concrete wall.

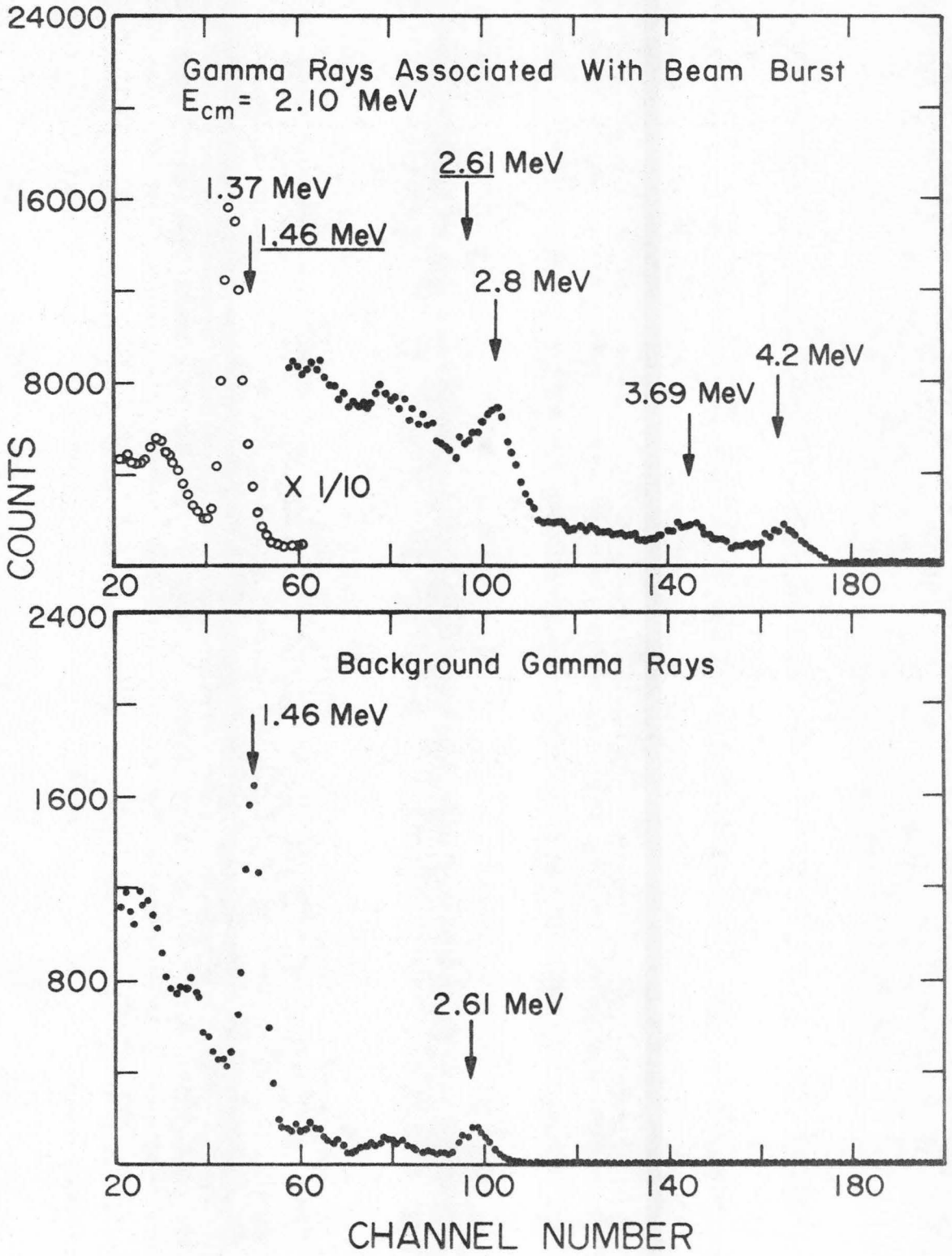
Gamma Rays Associated With Beam Burst
E_{cm}= 2.10 MeV
1.37 MeV
1.46 MeV
2.61 MeV
2.8 MeV
3.69 MeV
4.2 MeV
X 1/10
COUNTS
24000
16000
8000
20
60
100
140
180
Background Gamma Rays
1.46 MeV
2.61 MeV
2400
1600
800
CHANNEL NUMBER

Figure 11

Angular distribution of the 1.37 Mev gamma rays from the reaction $^{21}Ne(\alpha,n)^{24}Mg$. The dashed curve is a least-squares Legendre-Polynomial fit,

$$W(\theta) = 2.78 + 0.084 \frac{J_2}{J_o} P_2(\cos\theta) + 0.065 \frac{J_4}{J_o} P_4(\cos\theta) ,$$

where J_L is defined by equation C5.

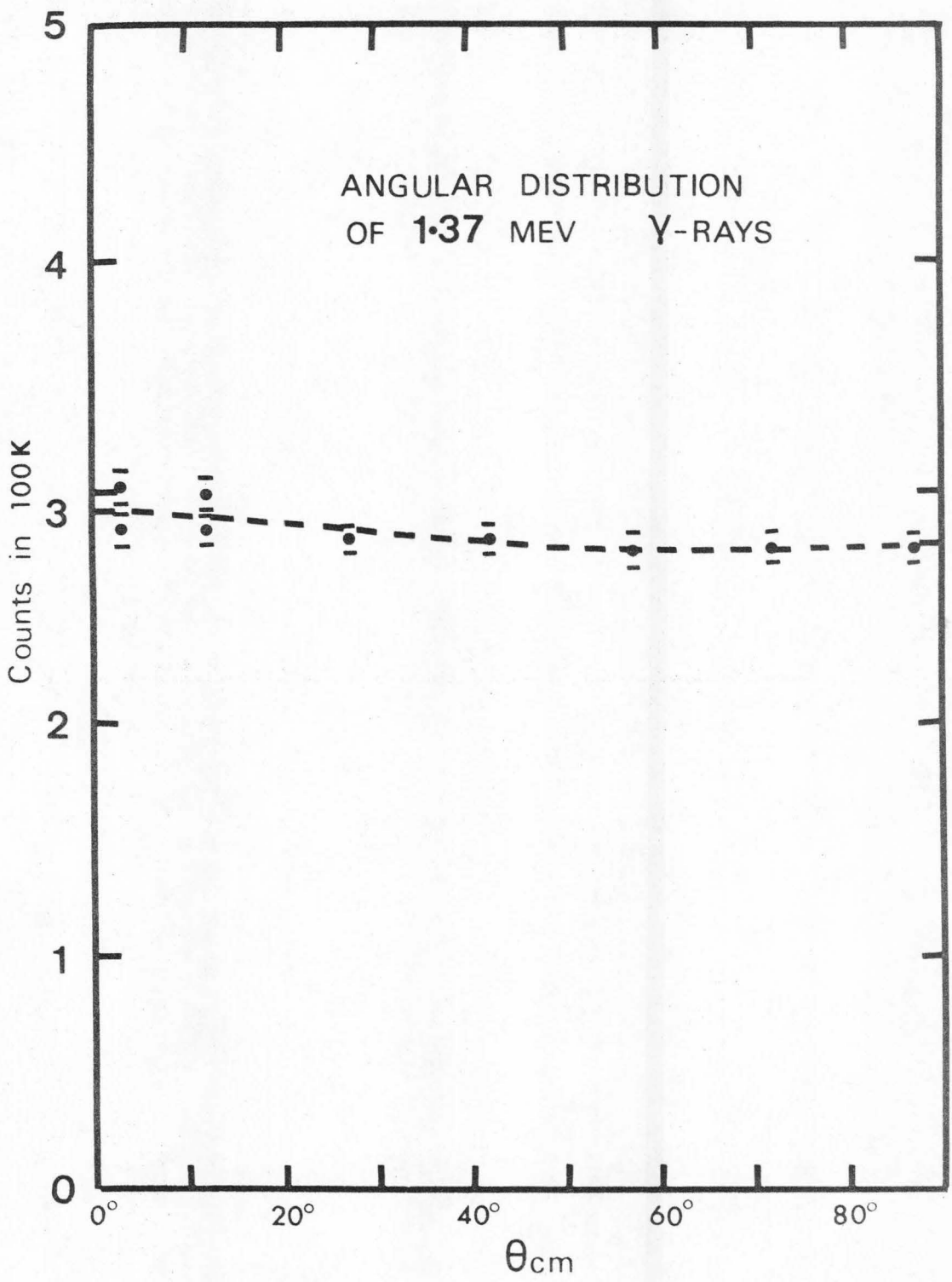
ANGULAR DISTRIBUTION
OF 1·37 MEV γ-RAYS
Counts in 100 K
0
1
2
3
4
5
0°
20°
40°
60°
80°
θcm

Figure 12

Angular distribution of the 2.86 Mev gamma rays from the $^{21}Ne(\alpha,n)^{24}Mg$ reaction. The dashed curve is a least-squares Legendre-Polynomial fit to the data points,

$$W(\theta) = 7.23 + 1.83 \frac{J_2}{J_o} P_2(\cos\theta) + 0.65 \frac{J_4}{J_o} P_4(\cos\theta) ,$$

where J_L is defined by equation C5.

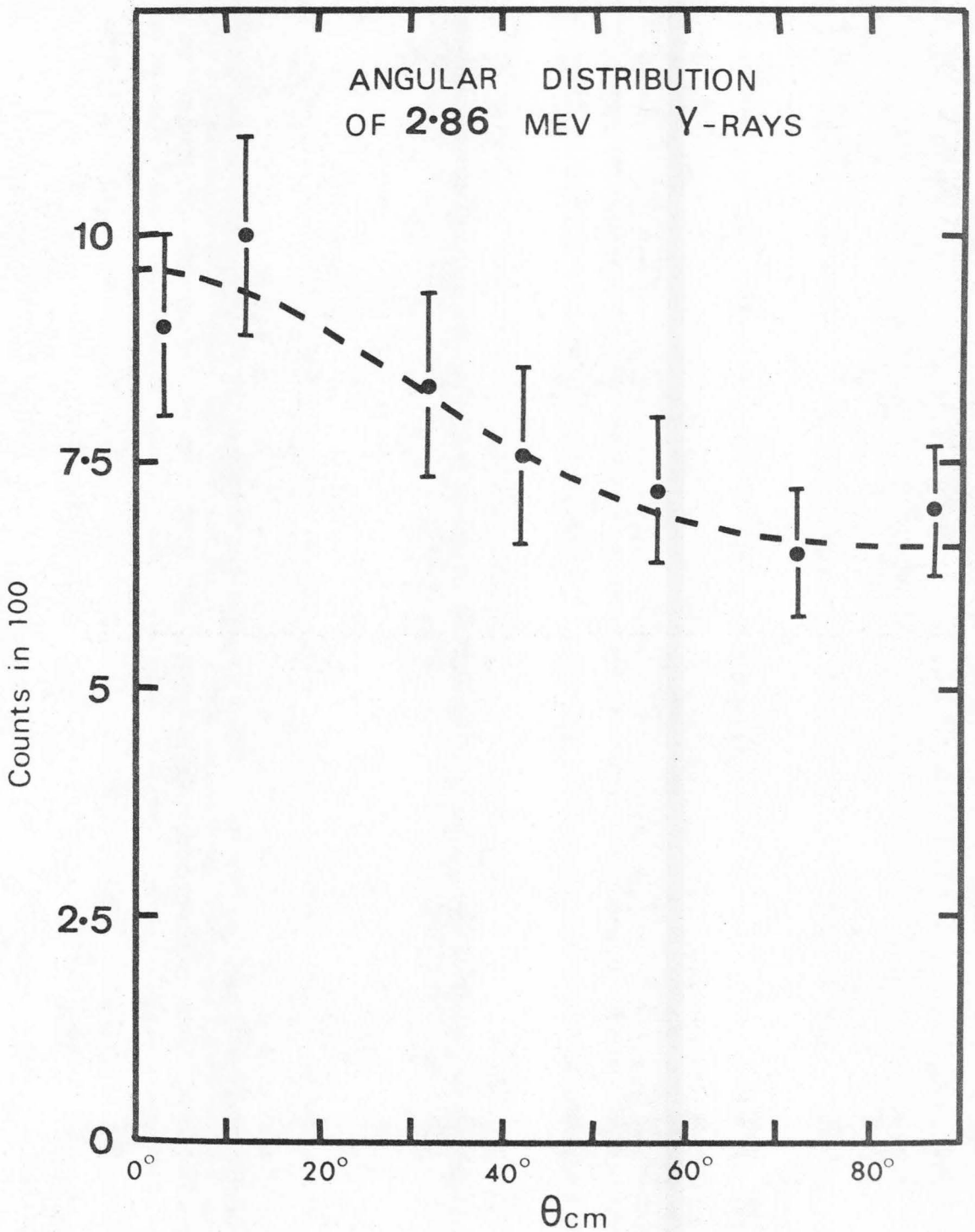
ANGULAR DISTRIBUTION
OF 2·86 MEV γ-RAYS
10
7·5
5
2·5
0
Counts in 100
0°
20°
40°
60°
80°
θcm

Figure 13

Angular distribution of the 4.2 Mev gamma rays from the reaction $^{21}Ne(\alpha,n)^{24}Mg$. The dashed curve is a least-squares Legendre-Polynomial fit,

$$W(\theta) = 9.02 + 2.67 \frac{J_2}{J_o} P_2(\cos\theta) + 0.186 \frac{J_4}{J_o} P_4(\cos\theta)$$

where J_L is defined by equation C5.

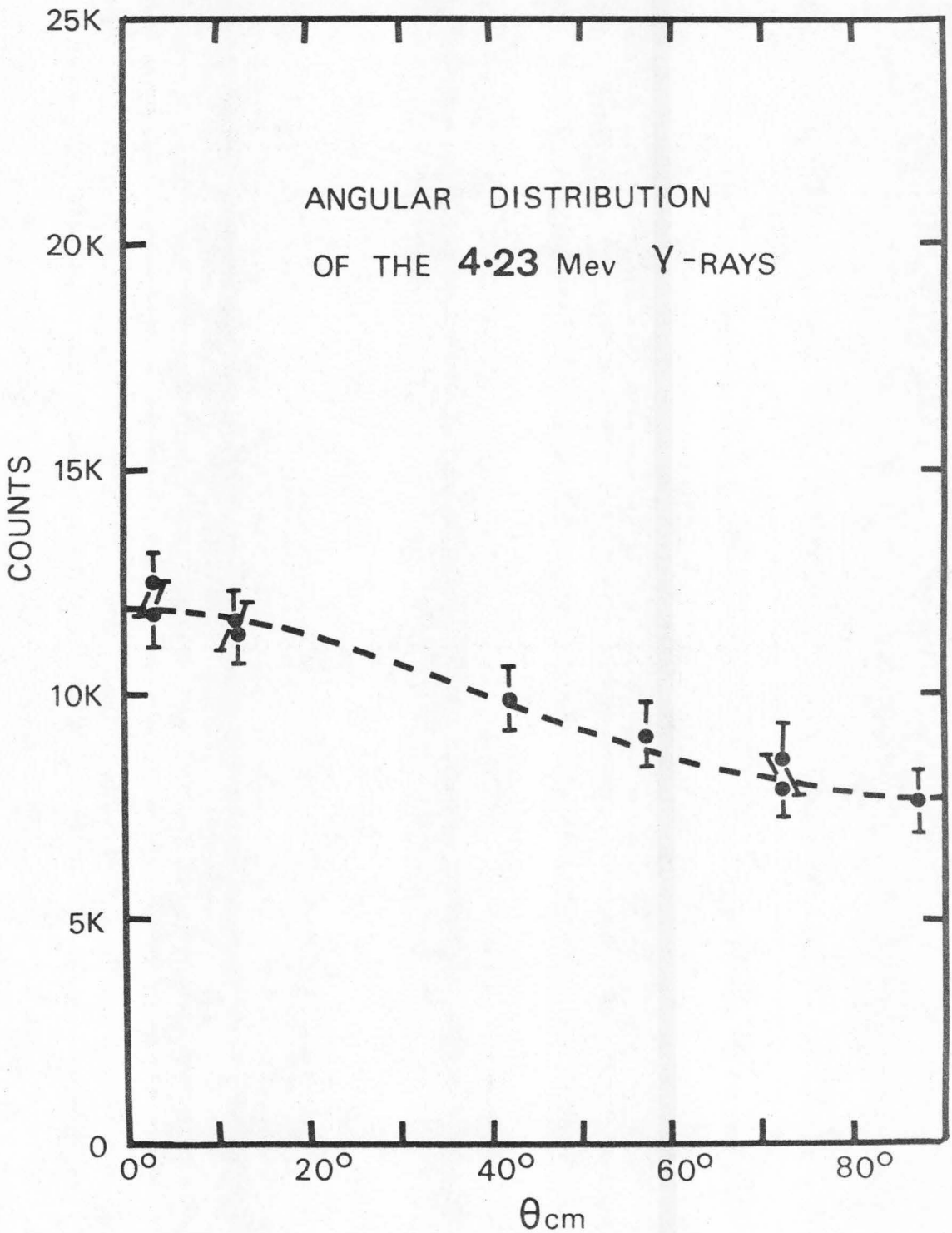
ANGULAR DISTRIBUTION
OF THE 4·23 Mev γ-RAYS
COUNTS
25K
20K
15K
10K
5K
0
0°
20°
40°
60°
80°
θcm

Figure 14

Angular distributions of $(n_o + n_1)$ groups from the reaction $^{21}Ne(\alpha,n)^{24}Mg$.

* E_{cm} = 2.36 Mev

○ E_{cm} = 2.08 Mev

△ E_{cm} = 1.82 Mev

● E_{cm} = 1.65 Mev

The curves are fits with Legendre-Polynomials up to order 3.

Table 2 lists the angular distributions of the $(n_o + n_1)$ groups in the energy range 1.49 Mev $\leq E_{cm} \leq$ 2.57 Mev.

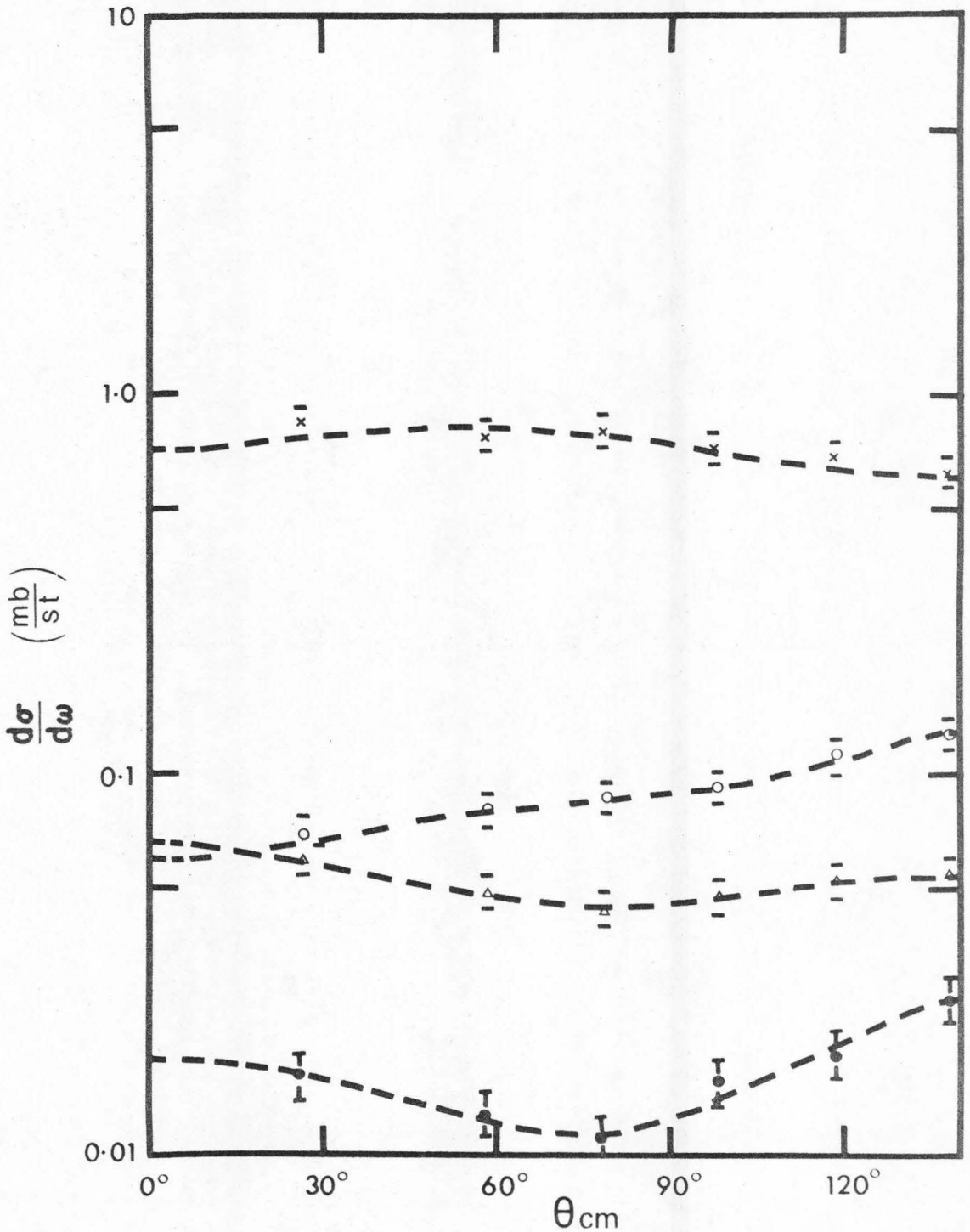
10
1·0
0·1
0·01
dσ/dω (mb/st)
0°
30°
60°
90°
120°
θcm

Figure 15

Excitation function for the reaction $^{21}Ne(\alpha,n)^{24}Mg$. The solid curve is a theoretical calculation using formula D16 in the text, and the following values for the parameters:

$R = 6.0$ fm,

$\beta\Gamma_n/\Gamma = 0.435$,

$E_\gamma = 1.93$ Mev,

$\Gamma_\gamma = 0.07$ Mev,

$\ell = 1$,

$\gamma^2_{\alpha,\ell} = 0.046$ Mev.

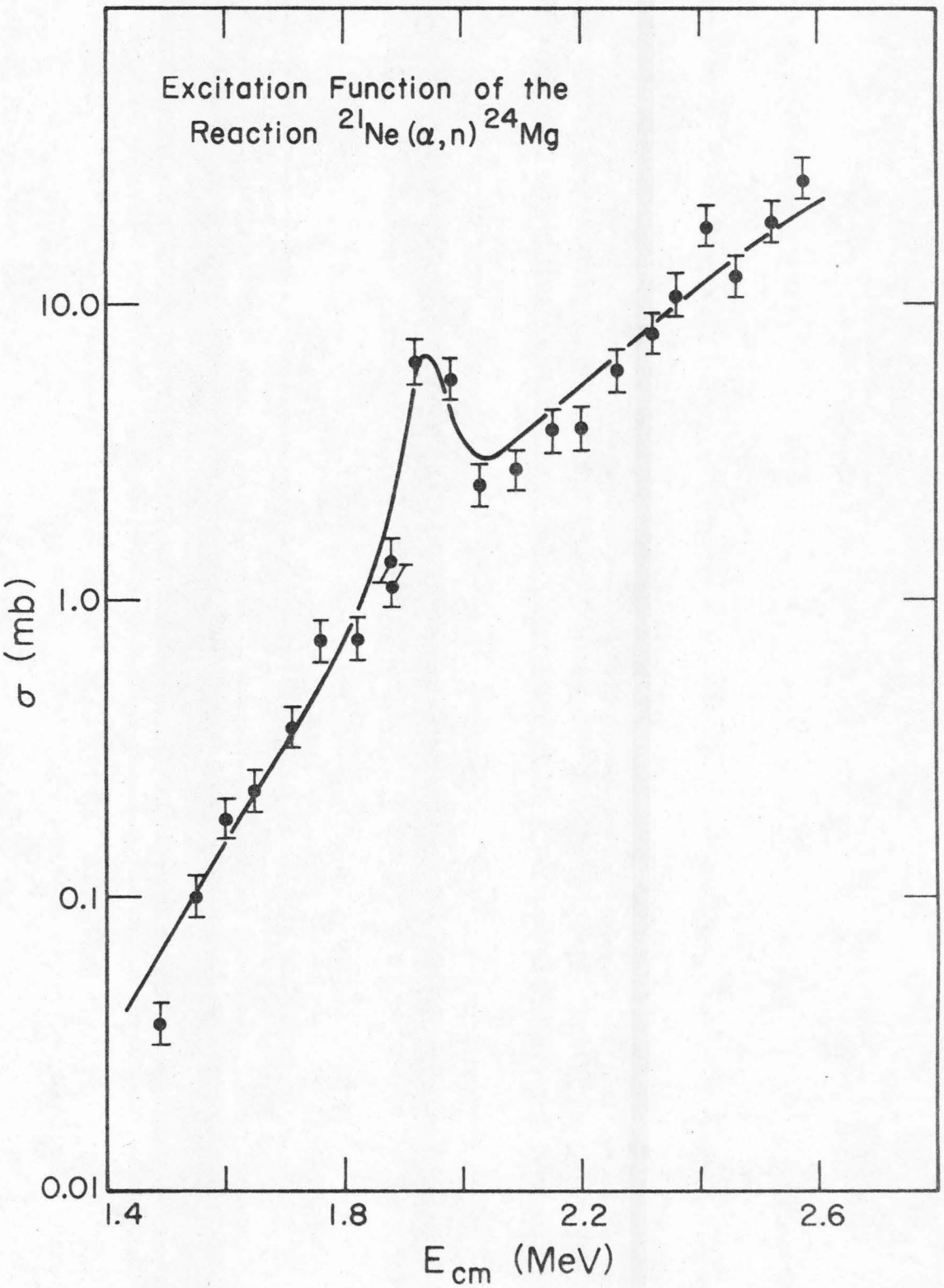
Excitation Function of the
Reaction $^{21}Ne(\alpha,n)^{24}Mg$
10.0
1.0
0.1
0.01
σ (mb)
1.4
1.8
2.2
2.6
E_{cm} (MeV)

Figure 16

Cross-section factor S(E)

The solid curve is a calculation using equation E8 with $R = 6.0$ fm and $\beta\Gamma_n/\Gamma = 0.435$.

The dashed line is a least-squares fit of the experiment S(E) data, excluding the two points at 1.92 Mev and 1.98 Mev, using equation D11.

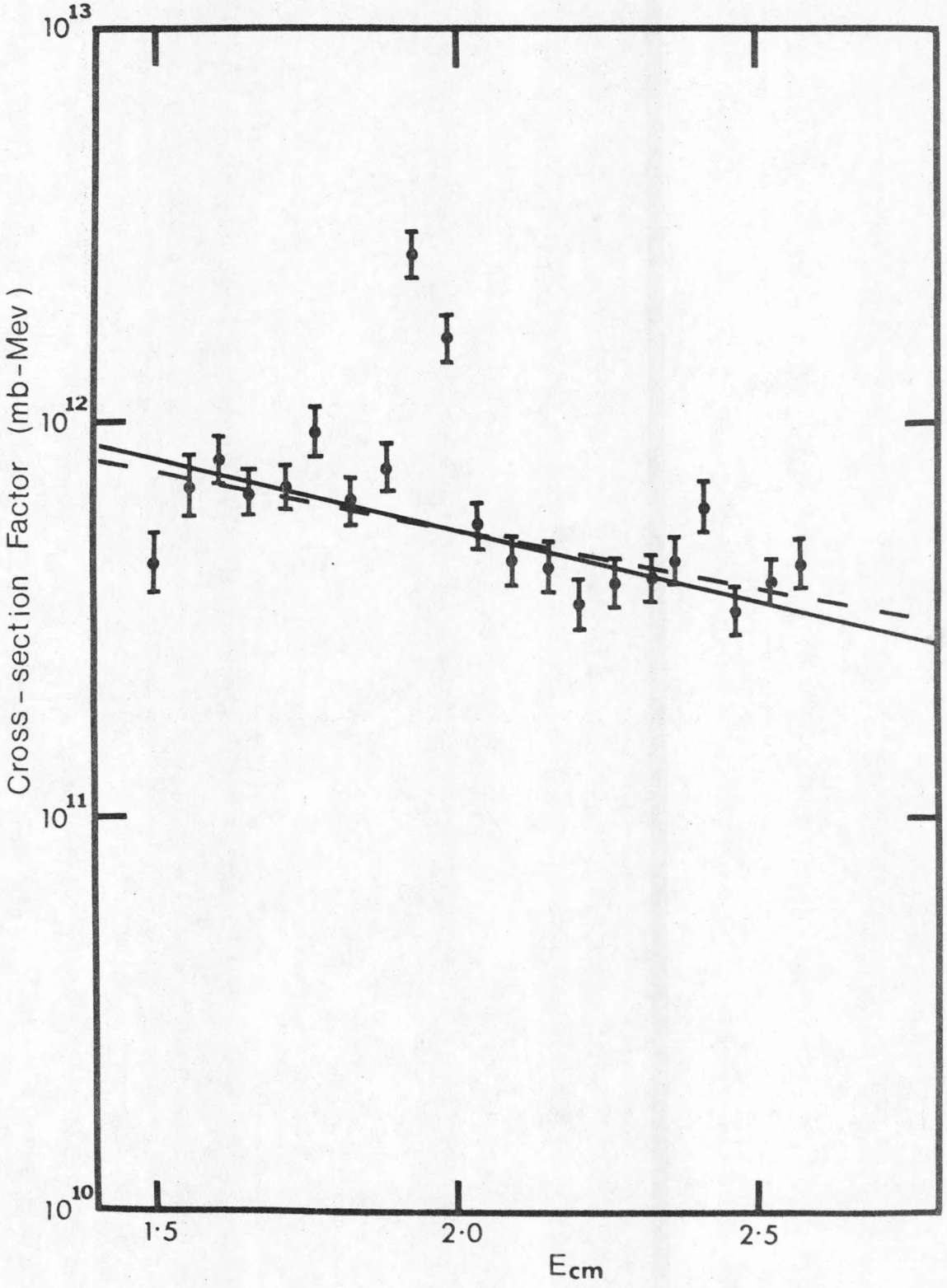
10^{13}
10^{12}
10^{11}
10^{10}
Cross-section Factor (mb-Mev)
1·5
2·0
2·5
E_{cm}

PART II

A Study of the Reaction

$^{12}C(^{3}He,p)^{14}N$

A. INTRODUCTION

Direct reactions have long been used to extract information about nuclear structure. From the angular distributions, the angularmomentum transfers can be determined, and, with the selection rules, the spins and parities of the nuclear states involved can be obtained or, at least, restricted to a narrow range of possible values. From the strength of a particulartransition, the spectroscopic factor can be obtained; this quantity identifies the specific configuration of the nuclear state involved.

It is generally assumed that the differential cross-section for a direct transfer reaction can be written in the factorized form

$$\frac{d\sigma}{d\Omega} = R \sum_{LSJ} S_{LSJ}\, \sigma_{LSJ} \quad ,$$

where R is a statistical factor involving the spin and isospin of the nuclear states, S_{LSJ} is the spectroscopic factor, which includes the overlap between the initial and the final states and contains the detailed nuclear structure information, and σ_{LSJ} is a kinematic factor which contains the energy and angle dependence.

In order to facilitate computations, a number of simplifications are generally made in applying the direct

transfer theory to calculate the kinematic factor σ_{LSJ}. In most cases it appears that the spins and parities can be deduced rather well (Hen 69, Ade 67). There remains the important question of how accurately the spectroscopic factor can be extracted from the experimental data. (AM 70, Bar 69).

A major difficulty in extracting the spectroscopic factor is caused by the uncertainties introduced in simplifying the calculation. Recently a lot of theoretical work has been carried out to improve the approximations but, due to the complexity of the problem, it is not obvious that these improvements have significantly increased the accuracy of extracting spectroscopic factors.

Another difficulty lies in determining the magnitude of the contributions from compound nucleus formation, which may have a strong energy dependence. In many cases, direct transfer reaction theory has been used to interpret reactions at isolated energies, and parameters have been adjusted freely to fit the data. It is rather doubtful that the spectroscopic factor so obtained can be very significant. It is essential to establish the nature of the reaction mechanism first by studying the reaction systematically through a reasonable energy range. If the reaction changes smoothly with energy, direct reaction theory can then be applied to obtain spectroscopic

information, with a little more confidence.

In the present experiment, the $^{12}C(^{3}He,p)^{14}N$ reaction was studied over the energy range 12 Mev $\leq E_{lab} \leq$ 18 Mev. This reaction was chosen because the first excited state in ^{12}C has an excitation energy of 4.439 Mev; hence the problem of core excitation should not be as important as in cases where the target nucleus has low-lying levels. (However, there is a large electromagnetic matrix element between the ground state and first excited state of ^{12}C; thus one should be wary of the assumption that no core excitation is involved.) In addition the energy levels of ^{14}N below 6 Mev excitation are at least partially understood, and several theoretical calculations for the wave functions of ^{14}N are available (Tru 63, CK 65, WP 60, TU 60, GFGH 66).

This reaction has been studied by several workers: Hinds and Middleton (HM 60) at several energies below 10 Mev, Holbrow et al. (HMPB 66) and Priest et al. (PTB 60) at 14.0 Mev, and Mangelson (Man 67) at 20.1 Mev.

The aim of the present work is to examine whether two-nucleon transfer theory can be applied to interpret the reaction $^{12}C(^{3}He,p)^{14}N$ in a meaningful way or not, by systematically studying the reaction in the energy range 12 Mev $\leq E_{lab} \leq$ 18 Mev in 0.5 Mev steps.

The two-nucleon stripping formalism of Glendenning

(Gle 65) was used to interpret the results. The computer code 'JULIE' compiled by Bassel et al. (BDS 67), which is based on the zero-range and local potential approximations, was used to facilitate the computation.

B. EXPERIMENTAL METHOD

1. ^{3}He Beam

The ONR-CIT tandem accelerator was used to provide a doubly-charged ^{3}He beam for this experiment. The beam energy, selected by a 90° momentum-analysing magnet, has a resolution of approximately one part per thousand. The beam current at the target was kept at approximately 150 nano-amp, except when taking data at forward angles ($\theta_{lab} \leq 25^\circ$), where it was necessary to reduce the current because of the high counting rate from the elastic scattering of ^{3}He on ^{12}C.

2. Scattering Chamber

Figure 1 shows the scattering chamber and its associated parts. The chamber itself is a cylindrical section, 8 inches high and 24 inches in diameter. The target holder was a stainless steel rod, which was electrically insulated from ground, passing through the center of the lid.

Two arms, which could be rotated independently around the stainless steel rod from outside of the chamber, were used as detector mounts. The angular positions of the arms could be read on a dial to an

accuracy of 0.25°.

The beam direction was defined by two sets of slits. One, with a 150-mil square aperture, was at a distance of 62.5 inches before the target, while the other, with a 50-mil square aperture, was at a distance of 17 inches before the target. The stray beam scattered off the slits was stopped by a collimator with a circular opening, 0.19 inches in diameter, approximately 3.5 inches in front of the target.

A Faraday cup assembly consisting of a tantalum cup at +300 volts and a magnet, which provides magnetic and electric electron suppression, at -300 volts, was placed in the beam exit port 12 inches behind the target. The Faraday cup subtended an angle of 5° at the target. It was estimated that the loss of beam particles, due to multiple scattering in the target, was less than 1%.

A monitor detector was mounted on one of the detector arms, and was kept fixed at 90° throughout the experiment. The circular opening of the collimator in front of the detector subtended an angle of 1.8° at the target. A "telescope detector" system was mounted on the other arm, and was collimated to subtend an angle of 0.8° at the target.

3. Target

Natural carbon foil, approximately 200 μgm/cm^2 thick, was mounted on a tantalum frame over a 0.38 inches diameter hole. For all the $^{12}C(^3He,p)^{14}N$ measurements, the foil was placed at an angle of $\pm 45^o$ to the beam.

For the cross-section measurement of the $^{12}C(^3He,^3He)^{12}C$ reaction at $\theta_{lab} = 45^o$, a 0.5 inch x 0.5 inch natural carbon foil was weighed by an electronic micro-balance after its area had been estimated. It was then mounted on a tantalum frame and positioned perpendicular to the beam. The thickness of the carbon foil used was found to be 129 ± 13 μgm/cm^2. The main sources of error in determining the target thickness were the uncertainty in estimating the area and the uncertainty in the uniformity of the target.

4. Electronic Circuitry

A block diagram of the electronic circuits used in this experiment is shown in figure 2. The system employed a ΔE and E telescope arrangement for particle identification and energy detection. The telescope arrangement consisted of a 200 μ-thick transmission-mounted silicon counter, backed up by a 3 mm-thick lithium drifted silicon counter. The gains of the E and ΔE counters were matched

by attenuating the signals from the ΔE counter. The E and ΔE pulses were then added by a summing amplifier of unit gain, amplified and routed into two separate pulse-height-analysers, according to the size of the pulses in the E-counter, as described below.

Only the seven most energetic proton groups produced in the reaction $^{12}C(^{3}He,p)^{14}N$ were being studied, and they all lost a major fraction of their energy in the E counter, while the ^{3}He and ^{4}He particle from the reactions $^{12}C(^{3}He,^{3}He)^{12}C$ and $^{12}C(^{3}He,\alpha)^{11}C$ lost the major fraction of their energy in the ΔE counter. Particle identification was done very simply by setting up a single channel analyser to inspect the output from the E counter. The threshold of the single channel analyser was set to block the small signals produced by ^{3}He and ^{4}He particles. The output of this single channel analyser was then branched off into two pulse stretchers, the output of one of which was used to gate a 4096-channel analyser, while the output of the other was fed into the anti-coincidence input of a slow coincidence gate. The signals of the ΔE counter were also inspected by a single channel analyser which was set to cut off the noise. The output of this single channel analyser was fed into the coincidence input of the slow coincidence gate, whose output was used to gate a 400-channel pulse-

height-analyser.

A 2 mm-thick lithium-drifted silicon counter, kept fixed at $\theta_{lab} = 90^{o}$, was used to normalize the yields obtained by the telescope counters at different angles and bombarding energies. No particle identification was made for the monitor counter system.

C. DATA REDUCTION

1. Absolute Differential Cross-section Measurement

In this experiment, the carbon-foil targets used had large uncertainties in their thickness. In order to convert the yields into differential cross-sections, a monitor counter set at $\theta_{lab} = 90^{o}$ was used.

The differential cross-sections of the reaction $^{12}C(^{3}He,^{3}He)^{12}C$ at $\theta_{lab} = 45^{o}$ were measured over the energy range 12 Mev $\leqslant E_{lab} \leqslant$ 18 Mev. Figure 3 shows the spectra obtained at $E_{lab} = 17.0$ Mev by the telescope counters at 45^{o}.

The following equation was used in calculating the differential cross-sections,

$$\frac{d\sigma}{d\Omega} = Y \cdot \frac{d^2}{a} \cdot \frac{\text{mole. wt.}}{N. N_o} \cdot \frac{1}{x} \cdot \frac{q}{Q} \cdot CMF \quad , \quad Cl$$

where $\frac{d\sigma}{d\Omega}$ = differential cross-section in the center-of-mass system,

d = distance between target and detector,

a = area of detector,

mole wt = molecular weight of the target atom,

N = number of target atoms per target molecule,

N_o = Avogardro's number,

x = target thickness,

q = charge of incident particles,

Q = total charge collected,

Y = number of counts within the peak,

CMF = center of mass factor for transforming from the laboratory system to the center-of-mass system.

Substituting appropriate numerical values, equation C1 becomes

$$\frac{d\sigma}{d\Omega} = 0.001935 \cdot Y \cdot CMF \quad mb/st \qquad C2$$

Figure 4 shows the excitation function of the reaction $^{12}C(^{3}He,^{3}He)^{12}C$ at $\theta_{lab} = 45^{o}$. The corresponding differential cross-sections are listed in Appendix B.

The uncertainty due to counting statistics and background subtraction was 3%, while the charge integration was good to 1%. These, together with a 10% uncertainty in target thickness, yield an uncertainty of approximately 10% in the differential cross-section.

Fortune et. al. (FGTF 68) have recently measured the excitation function of the $^{12}C(^{3}He,^{3}He)^{12}C$ reaction at various laboratory angles in the same energy range, and their results are in good agreement with the present experiment.

These 45^{o} differential cross-sections were used

to convert the yields of the reactions $^{12}C(^{3}He,^{3}He)^{12}C$ and $^{12}C(^{3}He,p)^{14}N$ into differential cross-sections by the following equation:

$$\frac{d\sigma(\theta_{cm})}{d\Omega} = \frac{d\sigma}{d\Omega} \cdot \frac{MON}{MON(\theta_{cm})} \cdot \frac{Y(\theta_{cm})}{Y} \cdot \frac{CMF(\theta_{cm})}{CMF} \cdot \frac{DT}{DT(\theta_{cm})} \quad , \qquad C3$$

where $\frac{d\sigma}{d\Omega}$ = differential cross-section of the reaction $^{12}C(^{3}He,^{3}He)^{12}C$ at $\theta_{lab} = 45^{o}$,

MON = number of monitor counts when the telescope counters were at $\theta_{lab} = 45^{o}$,

Y = number of elastically scattered ^{3}He particles detected by telescope counters at $\theta_{lab} = 45^{o}$,

DT = dead time correction when the telescope counters were at $\theta_{lab} = 45^{o}$,

CMF = center of mass factor, at $\theta_{lab} = 45^{o}$, for the reaction $^{12}C(^{3}He,^{3}He)^{12}C$,

$Y(\theta_{cm})$ = number of counts within the peak,

$CMF(\theta_{cm})$ = center of mass factor,

$DT(\theta_{cm})$ = dead time correction,

$MON(\theta_{cm})$ = number of monitor counts.

2. $^{12}C(^{3}He,^{3}He)^{12}C$

The $^{12}C(^{3}He,^{3}He)^{12}C$ reaction was studied using a self supporting natural carbon foil, approximately 200 $\mu gm/cm^2$ thick, placed at an angle of 45^{o} to the beam. In the backward angles, the elastically scattered ^{3}He particles could not be resolved from the ^{4}He particles from the reaction $^{12}C(^{3}He,\alpha)^{11}C$. In the forward angles, the ^{3}He particles scattered by the impurities in the target, mainly ^{16}O and ^{13}C, could not be resolved from those scattered by ^{12}C. The contribution from the impurities was , however, estimated to be less than 4%.

Angular distributions of the elastically scattered ^{3}He by ^{12}C are shown in figure 5, and the differential cross-sections are tabulated in Appendix B.

In addition to the 10% uncertainty from the normalization factor, the statistical uncertainties and the scattering from impurities introduced an error of approximately 4%. In the forward angles, the dead time correction had a large uncertainty, up to 50%, due to the high counting rate.

The $^{12}C(^{3}He,^{3}He)^{12}C$ elastic scattering has been studied extensively within the last few years. Fortune et. al. (FGTF 68) at 16 Mev, 17 Mev and 18 Mev, Baugh et. al. (BPRS 67) at 29 Mev, Warshaw et. al.(WBBB 68)

at 18 Mev, 20 Mev, 22.2 Mev and 24 Mev, Scheklinski et. al. (SSG 70) at 11 Mev, and Zurmuhle et. al. (ZF 69) at 15 Mev. Hodgson (Hod 68) and Park (Par 68) have compiled information on the same reaction from earlier work.

3. $^{12}C(^{3}He,p)^{14}N$

The $^{12}C(^{3}He,p)^{14}N$ reaction was studied using a self-supporting natural carbon foil approximately 200 $\mu gm/cm^2$ thick placed at an angle of 45^{o} to the beam direction.

Figure 6 shows the energy level diagram of ^{14}N taken from F. Ajzenberg-Selove (Ajz 70). Figure 3 shows the proton spectrum obtained at 17.0 Mev and $\theta_{lab} = 45^{o}$. A small contribution from the reaction $^{16}O(^{3}He,p)^{18}F$ indicated a 1-2% oxygen impurity in the target.

Angular distributions of the proton groups leading to the lowest 7 states in ^{14}N are shown in figures 7-13 and their differential cross-sections are tabulated in Appendix B.

The statistical errors were between 1% and 10% in most cases. In the forward angles, the background subtraction and dead time correction introduced a 20-30% uncertainty due to the high count rate in the ΔE counter, which resulted in pulse pile-up in the proton spectra.

The differential cross-section for $^{12}C(^{3}He,p)^{14}N$ has been measured by several workers; Priest et. al. (PTB 60) at 14 Mev, Hinds and Middleton (HM 60) at 10.23 Mev and lower energies, Holbrow et. al. (HMPB 66) at 14 Mev, Mangelson (Man 67) at 20.1 Mev, J. Singh (Sin 70) from 16 Mev to 30.6 Mev.

D. ANALYSIS

1. $^{12}C(^{3}He,^{3}He)^{12}C$

The $^{12}C(^{3}He,^{3}He)^{12}C$ elastic scattering was analysed using the optical-model potential

$$U(r) = Vf_r(r) + iWf_w(r) + V_c(r) \qquad D1$$

where

$$f_r(r) = \left\{1 + \exp[(r - R_r)/A_r]\right\}^{-1}$$

$$f_w(r) = \left\{1 + \exp[(r-R_w)/A_w]\right\}^{-1}$$

$$V_c(r) = \frac{Z_1 Z_2 e^2}{2R_c}\left\{3 - \frac{r^2}{R_c^2}\right\} \qquad r \leqslant R_c$$

$$= Z_1 Z_2 \frac{e^2}{r} \qquad r \geqslant R_c$$

The parameters V and W are the well depths of the real potential and the volume-absorption imaginary potential. R_r, and R_w are the corresponding radius parameters, and A_r, and A_w are the corresponding diffuseness parameters. R_c is the so-called Coulomb radius.

The quality of the fits was rather insensitive to

small changes in R_c, so it was kept fixed at $R_c = 3.21$ fm. The inclusion of a spin-orbital potential improves the fit slightly; it was not included in the analysis since the improvement is not significant.

A complete six-parameter search was carried out at 12 Mev, 15 Mev and 18 Mev, using as starting points the parameters given by Fortune et. al. (FGTF 68) and Park (Par 68). Two sets of average shape parameters (R_r, A_r, R_w and A_w) were obtained. Then a two-parameter search was made over V and W at each energy, using one set of shape parameters at a time. Only one set of shape parameters could fit the data over the whole energy range reasonably well. The parameters are listed in Table 1, and the calculated curves are shown in figure 5.

It was possible to improve the fits slightly by varying the shape parameters slightly at different energies, but it seems contrary to the spirit of an optical model to use different shape parameters at different energies, and it was felt more proper to keep them constant.

There is considerable evidence that ^{12}C is a highly non-spherical nucleus, and the cross-section for inelastic scattering to the 4.43 Mev first excited state is very large. Thus a complete description of elastic scattering process would have to take into

account the coupling between the ground state and first excited state.

2. $^{12}C(^{3}He,p)^{14}N$

The distorted-wave Born Approximation (DWBA) was used to calculate the cross-sections. For a $A(^{3}He,p)B$ stripping reaction, the cross-section is given by the expression (Gle 65),

$$\frac{d\sigma}{d\Omega} = \frac{2J_B+1}{2J_A+1} \frac{M_T M_p}{(2\pi\hbar^2)^2} \frac{k_p}{k_T} \sum_{LSJT} C^2_{ST} \left| \sum_M G_{NLSJT} B^M_{NL} \right|^2 ,$$

where S and T are the spin and isospin of the transferred (pn) pair, whose center-of-mass motion around the core is described by the quantum numbers (NLM). J is the total angular momentum transferred (See Appendix A for more detail).

(i) Calculation of the Structural factor, $G_{NSLJT\gamma}$

Two sets of wave functions have been found to predict physical quantities in good agreement with many experimental quantities for ^{14}N. Cohen and Kurath (CK 65) made an intermediate-coupling shell model calculation for all nuclei in the p shell. True (Tru 63) calculated the levels of ^{14}N on a model which assumed that the ^{14}N

nucleus consisted of a closed $p_{3/2}$ core with two particles in the following single-particle states; $1p_{1/2}$, $1d_{5/2}$, $2s_{1/2}$, $1d_{3/2}$ and $1f_{7/2}$.

In order to evaluate G_{NLSJT} from the wave function of Cohen and Kurath (CK 65), the two-particle coefficient-of-fractional-parentage (c.f.p.) (CK 70) is needed. $B_{NLSJT\gamma}$ is then equal to the product of the c.f.p. and the binomial coefficient $\binom{10}{2}$.

The wave functions of True (Tru 63) are two-particle wave functions, so the c.f.p. is identically one, and $B_{NLSJT\gamma}$ is given by

$$B_{NLSJT\gamma} = D_\gamma \begin{bmatrix} \ell_1 & \frac{1}{2} & j_1 \\ \ell_2 & \frac{1}{2} & j_2 \\ L & S & J \end{bmatrix} \delta_{JJ_B} \delta_{TT_B}$$

where the bracket is a 9-j symbol for transforming from j-j coupling into the L-S coupling scheme. D_γ is the mixing coefficient for the configuration. The overlap integral of the wave functions describing the relative motion of the transferred (pn) pair inside the ^{14}N nucleus and ^3He nucleus, respectively, can be calculated, assuming a Gaussian wave function for ^3He. Glendenning gave the following expression (Gle 65),

$$\Omega_{\gamma}(n) = \frac{[(2n-1)!]^{\frac{1}{2}}}{2^{n-1}(n-1)!} (xy)^{3/2} (1-x)^{n-1} ,$$

$$n = 1, 2, \ldots$$

where $x = 2v/(2a\eta^2 + v)$,

$y = \eta(6/v)^{\frac{1}{2}}$,

η = radius parameter, and

v = harmonic oscillator potential parameter.

The spectroscopic factor $G_{NLSJT\gamma}$ for the reaction $^{12}C(^3He,p)^{14}N$ has been calculated, in the way described above, by Mangelson (Man 67) and Dragún et. al. (DMT 70). Cohen and Kurath (CK 70) also calculated the strength of the L = 0 and L = 2 transfers. Table 2 lists the calculated values of $G_{NLSJT\gamma}$, taken from Mangelson's work (Man 67), of the reaction $^{12}C(^3He,p)^{14}N$.

(ii) Calculation of Form Factor B^M_{NL}

The quantity

$$\frac{M_\tau M_p}{(2\pi\hbar^2)^2} \frac{k_p}{k_\tau} \left| B^M_{NL} \right|^2$$

was evaluated using the computer code 'JULIE' (BDS 67). The function U^M_{NL} was obtained by solving the Schrödinger equation for the motion of the transferred (pn) pair

relative to the ^{12}C core in a Coulomb + Woods-Saxon potential

$$V(r) = V_c(r) + V_o \left\{ 1 + \exp[(r - R)/A] \right\}^{-1} ,$$

where

$$V_c(r) = \frac{3.5}{R_c} e^2 \left(3 - \frac{r^2}{R_c^2} \right) \qquad r \leq R_c$$

$$= \frac{7e^2}{r} . \qquad r \geq R_c$$

V_o was varied until a solution, with the right binding energy, was found.

The values of R, A and R_c were determined from elastic scattering data for the $^{12}C(d,d)^{12}C$ reaction. Wilsch and Clausnitzer (WC 71) and Satchler (Sat 66) have analysed the elastic scattering of d by ^{12}C at various energies, and gave the following values for the shape parameters

$$R = 2.06 \text{ fm} \qquad a = 0.9 \text{ fm} \qquad R_c = 2.97 \text{ fm}$$

(iii) Optical-Model Parameters

The optical parameters used in the DWBA calculations for the $^{12}C(^3He,p)^{14}N$ reactions were listed in Tables

1 and 3. Table 1 lists the optical parameters obtained by fitting the $^{12}C(^{3}He,^{3}He)^{12}C$ elastic scattering data. Table 3 lists the proton parameter used, obtained by fitting the elastic scattering data of Kim et. al. (KBDF 64) at 30.1 Mev and Rush et. al. (RBS 71) at 49.4 Mev without a spin-orbit potential, and extrapolated to the region of interest, keeping the shape parameters and the imaginary potential fixed. The proton parameters were varied over a 10% range, in different combinations, in a few calculations, and no significant change in angular distribution was found, although the magnitude of the cross-section changed (by 15% or less).

(iv) Distorted-wave calculations

The curves in Figures 7 to 13 are DWBA calculations using the code 'JULIE', with optical parameters and form factor parameters listed in Tables 1 and 3. The curves are individually (and arbitrarily) normalized to the data. In general the curves fit the data reasonably well above 16 Mev. However, below 15.0 Mev, the fits are rather poor. This is not surprising considering the drastic changes in the experimental angular distributions.

Both the 2.311 Mev and 3.945 Mev transitions have a dominant L = 0 character. In general the positions of

the maxima and minima are reproduced quite well by the calculated angular distributions. However, the relative magnitudes of the maxima are quite far off, especially at low energies.

The 4.91 Mev, 5.10 Mev and 5.69 Mev-state transitions have a dominant L = 1 character. For the 4.91 Mev state, the fit is reasonably good at energies higher than 15.0 Mev. For the 5.10 Mev state, the maximum at 20^{o} cannot be reproduced. Also, the sharp change in angular distribution at 14.0 Mev fails to show up in the calculated cross-sections. For the 5.69 Mev state, the fit is not too bad, throughout the whole energy range.

The ground state transition has a dominant L = 2 character. At energies higher than 17 Mev, the fit is quite good out to an angle of about 80^{o} center-of-mass, beyond which the calculated value falls below the experimental values. At lower energies, however, the fit is quite poor.

The 5.83 Mev-state transition has a major L = 3 character. At low energies, the calculated angular distribution has a strong forward peak which is not present in the experimental data. Above 17 Mev, the fit is quite good.

The angular distributions for L = 0, 1 and 2

transitions were also calculated with different optical-model and form factor parameters. Figure 14 shows the results of such calculations at 18 Mev. In general, the main feature of the angular distributions, the position of maxima and minima, are well determined by the L-value of the transfer, and not by the optical-model or form factor parameters used.

A comparison with the calculated values of $G_{NLSJT\gamma}$ listed in table 2 indicates that the DWBA stripping theory, together with the shell model wave-functions of ^{14}N, predicts quite accurately the dominant L-value for the reaction. This is particularly striking for the ground-state transition which, purely from relative spin and parity considerations, could be either an L = 0 or L = 2 transition. The theory predicts an almost pure L = 2 transition, and this is confirmed by the experimental data.

The form-factor shape parameters, and the optical-model parameters, affect the magnitude of the calculated transfer amplitudes differently for different levels, making a comparison of the relative cross-sections rather meaningless unless the parameters are specified In the case of $^{12}C(^{3}He,p)^{14}N$, as well as in the case of many light nuclei, both the optical parameters and the form factor parameters are not without ambiguity;

hence it is quite difficult to draw conclusions as to the value of the spectroscopic factors obtained for the reaction, as conjectured before the work was begun. Perhaps previous investigators have underestimated the ambiguity in the determination of spectroscopic factors.

E. CONCLUSION

It has been demonstrated in this experiment that in using the distorted-wave Born Approximation (DWBA) to interpret the results of two-nucleon stripping reactions in light nuclei, it is necessary to exercise extreme care.

The reaction should be followed through a reasonable range of energy to establish the "direct" nature of the reaction mechanism taking place. In the $^{12}C(^{3}He,p)^{14}N$ reaction, there is a change in the shape of angular distributions for some levels around E_{lab} = 15.0 Mev, indicating a change in reaction mechanism, and the DWBA calculations cannot fit the experimental data at energies lower than 15.0 Mev, even though the angular distributions still show a 'characteristic' stripping angular distribution, i.e. with maxima and minima.

The main features in the angular distribution of a stripping reaction are determined by the value of the orbital-angular momentum transfer, L. The form-factor geometrical parameters, which are not known in many cases, do not seem to affect the shape of the angular distributions appreciably. The optical parameters do affect the shapes slightly, but not sufficiently to

cause any confusion about which L-value is required. This means that such DWBA calculations are very useful in obtaining information on the spins and parities of the nuclear states involved in a double stripping reaction, as has been assumed many times in the past.

Both the optical-model parameters and the form-factor geometrical parameters affect the magnitude of the calculated transfer amplitude B^{M}_{NL}, differently for different transitions. Since, for light nuclei, these parameters are not well determined, it is quite impossible to extract accurate spectroscopic factors, or even relative spectroscopic factors for different levels.

The DWBA calculations, together with the shell-model wave functions, do predict the value of the orbital angular momentum transfers reasonably well. Considering the fact that ^{12}C is known to have strong deformation and that elastic scattering of many different kinds of particles by ^{12}C is known to be difficult to fit in terms of optical-model theory, it is remarkable (and fortunate) that the DWBA calculations can predict the L-values so well.

In a few cases, DWBA calculations have been used to interpret double stripping reactions at isolated energies, and the optical parameters were adjusted to

obtain good fits to the data (Man 67). However, the result of this experiment indicates that one should not place confidence in the spectroscopic factors so extracted from the data.

APPENDIX A

A. Two-Nucleon Stripping Theory

For a $A(^3He,p)B$ reaction, the cross-section can be expressed as (Gle 65)

$$\frac{d\sigma}{d\Omega} = \frac{2J_B+1}{2J_A+1} \frac{M_T M_p}{(2\pi\hbar^2)^2} \frac{k_p}{k_T} \sum_{LSJT} C_{ST}^2 \left| \sum_M G_{NLSJT} B_{NL}^M \right|^2 ,$$

where M is the reduced mass, and k_p and k_T are the wave numbers of the incoming ^3He and the outgoing proton. J_A and J_B are the spins of the target and residual nuclei, respectively. N, L and M are the radial and orbital quantum numbers of the transferred (np) pair whose spin and isospin are S and T. The orbital angular momentum transferred is L and the total angular momentum transferred is J.

C_{ST} is related to the isospin coupling between the (np) pair and the target nucleus as well as the nature of the potential between the (np) pair and the outgoing proton. If it is assumed that the triplet potential is proportional to the singlet potential, and if the potentials are central, C_{ST} can be expressed as (Man 67)

$$C^2_{ST} = C^2(T_B T T_A)\ b^2_{ST}\ D^2(S) \quad ,$$

where $C(T_B T T_A)$ is the Clebsch-Gordan coefficient for coupling the isospins of the transferred pair and target nucleus A to that of residual nucleus B. b^2_{ST} is the spin-isospin overlap integral of ^{3}He and the transferred pair, and has the value (Gle 65)

$$b_{ST} = \tfrac{1}{2}\,(\delta_{S0}\delta_{T1} + \delta_{S1}\delta_{T0}) \quad .$$

The factor D(S) is discussed by Fleming et. al. (FCG 68). If the singlet and triplet nucleon potentials are equal, then $D(S) = 1$ for $S = 0, 1$. For a spin-dependent potential, the ratio $R = |D(1)/D(0)|$ is approximately 0.3.

B^M_{NL} is the transfer amplitude, which, in the zero range approximation, is given by

$$B^M_{NL} = D_0 \int X^{(-)*}(\vec{k}_p \vec{R}_p)\ U^{M*}_{NL}(\vec{R})\ \delta(\vec{\rho})\ X^{(+)}(\vec{k}_\tau \vec{R}_\tau)\ d\vec{R}_\tau d\vec{R}_p \quad ,$$

where $X^{(-)}$ and $X^{(+)}$ are the incoming and outgoing spherical waves generated from optical potentials determined by elastic scattering of ^{3}He on A and proton on B. $U^M_{NL}(\vec{R})$ is the wave function describing the motion of the center of mass of the transferred (np) pair around the core, and is obtained by solving the

Schrödinger equation for the motion of the (np) pair in a Coulomb + Woods-Saxon potential (BDS 67). The $\vec{k}_p$ and $\vec{k}_\tau$ are the wave numbers of the proton and ^{3}He respectively. The position vectors are shown in figure 15. The factor D_0, which is a measure of the strength of the potential between the (pn) pair and the proton, has been studied by Bassel (Bas 66), Rook (Roo 67) and Mathur and Rook (MR 67).

The structural factor G_{NLSJT} is the product of three overlap integrals, (Gle 65),

$$G_{NLSJT} = g \sum_{\gamma} B_{NLSJT\gamma} P_{NLSJT\gamma} \Omega_{\gamma} \quad .$$

Here $P_{NLSJT\gamma}$ is the Moshinsky bracket (Mos 59) for coupling two p-shell particles, denoted by quantum numbers $n_1\ell_1$ and $n_2\ell_2$, to center of mass motion designated by N and L and relative motion designated by principal quantum number n and angular momentum quantum number $\ell = 0$. Ω_γ is the spatial overlap integral of the wave functions describing the internal motion of the transferred pair before and after the reaction. It can be calculated using a Gaussian wave function for ^{3}He (Gle 65). The factor $B_{NLSJT\gamma}$, is a measure of the extent to which the nucleus B appears as the ground state of the nucleus A plus two nucleons in the states $n_1\ell_1$ and $n_2\ell_2$. If a two-

particle wave function is used, it is just the product of 9-j symbols for transforming from j-j coupling to L-S coupling and the mixing coefficients of the configuration. If intermediate coupling of q ($q > 2$) particles is used, it is the product of the two-particle coefficient-of-fractional-parentage, c.f.p., and the statistical factor $\binom{2}{q}$, indicating 2 taken out of q particles. The factor g is a symmetry factor, for two identical single particle orbits, and $1/\sqrt{2}$ otherwise. The G_{NLSJT} contain a sum over the configurations $\gamma = (n_1 \ell_1 j_1, n_2 \ell_2 j_2)$ of the wave function. There is, however, no explicity sum over n due to the relationship (for $\ell = 0$),

$$2(n+N) + L = 2(n_1 + n_2) + \ell_1 + \ell_2 \quad .$$

B. Examination of Approximations

In order to facilitate numerical computation, a few approximations are commonly used in current DWBA calculations in evaluating the transfer amplitude B^M_{NL}. Some of the approximations will be discussed in this section.

1. Zero-range Approximation

In this approximation, the potential between the

transferred (pn) pair and the outgoing proton is taken to be a δ-function, $\delta(\vec{\rho})$. Physically, this means that the (pn) pair is captured at a point and the proton is emitted at the same point. Under this assumption, the 6-dimensional integral for B_{NL}^{M} is reduced to a 3-dimensional integral.

The effect of the zero-range approximation has been treated by many workers (ADHS 64, HNB 67, Bas 66, BZ 66). Recently Rost and Kunz (RK 71), Bayman (Bay 71) Chant and Mangelson (CM 70) compared the effects of zero-range approximation and finite range approximation, and propose simple approximations to correct for finite range effects.

In many cases, the angular distributions calculated by the zero-range approximation and the finite range approximation are quite similar as far as the location of the minima and maxima are concerned (RK 71, FDS 71), for the case of low angular momentum transfers from ^{3}He and ^{3}H projectile. However, the cross-sections can differ by as much as a factor of 2. Moreover, some levels are affected more than others, suggesting that zero-range calculation may introduce serious errors in the calculated relative cross-sections as well.

2. Local Potential Approximation

In most DWBA calculations, the optical potentials as well as the shell model potential used in computing the eigenfunctions are local potentials. There are, however, good reasons to believe that both types of potentials are non-local, (Aus 65, PS 64, PB 63), and the corrections have been studied by a number of workers recently (For 71, Hus 71).

Percy and Buck (PB 63) demonstrated that the scattering from a non-local optical potential can be reproduced by an equivalent local potential whose parameters vary with the bombarding energy. The eigenfunctions of the equivalent local potential, however, are increased in the nuclear interior in comparison with the eigenfunctions of the non-local potential. This effect is extremely important in DWBA calculations since the transfer amplitude B^{M}_{NL} contains two distorted waves, and integration has to be done over the interior of the nucleus. The net effect of nonlocality is to increase or decrease the calcultated cross-sections as compared with those calculated by local potentials. The relative angular distributions, however, are only slightly affected in most cases.

3. Radial Cutoffs

Due to the uncertainties in choosing the right form of potential to generate wave functions, and the related uncertainty as to whether the optical-potential wave functions inside the nuclear interior are meaningful, the nuclear interior region is sometimes excluded in DWBA calculations of the radius integral for B^{M}_{NL}. In many cases, the shape of the experimental angular distributions can be fitted better by the use of radial cutoffs in zero-range local-potential DWBA calculations.

It is certainly not possible to extract spectroscopic information using radial cutoffs, and the quality of the fits using radial cutoffs depends strongly on the cutoff radius. Recent developments in the use of finite-range non-local potentials indicate that such potentials produce better results for calculated differential cross-sections than the use of radial cutoffs. Thus such radial cutoffs should not be used. (DDPS 65)

4. Form Factor of Bound State

A serious problem associated with both the shapes and magnitudes of the predicted cross-sections is the choice of the proper form of U^{M}_{NL} used in the calculation

of B^M_{NL}. Through this form factor, U^M_{NL}, the nuclear structure and reaction mechanism are interdependent. For a bound state, it is quite clear that the asymptotic form of the form factor should decay exponentially as e^{-kr}, where the wave number k is given by

$$k^2 = \frac{2M^*_{pn}\, BE}{\hbar^2} \quad ,$$

with

BE = separation energy of the transferred (pn) pair, and

M_{pn} = reduced mass of the (pn) pair.

A common approximation is to use a finite Woods-Saxon spherical well to generate the form factor U^M_{NL}. The computer code 'JULIE' uses this approximation. The depth of the potential is varied to produce a wave function which is a good approximation to the exponential decaying wave function e^{-kr}. There are, however, uncertainties in choosing the shape parameters for this potential.

Another approximation frequently employed is to use an infinite spherical harmonic oscillator potential well to generate U^M_{NL} inside the interior of the nucleus, and the wave function is then matched to a Coulomb or Hankel function, with decay length based on the binding

energy of the (pn) pair. The uncertainties in this case arise from the choice of matching radius and harmonic oscillator potential parameter $\hbar\omega$.

Broglia and Riedel (BR 67) have compared calculations using U^M_{NL} generated by (1) a Woods-Saxon potential, (2) a harmonic oscillator potential, (3) a Woods-Saxon potential plus tail, and (4) a harmonic oscillator potential plus tail.

There is no obvious way to choose the form of the potential, or its parameters, to generate U^M_{NL}, the wave function for a complex particle. In the case of unbound final states, this problem is even more serious.

5. Multiple-step Processes

In most cases, two-nucleon transfer theory is based on the assumption that a single-step process takes place. It is quite possible for multiple-step processes to be confused with single-step processes, particularly when the cross-section is small. For example, the target nucleus may be excited to a higher state by the incident projectile, which is then stripped, forming the product nucleus B from an excited core.

The angular distribution of a multiple-step reaction may be quite similar to the single-step reaction,

but the cross-section is expected to be much smaller. However, for nuclei with large inelastic scattering cross-sections as compared with elastic cross-sections, multiple-processes may be important, and the angular distributions obtained may give false values for L if they are treated as single step processes.

6. Optical Parameters

The incoming and outgoing spherical waves used in DWBA calculations are generated by optical potentials. While it is always possible to test the optical potential parameters for the entrance channel, it is sometimes impossible to obtain experimental information for the optical potential parameters for the exit channel. In this case, an "average" potential, interpolated from nearby nuclei, is used. Unfortunately the magnitude of the calculated cross-sections depend strongly on the optical-model parameters. The spectroscopic factor obtained with a purely assumed potential is therefore unreliable. This problem is particularly important in light nuclei, where there are many cases in which the required elastic scattering experiment cannot be carried out because the target is radioactive. In any case, when one is dealing with stripping to excited states, the elastic scattering is impossible

and one has to assume the ground state optical potential is valid for the excited states.

APPENDIX B

Tables of center-of-mass differential cross-sections are given in this section. Errors listed in tables B2 to B105 are the standard deviations arising from statistics, background subtraction, and dead time correction.

TABLE B1 12C(3HE,3HE)12C

ANGLE(LAB) = 45 DEGREE
EXCITATION ENERGY = 0.0 MEV

E LAB C.M.	dσ/dω (MB/ST)	ERROR	E LAB C.M.	dσ/dω (MB/ST)	ERROR
12.0	28.8	10 %	15.2	5.72	10 %
12.2	26.84	10 %	15.4	6.94	10 %
12.4	23.68	10 %	15.5	7.73	10 %
12.5	22.55	10 %	15.6	7.88	10 %
12.6	21.06	10 %	15.8	8.48	10 %
12.8	17.80	10 %	16.0	7.62	10 %
13.0	14.98	10 %	16.2	7.53	10 %
13.2	12.91	10 %	16.4	7.39	10 %
13.4	12.50	10 %	16.5	7.42	10 %
13.5	12.78	10 %	16.6	7.25	10 %
13.6	12.80	10 %	16.8	6.92	10 %
13.8	12.67	10 %	17.0	6.58	10 %
14.0	12.53	10 %	17.2	5.88	10 %
14.2	10.76	10 %	17.4	4.28	10 %
14.4	8.87	10 %	17.5	5.18	10 %
14.5	8.34	10 %	17.6	4.81	10 %
14.6	7.04	10 %	17.8	4.89	10 %
14.8	5.58	10 %	18.0	4.52	10 %
15.0	5.50	10 %			

TABLE B2

12C(3HE,3HE)12C
BEAM ENERGY = 12.0 MEV
EX. ENERGY = 0.00 MEV

ANGLE C.M.	dσ/dω (MB/ST)	ERROR (MB/ST)
7.5	8.67E 04	4.3E 04
12.5	1.09E 04	4.4E 03
18.7	2.35E 03	7.0E 02
24.9	6.96E 02	1.4E 02
31.1	1.86E 02	1.6E 00
37.2	4.12E 01	4.4E-01
43.2	2.40E 01	4.1E-01
49.2	3.05E 01	3.4E-01
55.2	2.87E 01	3.3E-01
61.0	2.00E 01	2.5E-01
66.8	1.19E 01	1.7E-01
72.5	7.78E 00	1.2E-01
78.1	5.57E 00	9.9E-02
83.6	3.71E 00	7.6E-02
89.0	1.65E 00	4.5E-02
94.3	8.29E-01	3.0E-02
99.4	1.66E 00	5.1E-02
104.5	3.85E 00	8.8E-02
109.4	6.14E 00	1.2E-01
114.3	7.31E 00	1.4E-01
119.0	6.71E 00	1.3E-01
123.6	4.96E 00	1.1E-01
128.1	3.26E 00	8.6E-02
132.5	1.97E 00	6.4E-02

TABLE B3

12C(3HE,3HE)12C
BEAM ENERGY = 12.5 MEV
EX. ENERGY = 0.00 MEV

ANGLE C.M.	dσ/dω (MB/ST)	ERROR (MB/ST)
7.5	1.06E 05	5.3E 04
12.5	1.05E 04	4.2E 03
18.7	2.27E 03	6.7E 02
24.9	6.73E 02	1.4E 02
31.1	1.72E 02	1.7E 01
37.2	3.70E 01	4.0E-01
43.2	1.97E 01	2.4E-01
49.2	2.46E 01	2.9E-01
55.2	2.25E 01	2.7E-01
61.0	1.55E 01	2.0E-01
66.8	1.02E 01	1.5E-01
72.5	7.56E 00	1.2E-01
78.1	6.63E 00	1.1E-01
83.6	4.78E 00	9.0E-02
89.0	2.32E 00	5.6E-02
94.3	6.49E-01	2.6E-02
99.4	1.05E 00	3.5E-02
104.5	4.49E 00	1.0E-01
109.4	6.10E 00	1.2E-01
114.3	7.55E 00	1.5E-01
119.0	6.89E 00	1.4E-01
123.6	4.96E 00	1.1E-01
128.1	2.64E 00	7.6E-02

TABLE B4

12C(3HE,3HE)12C
BEAM ENERGY = 13.0 MEV
EX. ENERGY = 0.00 MEV

ANGLE C.M.	dσ/dω (MB/ST)	ERROR (MB/ST)
7.5	5.75E 04	2.9E 04
12.5	1.56E 04	4.2E 03
18.7	2.01E 03	6.0E 02
24.9	6.27E 02	1.3E 02
31.1	1.49E 02	1.5E 01
37.2	2.28E 01	3.8E-01
43.2	1.36E 01	2.5E-01
49.2	1.77E 01	3.1E-01
55.2	1.50E 01	2.8E-01
61.0	9.75E 00	2.0E-01
66.8	6.65E 00	1.5E-01
72.5	5.73E 00	1.4E-01
78.1	5.82E 00	1.4E-01
83.6	4.77E 00	1.3E-01
89.0	2.77E 00	8.9E-02
94.3	9.82E-01	4.7E-02
99.4	6.01E-01	3.5E-02
104.5	2.15E 00	7.7E-02
109.4	4.37E 00	1.3E-01
114.3	5.73E 00	1.5E-01
119.0	5.61E 00	1.5E-01
123.6	3.88E 00	1.2E-01
128.1	1.79E 00	7.5E-02

TABLE B5

12C(3HE,3HE)12C
BEAM ENERGY = 13.5 MEV
EX. ENERGY = 0.00 MEV

ANGLE C.M.	dσ/dω (MB/ST)	ERROR (MB/ST)
7.5	7.35E 04	3.7E 04
12.5	8.83E 03	3.5E 03
18.7	1.97E 03	5.9E 02
24.9	5.74E 02	1.1E 01
31.1	1.24E 02	1.2E 01
37.2	1.40E 01	3.8E-01
43.2	1.31E 01	2.5E-01
49.2	1.69E 01	3.0E-01
55.2	1.28E 01	2.4E-01
61.0	7.94E 00	1.7E-01
66.8	5.73E 00	1.4E-01
72.5	5.23E 00	1.3E-01
78.1	4.78E 00	1.2E-01
83.6	3.72E 00	1.0E-01
89.0	2.46E 00	8.0E-02
94.3	1.28E 00	5.4E-02
99.4	1.01E 00	4.8E-02
104.5	1.64E 00	6.5E-02
109.4	2.78E 00	9.4E-02
114.3	3.96E 00	1.2E-01
119.0	3.95E 00	1.2E-01
123.6	3.01E 00	1.0E-01

TABLE B6

12C(3HE,3HE)12C
BEAM ENERGY = 14.0 MEV
EX. ENERGY = 0.00 MEV

ANGLE C.M.	dσ/dω (MB/ST)	ERROR (MB/ST)
7.5	5.07E 04	2.5E 04
12.5	7.67E 03	3.1E 03
18.7	1.75E 03	5.3E 02
24.9	5.15E 02	1.0E 01
31.1	1.03E 02	1.0E 01
37.2	1.13E 01	2.2E-01
43.2	1.57E 01	2.9E-01
49.2	1.85E 01	3.4E-01
55.2	1.25E 01	2.5E-01
61.0	7.01E 00	1.6E-01
66.8	5.13E 00	1.3E-01
72.5	5.36E 00	1.3E-01
78.1	4.77E 00	1.3E-01
83.6	3.63E 00	1.0E-01
89.0	1.66E 00	6.4E-02
94.3	1.70E-01	1.7E-02
99.4	7.05E-01	3.9E-02
104.5	1.35E 00	5.9E-02
109.4	2.09E 00	7.9E-02
114.3	2.57E 00	9.3E-02
119.0	2.11E 00	8.0E-02
123.6	1.86E 00	7.7E-02

TABLE B7

12C(3HE,3HE)12C
BEAM ENERGY = 14.5 MEV
EX. ENERGY = 0.00 MEV

ANGLE C.M.	dσ/dω (MB/ST)	ERROR (MB/ST)
7.5	3.90E 04	1.8E 04
12.5	8.20E 03	3.4E 03
18.7	1.85E 03	5.1E 02
24.9	4.80E 02	9.5E 01
31.1	7.25E 01	7.3E 00
37.2	1.01E 01	5.0E-01
43.3	2.08E 01	1.4E 00
49.3	1.68E 01	8.4E-01
55.2	8.34E 00	4.2E-01
61.1	3.77E 00	1.9E-01
66.9	3.74E 00	1.9E-01
72.5	4.65E 00	2.3E-01
78.3	5.88E 00	2.9E-01
83.6	4.99E 00	2.5E-01
89.0	3.45E 00	1.7E-01
94.3	1.50E 00	1.5E-01
99.5	7.48E-01	1.5E-01
104.5	1.16E 00	1.6E-01
109.5	1.92E 00	2.0E-01
114.3	2.54E 00	2.0E-01
119.0	2.01E 00	2.0E-01

TABLE B8

12C(3HE,3HE)12C
BEAM ENERGY = 15.0 MEV
EX. ENERGY = 0.00 MEV

ANGLE C.M.	dσ/dω (MB/ST)	ERROR (MB/ST)
7.5	5.25E 04	2.6E 04
12.5	5.90E 03	2.5E 03
18.7	1.69E 03	5.1E 02
24.9	3.83E 02	7.7E 01
31.1	5.70E 01	1.2E 00
37.2	1.15E 01	1.8E-01
43.2	1.93E 01	2.7E-01
49.2	1.09E 01	1.7E-01
55.2	5.50E 00	1.1E-01
61.0	4.07E 00	8.6E-02
66.8	5.22E 00	1.0E-01
72.5	5.70E 00	1.1E-01
78.1	5.17E 00	1.0E-01
83.6	4.85E 00	7.3E-02
89.0	3.90E 00	8.6E-02
94.3	2.10E 00	5.6E-02
99.4	9.61E-01	3.5E-02
104.5	8.47E-01	3.3E-02
109.4	1.29E 00	4.3E-02
114.3	1.65E 00	5.2E-02
119.0	1.53E 00	2.7E-02
123.6	1.31E 00	4.6E-02

TABLE B9

12C(3HE,3HE)12C
BEAM ENERGY = 15.5 MEV
EX. ENERGY = 0.00 MEV

ANGLE C.M.	dσ/dω (MB/ST)	ERROR (MB/ST)
7.5	6.53E 04	3.3E 04
12.5	6.70E 03	2.7E 03
18.7	1.77E 03	4.9E 02
24.9	4.37E 02	8.4E 01
31.1	6.87E 01	6.9E 00
37.2	2.08E 01	2.9E-01
43.2	2.24E 01	3.1E-01
49.2	1.41E 01	2.1E-01
55.2	7.75E 00	1.3E-01
61.0	8.55E 00	1.5E-01
66.8	8.84E 00	1.5E-01
72.5	6.16E 00	1.2E-01
78.1	3.34E 00	7.8E-02
83.6	3.81E 00	8.6E-02
89.0	3.92E 00	8.9E-02
94.3	2.43E 00	6.6E-02
99.4	1.05E 00	3.5E-02
109.4	9.01E-01	3.3E-02

TABLE B10

12C(3HE,3HE)12C
BEAM ENERGY = 16.0 MEV
EX. ENERGY = 0.00 MEV

ANGLE C.M.	dσ/dω (MB/ST)	ERROR (MB/ST)
7.5	7.36E 04	3.7E 04
12.5	5.62E 03	2.2E 03
18.7	1.65E 03	5.0E 02
24.9	4.01E 02	8.0E 01
31.1	6.25E 01	6.1E 00
37.2	1.76E 01	1.8E 00
43.2	2.34E 01	3.6E-01
49.2	1.39E 01	2.4E-01
55.2	7.64E 00	1.5E-01
61.0	9.34E 00	1.8E-01
66.8	1.03E 01	1.9E-01
72.5	7.00E 00	1.4E-01
78.1	2.73E 00	7.5E-02
83.6	1.20E 00	4.4E-02
89.0	1.75E 00	5.7E-02
94.3	2.31E 00	7.0E-02
99.4	1.34E 00	4.8E-02
104.5	5.69E-01	2.9E-02

TABLE B11

12C(3HE,3HE)12C
BEAM ENERGY = 16.5 MEV
EX. ENERGY = 0.00 MEV

ANGLE C.M.	dσ/dω (MB/ST)	ERROR (MB/ST)
7.5	4.21E 04	2.1E 04
12.5	5.34E 03	2.2E 03
15.6	2.84E 03	8.6E 02
18.7	9.85E 02	3.0E 02
22.8	4.68E 02	9.4E 01
24.9	2.96E 02	6.0E 01
31.1	5.41E 01	5.4E 00
37.2	1.85E 01	3.1E-01
43.2	2.20E 01	3.5E-01
49.2	1.36E 01	2.4E-01
55.2	7.42E 00	1.6E-01
61.0	8.64E 00	1.8E-01
66.8	9.30E 00	1.9E-01
72.5	6.07E 00	1.4E-01
78.1	2.64E 00	8.3E-02
83.6	1.55E 00	6.0E-02
89.0	2.37E 00	8.0E-02
94.3	2.39E 00	8.1E-02
99.4	1.47E 00	6.5E-02
104.5	5.10E-01	3.5E-02

TABLE B12

12C(3HE,3HE)12C
BEAM ENERGY = 17.0 MEV
EX. ENERGY = 0.00 MEV

ANGLE C.M.	dσ/dω (MB/ST)	ERROR (MB/ST)
7.5	4.30E 04	2.2E 04
12.5	4.80E 03	1.9E 03
18.7	1.49E 03	4.5E 02
24.9	3.61E 02	6.2E 01
31.1	5.48E 01	4.7E 00
37.2	1.63E 01	2.9E-01
49.2	1.26E 01	2.4E-01
43.2	2.07E 01	3.4E-01
55.2	6.55E 00	1.5E-01
61.0	8.29E 00	1.8E-01
66.8	9.18E 00	1.9E-01
72.5	6.42E 00	1.5E-01
78.1	2.60E 00	8.4E-02
83.6	1.03E 00	4.8E-02
89.0	1.41E 00	5.9E-02
94.3	1.68E 00	6.7E-02
99.4	1.00E 00	5.0E-02

TABLE B13

12C(3HE,3HE)12C
BEAM ENERGY = 17.5 MEV
EX. ENERGY = 0.00 MEV

ANGLE C.M.	dσ/dω (MB/ST)	ERROR (MB/ST)
7.5	2.45E 04	1.2E 04
12.5	4.89E 03	2.0E 03
18.7	1.42E 03	4.3E 02
24.9	3.10E 02	6.2E 01
31.1	3.80E 01	3.8E 00
37.2	1.82E 01	2.9E-01
43.2	1.77E 01	2.7E-01
49.2	1.07E 01	2.0E-01
55.2	5.18E 00	1.3E-01
61.0	6.71E 00	1.5E-01
66.8	7.47E 00	1.7E-01
72.5	5.01E 00	1.3E-01
78.1	1.95E 00	6.8E-02
83.6	8.16E-01	4.1E-02
89.0	1.01E 00	4.7E-02
94.3	1.10E 00	5.1E-02
99.4	6.21E-01	3.7E-02

TABLE B14

12C(3HE,3HE)12C
BEAM ENERGY = 18.0 MEV
EX. ENERGY = 0.00 MEV

ANGLE C.M.	dσ/dω (MB/ST)	ERROR (MB/ST)
7.5	3.09E 04	1.6E 04
12.5	4.42E 03	1.3E 03
18.7	1.30E 03	3.9E 02
24.9	2.61E 02	5.2E 01
31.1	3.35E 01	3.3E 00
37.2	2.01E 01	3.2E-01
43.2	2.15E 01	3.4E-01
49.2	7.64E 00	1.6E-01
55.2	4.38E 00	1.1E-01
61.0	5.75E 00	1.3E-01
66.8	5.23E 00	1.2E-01
72.5	3.23E 00	9.2E-02
78.1	1.15E 00	4.8E-02
83.6	6.13E-01	3.4E-02
89.0	1.00E 00	4.6E-02
94.3	7.94E-01	4.0E-02
99.4	2.66E-01	2.2E-02

TABLE B15

12C(3HE,P)14N
BEAM ENERGY = 12.0 MEV
EX. ENERGY = 0.00 MEV

ANGLE C.M.	dσ/dω (MB/ST)	ERROR (MB/ST)
11.1	1.32E 00	2.6E-01
16.6	1.55E 00	3.2E-01
22.1	1.65E 00	3.8E-02
27.6	1.78E 00	4.4E-02
33.1	1.69E 00	4.4E-02
38.6	1.48E 00	6.3E-02
44.0	1.25E 00	3.7E-02
49.4	1.03E 00	3.3E-02
54.8	7.95E-01	2.9E-02
60.1	6.78E-01	2.6E-02
65.4	6.47E-01	2.6E-02
70.7	6.08E-01	2.5E-02
75.9	5.72E-01	2.4E-02
81.1	5.23E-01	2.3E-02
86.2	4.60E-01	2.1E-02
91.2	4.72E-01	2.4E-02
96.3	3.17E-01	1.9E-02
101.2	2.59E-01	1.7E-02
106.2	2.17E-01	1.6E-02
111.1	2.63E-01	1.8E-02
115.9	3.19E-01	2.0E-02
120.7	4.55E-01	2.5E-02
125.4	5.68E-01	2.8E-02
130.1	6.86E-01	3.2E-02
134.8	8.26E-01	3.5E-02
139.4	9.67E-01	3.9E-02
144.0	9.76E-01	3.9E-02
148.6	8.91E-01	3.8E-02
153.1	8.09E-01	3.6E-02

TABLE B16

12C(3HE,P)14N
BEAM ENERGY = 12.5 MEV
EX. ENERGY = 0.00 MEV

ANGLE C.M.	dσ/dω (MB/ST)	ERROR (MB/ST)
11.1	1.13E 00	2.3E-01
16.6	1.35E 00	2.7E-01
22.2	1.33E 00	5.3E-02
27.7	1.44E 00	5.5E-02
33.2	1.43E 00	4.0E-02
38.6	1.26E 00	3.7E-02
44.1	1.10E 00	3.5E-02
49.5	9.04E-01	3.1E-02
54.8	8.07E-01	2.9E-02
60.2	7.15E-01	2.8E-02
65.5	6.41E-01	2.5E-02
70.7	6.39E-01	2.5E-02
75.9	6.24E-01	2.5E-02
81.1	5.33E-01	2.3E-02
86.2	4.82E-01	2.2E-02
91.3	3.86E-01	2.0E-02
96.3	2.76E-01	1.8E-02
101.3	2.11E-01	1.5E-02
106.2	2.02E-01	1.5E-02
111.1	2.38E-01	1.7E-02
115.9	3.36E-01	2.1E-02
120.7	4.51E-01	2.5E-02
125.5	6.44E-01	3.0E-02
130.2	7.28E-01	3.3E-02
134.8	8.07E-01	3.5E-02
139.5	7.69E-01	3.4E-02
144.1	6.88E-01	3.2E-02
148.6	6.58E-01	3.2E-02
153.1	6.38E-01	3.1E-02

TABLE B17

12C(3HE,P)14N
BEAM ENERGY = 13.0 MEV
EX. ENERGY = 0.00 MEV

ANGLE C.M.	dσ/dω (MB/ST)	ERROR (MB/ST)
11.1	1.31E 00	2.6E-01
16.6	1.44E 00	2.9E-01
22.2	1.67E 00	5.4E-02
27.7	1.52E 00	5.6E-02
33.1	1.41E 00	5.2E-02
38.6	1.27E 00	5.1E-02
44.1	9.66E-01	4.4E-02
49.5	7.31E-01	3.8E-02
54.9	5.86E-01	3.3E-02
60.2	5.49E-01	3.2E-02
65.5	6.40E-01	3.5E-02
70.8	5.59E-01	3.3E-02
76.0	5.46E-01	3.3E-02
81.1	4.52E-01	3.0E-02
86.3	3.75E-01	2.7E-02
91.3	2.48E-01	2.1E-02
96.4	1.71E-01	1.7E-02
101.3	1.53E-01	1.6E-02
106.3	2.17E-01	2.0E-02
111.1	2.58E-01	2.2E-02
116.0	4.78E-01	3.2E-02
120.8	6.72E-01	3.9E-02
125.5	8.36E-01	4.5E-02
130.2	8.77E-01	4.7E-02
134.9	9.99E-01	5.1E-02
139.5	8.19E-01	4.5E-02
144.1	7.13E-01	4.2E-02
148.6	5.30E-01	3.6E-02
153.2	4.29E-01	3.2E-02

TABLE B18

12C(3HE,P)14N
BEAM ENERGY = 13.5 MEV
EX. ENERGY = 0.00 MEV

ANGLE C.M.	dσ/dω (MB/ST)	ERROR (MB/ST)
11.1	1.48E 00	3.0E-01
16.6	1.87E 00	3.7E-01
22.2	1.92E 00	6.2E-02
27.7	2.04E 00	6.7E-02
33.2	1.70E 00	6.2E-02
38.7	1.39E 00	5.5E-02
44.1	1.01E 00	4.5E-02
49.5	6.32E-01	3.4E-02
54.9	4.71E-01	2.9E-02
60.2	3.59E-01	2.5E-02
65.5	4.12E-01	2.7E-02
70.8	4.86E-01	3.0E-02
76.0	4.67E-01	2.9E-02
81.2	4.57E-01	2.9E-02
86.3	3.47E-01	2.5E-02
91.4	2.51E-01	2.1E-02
96.4	1.67E-01	1.7E-02
101.4	1.22E-01	1.5E-02
106.3	1.44E-01	1.6E-02
111.2	2.58E-01	2.3E-02
116.0	4.47E-01	3.1E-02
120.8	6.67E-01	3.9E-02
125.5	8.90E-01	4.7E-02
130.2	8.81E-01	4.7E-02
134.9	8.95E-01	4.8E-02
139.5	8.77E-01	4.8E-02

TABLE B19

12C(3HE,P)14N
BEAM ENERGY = 14.0 MEV
EX. ENERGY = 0.00 MEV

ANGLE C.M.	dσ/dω (MB/ST)	ERROR (MB/ST)
11.1	1.42E 00	2.8E-01
16.7	2.06E 00	4.1E-01
22.2	2.00E 00	7.0E-02
27.7	2.13E 00	7.1E-02
33.2	1.96E 00	6.9E-02
38.7	1.58E 00	6.1E-02
44.1	1.11E 00	4.9E-02
49.5	7.38E-01	3.8E-02
54.9	5.45E-01	3.2E-02
60.3	4.79E-01	2.9E-02
65.6	4.72E-01	3.0E-02
70.8	4.76E-01	3.0E-02
76.0	4.16E-01	2.8E-02
81.2	3.65E-01	2.6E-02
86.3	2.39E-01	2.1E-02
91.4	1.67E-01	1.7E-02
96.4	1.67E-01	1.7E-02
101.4	1.49E-01	1.6E-02
106.3	2.03E-01	2.0E-02
111.2	3.28E-01	2.6E-02
116.0	4.64E-01	3.2E-02
120.8	5.88E-01	3.7E-02
125.6	8.45E-01	4.8E-02
130.3	7.68E-01	4.4E-02
134.9	8.55E-01	4.7E-02
139.5	7.18E-01	4.2E-02
144.1	6.20E-01	3.9E-02
148.7	5.12E-01	3.5E-02
153.2	3.96E-01	4.3E-02

TABLE B20

12C(3HE,P)14N
BEAM ENERGY = 14.5 MEV
EX. ENERGY = 0.00 MEV

ANGLE C.M.	dσ/dω (MB/ST)	ERROR (MB/ST)
11.1	1.02E 00	2.0E-01
16.7	8.30E-01	1.7E-01
22.2	1.82E 00	1.0E-01
27.7	2.42E 00	1.3E-01
33.2	2.31E 00	1.2E-01
38.7	1.98E 00	1.1E-01
44.1	1.45E 00	8.4E-02
49.6	1.18E 00	7.1E-02
54.9	8.66E-01	5.6E-02
60.3	7.74E-01	5.2E-02
65.6	6.68E-01	4.6E-02
70.8	6.30E-01	4.5E-02
76.1	5.48E-01	4.0E-02
81.2	4.49E-01	3.5E-02
86.4	3.44E-01	2.9E-02
91.4	2.62E-01	2.4E-02
96.5	2.31E-01	2.2E-02
101.4	2.12E-01	2.1E-02
106.4	2.84E-01	2.6E-02
111.2	4.28E-01	3.5E-02
116.1	5.64E-01	4.3E-02
120.8	6.71E-01	4.9E-02
125.6	8.23E-01	5.7E-02
130.3	8.14E-01	5.0E-02
134.9	7.13E-01	4.9E-02
139.6	6.28E-01	4.7E-02
144.1	4.55E-01	3.8E-02
148.7	3.76E-01	3.3E-02
153.2	2.93E-01	2.8E-02

TABLE B21

12C(3HE,P)14N
BEAM ENERGY = 15.0 MEV
EX. ENERGY = 0.00 MEV

ANGLE C.M.	dσ/dω (MB/ST)	ERROR (MB/ST)
11.1	1.03E 00	2.1E-01
16.7	1.68E 00	3.4E-01
22.2	2.23E 00	1.0E-01
27.7	2.26E 00	1.0E-01
33.2	2.18E 00	5.7E-02
38.7	1.69E 00	4.8E-02
44.2	1.28E 00	4.1E-02
49.6	9.73E-01	3.5E-02
55.0	8.29E-01	3.2E-02
60.3	6.93E-01	2.8E-02
65.6	6.77E-01	2.8E-02
70.9	6.59E-01	2.8E-02
76.1	5.87E-01	2.6E-02
81.3	4.88E-01	2.4E-02
86.4	3.70E-01	1.9E-02
91.4	2.18E-01	1.7E-02
96.5	1.73E-01	1.3E-02
101.5	1.79E-01	1.3E-02
106.4	1.88E-01	1.4E-02
111.3	2.76E-01	1.7E-02
116.1	4.20E-01	2.2E-02
120.9	5.60E-01	2.7E-02
125.6	6.65E-01	3.0E-02
130.3	6.94E-01	3.1E-02
135.0	6.48E-01	2.9E-02
139.6	5.76E-01	2.8E-02
144.2	4.86E-01	2.6E-02
148.7	3.58E-01	2.2E-02
153.2	3.01E-01	2.0E-02

TABLE B22

12C(3HE,P)14N
BEAM ENERGY = 15.5 MEV
EX. ENERGY = 0.00 MEV

ANGLE C.M.	dσ/dω (MB/ST)	ERROR (MB/ST)
11.1	9.83E-01	2.0E-01
16.7	1.60E 00	3.2E-01
22.2	1.75E 00	8.9E-02
27.8	1.84E 00	9.0E-02
33.3	1.57E 00	4.7E-02
38.7	1.31E 00	4.2E-02
44.2	9.48E-01	3.5E-02
49.6	6.48E-01	2.7E-02
55.0	5.70E-01	2.6E-02
60.3	5.72E-01	2.6E-02
65.6	5.82E-01	2.6E-02
70.9	6.20E-01	2.7E-02
76.1	5.46E-01	2.6E-02
81.3	4.95E-01	2.5E-02
86.4	3.42E-01	1.6E-02
91.5	3.03E-01	1.7E-02
96.5	2.24E-01	1.4E-02
101.5	1.85E-01	1.3E-02
106.4	1.81E-01	1.3E-02
111.3	2.93E-01	1.7E-02
116.1	3.93E-01	2.0E-02
120.9	5.06E-01	2.4E-02
125.6	6.14E-01	2.7E-02
130.3	7.05E-01	2.9E-02
135.0	6.97E-01	2.9E-02
139.6	6.69E-01	2.9E-02
144.2	6.29E-01	2.8E-02
148.7	5.40E-01	2.6E-02
153.3	4.19E-01	2.2E-02

TABLE B23

12C(3HE,P)14N
BEAM ENERGY = 16.0 MEV
EX. ENERGY = 0.00 MEV

ANGLE C.M.	dσ/dω (MB/ST)	ERROR (MB/ST)
11.0	1.21E 00	2.4E-01
16.7	1.35E 00	2.7E-01
22.2	1.71E 00	8.5E-02
27.8	1.45E 00	7.9E-02
33.3	1.26E-01	3.1E-02
38.8	8.60E-01	2.5E-02
44.2	5.90E-01	2.0E-02
49.6	4.44E-01	2.2E-02
55.0	4.65E-01	2.5E-02
60.4	5.16E-01	2.6E-02
65.7	5.02E-01	2.6E-02
70.9	3.67E-01	2.2E-02
76.2	2.79E-01	1.9E-02
81.3	1.79E-01	1.5E-02
86.4	1.94E-01	1.6E-02
91.5	2.14E-01	1.6E-02
96.5	2.40E-01	1.7E-02
101.5	2.97E-01	2.0E-02
106.4	2.97E-01	2.0E-02
111.3	2.96E-01	2.0E-02
116.2	3.64E-01	2.3E-02
120.9	3.82E-01	2.3E-02
125.7	4.67E-01	2.7E-02
130.4	5.73E-01	3.0E-02
135.0	5.43E-01	3.0E-02
139.6	4.68E-01	2.7E-02
144.2	4.96E-01	2.8E-02
148.8	4.05E-01	2.5E-02
153.3	3.49E-01	2.2E-02

TABLE B24

12C(3HE,P)14N
BEAM ENERGY = 16.5 MEV
EX. ENERGY = 0.00 MEV

ANGLE C.M.	dσ/dω (MB/ST)	ERROR (MB/ST)
11.1	9.82E-01	2.0E-01
13.9	8.52E-01	1.7E-01
16.7	1.03E 00	2.1E-01
22.2	1.26E 00	4.8E-02
27.8	1.31E 00	5.2E-02
33.3	1.04E 00	4.7E-02
38.8	8.35E-01	4.1E-02
44.2	5.47E-01	3.2E-02
49.6	4.95E-01	3.1E-02
55.0	4.85E-01	3.0E-02
60.4	5.32E-01	3.2E-02
65.7	5.28E-01	3.2E-02
71.0	4.44E-01	3.0E-02
76.2	3.50E-01	2.6E-02
81.3	2.22E-01	2.0E-02
86.5	1.73E-01	1.8E-02
91.5	1.86E-01	2.0E-02
96.6	2.33E-01	2.2E-02
101.5	2.60E-01	2.2E-02
106.5	2.64E-01	2.3E-02
111.3	2.93E-01	2.4E-02
116.2	3.89E-01	2.8E-02
121.0	3.78E-01	2.8E-02
125.7	4.83E-01	3.3E-02
130.4	4.89E-01	3.3E-02
135.0	6.27E-01	3.9E-02
139.6	5.98E-01	3.8E-02
144.2	5.64E-01	3.7E-02
148.8	5.35E-01	3.5E-02

TABLE B25

12C(3HE,P)14N
BEAM ENERGY = 17.0 MEV
EX. ENERGY = 0.00 MEV

ANGLE C.M.	dσ/dω (MB/ST)	ERROR (MB/ST)
11.1	7.83E-01	1.6E-01
16.7	8.50E-01	1.7E-01
22.3	8.65E-01	6.0E-02
27.8	7.92E-01	3.9E-02
33.3	5.96E-01	3.4E-02
38.8	4.21E-01	2.8E-02
44.2	3.06E-01	2.3E-02
49.7	3.44E-01	2.5E-02
55.1	4.33E-01	2.9E-02
60.4	4.24E-01	2.9E-02
65.7	4.59E-01	3.1E-02
71.0	3.69E-01	2.7E-02
76.2	2.12E-01	2.0E-02
81.4	1.97E-01	2.0E-02
86.5	1.28E-01	1.6E-02
91.6	1.81E-01	1.9E-02
96.6	2.30E-01	2.2E-02
101.6	2.43E-01	2.3E-02
106.5	2.91E-01	2.6E-02
111.4	2.72E-01	2.5E-02
116.2	3.53E-01	3.0E-02
121.0	4.07E-01	3.2E-02
125.7	4.06E-01	3.2E-02
130.4	3.90E-01	3.2E-02
135.1	5.22E-01	3.8E-02
139.7	3.96E-01	3.2E-02
144.2	3.61E-01	3.2E-02
148.8	3.59E-01	3.1E-02
153.3	2.86E-01	2.8E-02

TABLE B26

12C(3HE,P)14N
BEAM ENERGY = 17.5 MEV
EX. ENERGY = 0.00 MEV

ANGLE C.M.	dσ/dω (MB/ST)	ERROR (MB/ST)
11.1	4.76E-01	9.5E-02
16.7	4.96E-01	9.9E-02
22.3	6.38E-01	2.5E-02
27.8	6.74E-01	6.0E-02
33.3	4.65E-01	2.9E-02
38.8	2.99E-01	2.2E-02
44.3	2.35E-01	2.0E-02
49.7	3.12E-01	2.3E-02
55.1	4.16E-01	2.8E-02
60.4	4.75E-01	3.0E-02
65.7	4.12E-01	2.8E-02
71.0	3.02E-01	2.4E-02
76.2	1.95E-01	1.9E-02
81.4	1.29E-01	1.5E-02
86.5	1.49E-01	1.7E-02
91.6	2.09E-01	1.9E-02
96.6	2.27E-01	2.2E-02
101.6	2.65E-01	2.5E-02
106.5	2.80E-01	2.6E-02
111.4	2.67E-01	2.5E-02
116.2	2.57E-01	2.5E-02
121.0	2.36E-01	2.4E-02
125.7	2.31E-01	2.4E-02
130.4	3.05E-01	2.8E-02
135.1	2.70E-01	2.6E-02
139.7	3.51E-01	3.1E-02
144.3	2.79E-01	2.7E-02
148.8	2.65E-01	2.7E-02
153.3	2.49E-01	2.6E-02

TABLE B27

12C(3HE,P)14N
BEAM ENERGY = 18.0 MEV
EX. ENERGY = 0.00 MEV

ANGLE C.M.	dσ/dω (MB/ST)	ERROR (MB/ST)
11.2	5.45E-01	1.1E-01
16.7	6.61E-01	1.3E-01
22.3	7.20E-01	4.3E-02
27.8	6.58E-01	3.4E-02
33.3	3.75E-01	2.5E-02
38.8	2.55E-01	2.0E-02
44.3	2.18E-01	1.9E-02
49.7	2.74E-01	2.3E-02
55.1	3.79E-01	2.6E-02
60.4	4.94E-01	3.0E-02
65.8	4.79E-01	3.0E-02
71.0	3.78E-01	2.6E-02
76.2	2.23E-01	2.0E-02
81.4	1.42E-01	1.6E-02
86.5	1.23E-01	1.4E-02
91.6	1.94E-01	1.9E-02
96.6	2.56E-01	2.3E-02
101.6	3.35E-01	2.8E-02
106.5	3.25E-01	2.3E-02
111.4	2.96E-01	2.6E-02
116.2	2.43E-01	2.4E-02
121.0	2.05E-01	2.2E-02
125.8	1.94E-01	2.1E-02
130.4	1.92E-01	2.2E-02
135.1	1.99E-01	2.2E-02
139.7	2.01E-01	2.2E-02
144.3	2.08E-01	2.3E-02
148.8	2.08E-01	2.3E-02
153.3	2.41E-01	2.5E-02

TABLE B28

12C(3HE,P)14N
BEAM ENERGY = 12.0 MEV
EX. ENERGY = 2.311 MEV

ANGLE C.M.	dσ/dω (MB/ST)	ERROR (MB/ST)
6.7	1.97E 00	5.9E-01
11.2	1.47E 00	2.9E-01
16.8	7.29E-01	1.4E-01
22.3	4.32E-01	1.7E-02
27.9	1.88E-01	1.2E-02
33.4	2.63E-01	1.5E-02
38.9	3.31E-01	1.7E-02
44.4	3.75E-01	1.8E-02
49.8	3.00E-01	1.6E-02
55.2	2.05E-01	1.3E-02
60.6	1.19E-01	9.8E-03
65.9	5.08E-02	6.3E-03
71.2	8.46E-02	8.3E-03
76.4	1.18E-01	1.0E-02
81.6	2.10E-01	1.4E-02
86.7	2.55E-01	1.5E-02
91.8	2.63E-01	1.7E-02
96.8	2.87E-01	1.8E-02
101.8	2.83E-01	1.8E-02
106.7	3.05E-01	1.9E-02
111.6	2.49E-01	1.7E-02
116.4	2.57E-01	1.8E-02
121.2	2.42E-01	1.7E-02
125.9	2.01E-01	1.6E-02
130.6	2.13E-01	1.6E-02
135.2	2.14E-01	1.7E-02
139.8	2.29E-01	1.7E-02
144.4	2.31E-01	1.8E-02
148.9	3.06E-01	2.1E-02
153.4	3.63E-01	2.3E-02

TABLE B29

12C(3HE,P)14N
BEAM ENERGY = 12.5 MEV
EX. ENERGY = 2.311 MEV

ANGLE C.M.	dσ/dω (MB/ST)	ERROR (MB/ST)
6.7	3.00E 00	9.9E-01
11.2	1.49E 00	3.0E-01
16.8	1.03E 00	2.1E-01
22.3	4.70E-01	2.7E-02
27.9	2.46E-01	1.9E-02
33.4	2.63E-01	1.5E-02
38.9	3.21E-01	1.7E-02
44.4	3.60E-01	1.8E-02
49.9	2.94E-01	1.6E-02
55.3	1.88E-01	1.2E-02
60.6	1.15E-01	9.6E-03
65.9	7.92E-02	7.8E-03
71.2	7.79E-02	7.8E-03
76.5	1.08E-01	9.5E-03
81.6	1.32E-01	1.0E-01
86.8	1.86E-01	1.3E-02
91.8	2.16E-01	1.4E-02
96.9	2.40E-01	1.7E-02
101.8	2.31E-01	1.6E-02
106.8	2.60E-01	1.8E-02
111.6	2.23E-01	1.6E-02
116.5	2.29E-01	1.7E-02
121.2	2.22E-01	1.8E-02
125.9	2.00E-01	1.6E-02
130.6	1.90E-01	1.5E-02
135.3	1.93E-01	1.6E-02
139.9	2.11E-01	1.7E-02
144.4	2.66E-01	1.9E-02
148.9	3.21E-01	2.1E-02
153.4	3.66E-01	2.3E-02

TABLE B30

12C(3HE,P)14N
BEAM ENERGY = 13.0 MEV
EX. ENERGY = 2.311 MEV

ANGLE C.M.	dσ/dω (MB/ST)	ERROR (MB/ST)
6.7	3.12E 00	9.4E-01
11.2	2.12E 00	4.2E-01
16.8	7.73E-01	1.5E-01
22.4	2.68E-01	1.8E-02
27.9	2.99E-01	2.2E-02
33.4	2.95E-01	2.2E-02
39.0	3.94E-01	2.5E-02
44.4	3.81E-01	2.5E-02
49.9	3.05E-01	2.3E-02
55.3	1.96E-01	1.8E-02
60.6	1.10E-01	1.3E-02
66.0	6.36E-02	9.7E-03
71.3	7.40E-02	1.1E-02
76.5	1.24E-01	1.4E-02
81.7	1.11E-01	1.5E-02
86.8	2.07E-01	1.9E-02
91.9	1.90E-01	1.8E-02
96.9	2.26E-01	2.0E-02
101.9	2.08E-01	1.9E-02
106.8	2.01E-01	1.9E-02
111.7	1.93E-01	1.9E-02
116.5	1.71E-01	1.7E-02
121.3	1.74E-01	1.8E-02
126.0	1.70E-01	1.8E-02
130.6	1.81E-01	1.9E-02
135.3	1.50E-01	1.7E-02
139.9	2.19E-01	2.2E-02
144.4	2.43E-01	2.3E-02
149.0	3.41E-01	2.8E-02
153.4	4.28E-01	3.2E-02

TABLE B31

12C(3HE,P)14N
BEAM ENERGY = 13.5 MEV
EX. ENERGY = 2.311 MEV

ANGLE C.M.	dσ/dω (MB/ST)	ERROR (MB/ST)
6.7	2.73E 00	8.2E-01
11.2	1.94E 00	3.9E-01
16.8	9.50E-01	1.9E-01
22.4	5.67E-01	2.9E-02
27.9	3.12E-01	2.2E-02
33.5	4.44E-01	2.7E-02
39.0	5.75E-01	3.2E-02
44.4	5.63E-01	3.1E-02
49.9	4.38E-01	2.7E-02
55.3	2.31E-01	1.9E-02
60.7	1.15E-01	1.3E-02
66.0	6.76E-02	9.9E-03
71.3	7.28E-02	1.0E-02
76.5	1.41E-01	1.5E-02
81.7	1.82E-01	1.7E-02
86.8	2.53E-01	2.1E-02
91.9	2.52E-01	2.1E-02
96.9	3.28E-01	2.5E-02
101.9	2.29E-01	2.1E-02
106.8	2.14E-01	2.0E-02
111.7	2.13E-01	2.0E-02
116.5	1.81E-01	1.9E-02
121.3	1.46E-01	1.7E-02
126.0	1.23E-01	1.5E-02
130.7	1.22E-01	1.5E-02
135.3	1.51E-01	1.8E-02
139.9	2.10E-01	2.1E-02

TABLE B32

12C(3HE,P)14N
BEAM ENERGY = 14.0 MEV
EX. ENERGY = 2.311 MEV

ANGLE C.M.	dσ/dω (MB/ST)	ERROR (MB/ST)
6.7	2.69E 00	6.0E-01
11.2	2.15E 00	4.3E-01
16.8	1.00E 00	2.0E-01
22.4	5.71E-01	3.2E-02
27.9	3.32E-01	2.3E-02
33.5	4.59E-01	2.8E-02
39.0	5.76E-01	3.3E-02
44.5	5.56E-01	3.2E-02
49.9	4.36E-01	2.8E-02
55.3	2.42E-01	2.0E-02
60.7	1.24E-01	1.4E-02
66.0	7.58E-02	1.1E-02
71.3	9.27E-02	1.2E-02
76.5	1.61E-01	1.6E-02
81.7	1.89E-01	1.8E-02
86.8	2.46E-01	2.1E-02
91.9	2.55E-01	2.1E-02
96.9	2.70E-01	2.3E-02
101.9	2.12E-01	2.0E-02
106.8	2.05E-01	2.0E-02
111.7	1.87E-01	1.9E-02
116.5	1.68E-01	1.8E-02
121.3	1.87E-01	1.9E-02
126.0	1.69E-01	1.9E-02
130.7	1.61E-01	1.8E-02
135.3	1.94E-01	2.0E-02
139.9	1.96E-01	2.0E-02
144.5	2.07E-01	2.1E-02
149.0	2.27E-01	2.2E-02
153.5	1.89E-01	2.9E-02

TABLE B33

12C(3HE,P)14N
BEAM ENERGY = 14.5 MEV
EX. ENERGY = 2.311 MEV

ANGLE C.M.	dσ/dω (MB/ST)	ERROR (MB/ST)
11.2	1.99E 00	6.0E-01
16.8	1.01E 00	2.0E-01
22.4	4.31E-01	3.3E-02
27.9	3.05E-01	2.5E-02
33.5	4.45E-01	3.3E-02
39.0	5.63E-01	4.0E-02
44.5	5.53E-01	3.9E-02
49.9	5.09E-01	3.7E-02
55.3	3.02E-01	2.6E-02
60.7	1.71E-01	1.7E-02
66.0	1.12E-01	1.3E-02
71.3	9.50E-02	1.2E-02
76.5	1.34E-01	1.5E-02
81.7	1.58E-01	1.7E-02
86.9	2.05E-01	2.0E-02
91.9	2.21E-01	2.2E-02
97.0	2.37E-01	2.3E-02
101.9	2.42E-01	2.3E-02
106.9	2.39E-01	2.3E-02
111.7	2.30E-01	2.3E-02
116.5	2.15E-01	2.2E-02
121.3	2.00E-01	2.1E-02
126.0	1.65E-01	1.9E-02
130.7	1.72E-01	2.1E-02
135.3	1.45E-01	1.7E-02
139.9	1.49E-01	1.8E-02
144.5	1.34E-01	1.7E-02
149.0	1.21E-01	1.6E-02
153.5	1.04E-01	1.4E-02

TABLE B34

12C(3HE,P)14N
BEAM ENERGY = 15.0 MEV
EX. ENERGY = 2.311 MEV

ANGLE C.M.	dσ/dω (MB/ST)	ERROR (MB/ST)
6.7	2.88E 00	8.6E-01
11.2	2.02E 00	4.0E-01
16.8	1.03E 00	2.1E-01
22.4	3.56E-01	3.2E-02
27.9	2.08E-01	2.4E-02
33.5	3.62E-01	1.9E-02
39.0	5.07E-01	2.3E-02
44.5	6.32E-01	2.6E-02
49.9	5.29E-01	2.4E-02
55.3	3.77E-01	2.0E-02
60.7	1.99E-01	1.4E-02
66.0	9.43E-02	9.2E-03
71.3	8.55E-02	8.8E-03
76.6	8.16E-02	8.5E-03
81.8	1.55E-01	1.2E-02
86.9	2.09E-01	1.4E-02
91.9	2.18E-01	1.5E-02
97.0	2.22E-01	1.5E-02
102.0	2.45E-01	1.6E-02
106.9	2.34E-01	1.6E-02
111.8	2.15E-01	1.5E-02
116.6	1.65E-01	1.3E-02
121.3	1.67E-01	1.3E-02
126.0	1.24E-01	1.1E-02
130.7	1.02E-01	1.0E-02
135.3	1.13E-01	1.1E-02
139.9	8.88E-02	9.9E-03
144.5	8.00E-02	9.5E-03
149.0	8.44E-02	9.9E-03
153.5	7.91E-02	9.6E-03

TABLE B35

12C(3HE,P)14N
BEAM ENERGY = 15.5 MEV
EX. ENERGY = 2.311 MEV

ANGLE C.M.	dσ/dω (MB/ST)	ERROR (MB/ST)
6.7	2.35E 00	7.0E-01
11.2	1.72E 00	3.5E-01
16.8	7.10E-01	1.4E-01
22.4	1.96E-01	2.4E-02
28.0	1.90E-01	3.0E-02
33.5	3.89E-01	1.7E-02
39.0	6.84E-01	2.8E-02
44.5	6.92E-01	2.8E-02
49.9	6.11E-01	2.6E-02
55.4	3.78E-01	2.0E-02
60.7	1.90E-01	1.4E-02
66.1	8.46E-02	8.8E-03
71.3	4.01E-02	5.9E-03
76.6	8.87E-02	9.2E-03
81.8	1.65E-01	1.6E-02
86.9	2.71E-01	1.6E-02
92.0	3.18E-01	1.7E-02
97.0	3.12E-01	1.7E-02
102.0	3.06E-01	1.7E-02
106.9	2.36E-01	1.5E-02
111.8	2.27E-01	1.5E-02
116.6	2.06E-01	1.4E-02
121.3	1.62E-01	1.3E-02
126.1	1.18E-01	1.1E-02
130.7	1.01E-01	9.9E-03
135.4	8.21E-02	8.9E-03
139.9	9.48E-02	9.7E-03
144.5	7.86E-02	8.9E-03
149.0	9.75E-02	1.0E-02
153.5	1.20E-01	2.0E-02

TABLE B36

12C(3HE,P)14N
BEAM ENERGY = 16.0 MEV
EX. ENERGY = 2.311 MEV

ANGLE C.M.	dσ/dω (MB/ST)	ERROR (MB/ST)
11.2	1.44E 00	2.9E-01
16.8	6.65E-01	1.3E-01
22.4	2.17E-01	2.4E-02
28.0	2.11E-01	2.3E-02
33.5	4.96E-01	4.0E-02
39.0	6.65E-01	3.0E-02
44.5	6.13E-01	2.9E-02
50.0	4.72E-01	2.5E-02
55.4	2.76E-01	1.8E-02
60.8	1.32E-01	1.2E-02
66.1	5.20E-02	7.3E-03
71.4	6.49E-02	8.3E-03
76.6	8.95E-02	1.0E-02
81.8	1.79E-01	1.5E-02
86.9	2.39E-01	1.7E-02
92.0	2.43E-01	1.7E-02
97.0	2.37E-01	1.7E-02
102.0	2.39E-01	1.8E-02
106.9	1.51E-01	1.4E-02
111.8	1.13E-01	1.2E-02
116.6	8.92E-02	1.0E-02
121.4	6.22E-02	8.6E-03
126.1	5.96E-02	8.6E-03
130.8	4.68E-02	7.6E-03
135.4	4.02E-02	7.1E-03
140.0	3.56E-02	6.6E-03
144.5	4.72E-02	7.8E-03
149.0	5.41E-02	8.4E-03
153.5	6.33E-02	9.1E-03

TABLE B37

12C(3HE,P)14N
BEAM ENERGY = 16.5 MEV
EX. ENERGY = 2.311 MEV

ANGLE C.M.	dσ/dω (MB/ST)	ERROR (MB/ST)
6.7	1.96E 00	5.9E-01
11.2	9.93E-01	2.0E-01
14.0	8.14E-01	1.6E-01
16.8	5.12E-01	1.0E-01
22.4	2.30E-01	1.9E-02
28.0	2.58E-01	2.1E-02
33.5	4.77E-01	3.0E-02
39.0	5.95E-01	3.4E-02
44.5	5.91E-01	3.4E-02
50.0	4.56E-01	2.9E-02
55.4	2.82E-01	2.2E-02
60.8	1.48E-01	1.6E-02
66.1	4.72E-02	8.6E-03
71.4	6.08E-02	1.0E-02
76.6	9.43E-02	1.3E-02
81.8	1.94E-01	1.9E-02
86.9	1.96E-01	1.9E-02
92.0	2.54E-01	2.4E-02
97.0	2.35E-01	2.2E-02
102.0	2.19E-01	2.0E-02
106.9	1.80E-01	1.8E-02
111.8	1.34E-01	1.6E-02
116.6	1.31E-01	1.6E-02
121.4	7.48E-02	1.2E-02
126.1	6.69E-02	1.1E-02
130.8	8.41E-02	1.3E-02
135.4	1.07E-01	1.5E-02
140.0	9.51E-02	1.4E-02
144.5	7.94E-02	1.3E-02
149.0	7.92E-02	1.3E-02
153.5	1.01E-01	1.5E-02

TABLE B38

12C(3HE,P)14N
BEAM ENERGY = 17.0 MEV
EX. ENERGY = 2.311 MEV

ANGLE C.M.	dσ/dω (MB/ST)	ERROR (MB/ST)
6.7	1.95E 00	5.9E-01
11.2	1.27E 00	2.3E-01
16.8	6.82E-01	1.4E-01
22.4	2.74E-01	2.1E-02
28.0	2.19E-01	1.9E-02
33.5	4.35E-01	2.8E-02
44.5	6.38E-01	3.5E-02
39.0	6.15E-01	3.4E-02
50.0	4.10E-01	2.8E-02
55.4	2.63E-01	2.2E-02
60.8	1.08E-01	1.4E-02
66.1	6.62E-02	1.1E-02
71.4	6.43E-02	1.0E-02
76.6	1.06E-01	1.4E-02
81.8	1.76E-01	1.8E-02
87.0	1.91E-01	1.9E-02
92.0	1.98E-01	2.0E-02
97.1	2.18E-01	2.2E-02
102.0	2.00E-01	2.1E-02
107.0	1.58E-01	1.8E-02
111.8	1.06E-01	1.6E-02
116.6	9.47E-02	1.5E-02
121.4	4.22E-02	9.6E-03
126.1	4.47E-02	9.9E-03
130.8	5.52E-02	1.1E-02
135.4	4.46E-02	1.1E-02
140.0	4.43E-02	1.0E-02
144.5	4.89E-02	1.0E-02
149.0	4.45E-02	1.6E-03
153.5	5.76E-02	1.2E-02

TABLE B39

12C(3HE,P)14N
BEAM ENERGY = 17.5 MEV
EX. ENERGY = 2.311 MEV

ANGLE C.M.	dσ/dω (MB/ST)	ERROR (MB/ST)
6.7	1.83E 00	5.5E-01
11.2	1.46E 00	3.0E-01
16.8	5.82E-01	1.2E-01
22.4	2.41E-01	1.5E-02
28.0	1.69E-01	1.4E-02
33.5	4.47E-01	2.8E-02
39.1	6.90E-01	2.8E-02
44.5	6.24E-01	3.6E-02
50.0	5.10E-01	3.1E-02
55.4	3.06E-01	2.3E-02
60.8	1.44E-01	1.6E-02
66.1	4.24E-02	8.1E-03
71.4	3.88E-02	7.8E-03
76.6	1.17E-01	1.4E-02
81.8	1.85E-01	1.8E-02
87.0	2.03E-01	2.0E-02
92.0	2.61E-01	2.3E-02
97.1	2.80E-01	2.5E-02
102.0	1.97E-01	2.1E-02
107.0	1.07E-01	1.5E-02
111.8	8.24E-02	1.3E-02
116.6	6.11E-02	1.1E-02
121.4	5.69E-02	1.2E-02
126.1	3.28E-02	8.5E-03
130.8	3.78E-02	9.3E-03
135.4	4.20E-02	9.8E-03
140.0	2.63E-02	7.9E-03
144.5	2.85E-02	8.2E-03
149.1	3.14E-02	8.7E-03
153.5	3.38E-02	9.1E-03

TABLE B40

12C(3HE,P)14N
BEAM ENERGY = 18.0 MEV
EX. ENERGY = 2.311 MEV

ANGLE C.M.	dσ/dω (MB/ST)	ERROR (MB/ST)
6.7	2.29E 00	6.9E-01
11.2	1.56E 00	3.1E-01
16.8	6.56E-01	1.3E-01
22.4	1.82E-01	1.8E-02
28.0	1.43E-01	1.5E-02
33.5	4.08E-01	2.7E-02
39.1	6.01E-01	3.3E-02
44.6	6.03E-01	3.3E-02
50.0	4.46E-01	2.9E-02
55.4	2.45E-01	2.0E-02
60.8	1.07E-01	1.2E-02
66.1	3.83E-02	7.6E-03
71.4	4.52E-02	8.3E-03
76.7	1.08E-01	1.3E-02
81.8	1.63E-01	1.7E-02
87.0	1.89E-01	1.8E-02
92.1	2.20E-01	2.0E-02
97.1	2.18E-01	2.0E-02
102.1	1.77E-01	2.0E-02
107.0	1.14E-01	1.6E-02
111.8	7.68E-02	1.3E-02
116.7	4.85E-02	1.0E-02
121.4	4.63E-02	9.9E-03
126.1	4.39E-02	9.8E-03
130.8	5.11E-02	1.1E-02
135.4	3.99E-02	9.5E-03
140.0	4.50E-02	1.0E-02
144.6	3.86E-02	8.6E-03
149.1	2.20E-02	7.2E-03
153.5	2.89E-02	8.3E-03

TABLE B41

12C(3HE,P)14N
BEAM ENERGY = 12.0 MEV
EX. ENERGY = 3.945 MEV

ANGLE C.M.	dσ/dω (MB/ST)	ERROR (MB/ST)
11.3	7.03E 00	1.4E 00
16.9	4.45E 00	8.9E-01
22.5	2.41E 00	4.7E-02
28.1	1.49E 00	3.9E-02
33.7	1.21E 00	3.5E-02
39.2	1.15E 00	3.4E-02
44.7	9.65E-01	3.1E-02
50.2	8.12E-01	2.8E-02
55.6	5.23E-01	2.2E-02
61.0	3.65E-01	1.8E-02
66.4	2.51E-01	1.5E-02
71.7	2.96E-01	1.6E-02
76.9	3.94E-01	1.9E-02
82.1	4.93E-01	2.2E-02
87.3	5.89E-01	2.5E-02
92.3	6.64E-01	2.9E-02
97.4	6.67E-01	3.0E-02
102.3	6.14E-01	2.8E-02
107.3	5.13E-01	2.6E-02
112.1	4.97E-01	2.6E-02
116.9	4.24E-01	2.4E-02
121.7	4.34E-01	2.4E-02
126.4	4.52E-01	2.5E-02
131.0	5.87E-01	2.9E-02
135.6	6.52E-01	3.1E-02
140.2	9.43E-01	3.9E-02
144.7	1.02E 00	4.1E-02
149.2	1.11E 00	4.4E-02
153.7	1.24E 00	4.7E-02

TABLE B42

12C(3HE,P)14N
BEAM ENERGY = 12.5 MEV
EX. ENERGY = 3.945 MEV

ANGLE C.M.	dσ/dω (MB/ST)	ERROR (MB/ST)
11.3	4.35E 00	8.7E-01
16.9	2.78E 00	5.6E-01
22.5	1.57E 00	5.3E-02
28.1	1.14E 00	4.7E-02
33.7	9.64E-01	3.1E-02
39.2	1.09E 00	3.4E-02
44.7	9.27E-01	3.1E-02
50.2	6.67E-01	2.5E-02
55.6	5.25E-01	2.2E-02
61.0	3.54E-01	1.8E-02
66.4	2.98E-01	1.6E-02
71.7	3.21E-01	1.7E-02
76.9	3.92E-01	1.9E-02
82.1	4.89E-01	2.2E-02
87.3	5.38E-01	2.3E-02
92.3	5.99E-01	2.5E-02
97.4	5.53E-01	2.7E-02
102.3	4.85E-01	2.5E-02
107.3	3.99E-01	2.2E-02
112.1	2.69E-01	1.8E-02
116.9	2.58E-01	1.8E-02
121.7	1.93E-01	1.5E-02
126.4	3.44E-01	2.1E-02
131.0	4.40E-01	2.5E-02
135.6	5.89E-01	3.0E-02
140.2	7.02E-01	3.3E-02
144.7	9.24E-01	3.9E-02
149.2	9.85E-01	4.1E-02
153.7	1.11E 00	4.4E-02

TABLE B43

12C(3HE,P)14N
BEAM ENERGY = 13.0 MEV
EX. ENERGY = 3.945 MEV

ANGLE C.M.	dσ/dω (MB/ST)	ERROR (MB/ST)
11.3	4.97E 00	9.8E-01
16.9	3.56E 00	7.1E-01
22.5	1.19E 00	4.3E-02
28.1	9.35E-01	4.0E-02
33.7	6.94E-01	3.5E-02
39.2	8.46E-01	5.0E-02
44.7	7.99E-01	3.9E-02
50.2	7.05E-01	3.7E-02
55.7	5.97E-01	3.3E-02
61.0	4.84E-01	3.0E-02
66.4	4.33E-01	2.8E-02
71.7	5.07E-01	3.1E-02
76.9	5.00E-01	3.1E-02
82.1	6.24E-01	3.6E-02
87.3	5.79E-01	3.4E-02
92.4	6.23E-01	3.6E-02
97.4	6.07E-01	3.5E-02
102.4	5.88E-01	3.5E-02
107.3	4.25E-01	2.9E-02
112.1	3.62E-01	2.7E-02
116.9	3.19E-01	2.5E-02
121.7	3.14E-01	2.5E-02
126.4	3.57E-01	2.8E-02
131.0	4.55E-01	3.2E-02
135.7	5.52E-01	3.6E-02
140.2	7.46E-01	4.4E-02
144.7	9.05E-01	4.9E-02
149.2	9.98E-01	5.2E-02
153.7	1.22E 00	6.0E-02

TABLE B44

12C(3HE,P)14N
BEAM ENERGY = 13.5 MEV
EX. ENERGY = 3.945 MEV

ANGLE C.M.	dσ/dω (MB/ST)	ERROR (MB/ST)
11.3	5.66E 00	1.1E 00
16.9	3.02E 00	6.0E-01
22.5	1.50E 00	5.2E-02
28.1	7.19E-01	3.5E-02
33.7	6.31E-01	3.3E-02
39.2	8.39E-01	4.0E-02
44.7	9.32E-01	4.2E-02
50.2	7.99E-01	3.9E-02
55.7	7.50E-01	3.8E-02
61.1	5.99E-01	3.3E-02
66.4	4.95E-01	3.0E-02
71.7	4.51E-01	2.9E-02
77.0	4.34E-01	2.8E-02
82.1	4.97E-01	3.1E-02
87.3	5.31E-01	3.2E-02
92.4	6.39E-01	3.6E-02
97.4	5.65E-01	3.4E-02
102.4	5.53E-01	3.4E-02
107.3	4.91E-01	3.2E-02
112.1	4.49E-01	3.1E-02
117.0	3.61E-01	2.7E-02
121.7	3.79E-01	2.9E-02
126.4	3.89E-01	2.9E-02
131.1	3.92E-01	3.0E-02
135.7	5.02E-01	3.5E-02
140.2	5.58E-01	3.7E-02

TABLE B45

12C(3HE,P)14N
BEAM ENERGY = 14.0 MEV
EX. ENERGY = 3.945 MEV

ANGLE C.M.	dσ/dω (MB/ST)	ERROR (MB/ST)
6.8	7.19E 00	2.2E 00
11.3	4.94E 00	8.9E-01
16.9	2.86E 00	5.7E-01
22.5	1.24E 00	5.0E-02
28.1	6.71E-01	3.5E-02
33.7	7.82E-01	3.9E-02
39.2	9.59E-01	4.4E-02
44.8	1.03E 00	4.6E-02
50.2	8.13E-01	4.0E-02
55.7	6.61E-01	3.5E-02
61.1	3.93E-01	2.6E-02
66.4	3.42E-01	2.4E-02
71.7	3.23E-01	2.4E-02
77.0	3.09E-01	2.3E-02
82.2	3.88E-01	2.7E-02
87.3	4.97E-01	3.1E-02
92.4	4.90E-01	3.1E-02
97.4	4.75E-01	3.1E-02
102.4	5.06E-01	3.3E-02
107.3	4.12E-01	3.0E-02
112.2	4.64E-01	3.1E-02
117.0	3.87E-01	2.9E-02
121.7	3.42E-01	2.7E-02
126.4	4.16E-01	3.2E-02
131.1	4.54E-01	3.4E-02
135.7	5.31E-01	3.6E-02
140.2	5.72E-01	3.7E-02
144.8	5.85E-01	3.8E-02
149.2	6.03E-01	3.9E-02
153.7	6.60E-01	5.9E-02

TABLE B46

12C(3HE,P)14N
BEAM ENERGY = 14.5 MEV
EX. ENERGY = 3.945 MEV

ANGLE C.M.	dσ/dω (MB/ST)	ERROR (MB/ST)
11.2	4.80E 00	1.4E 00
16.8	2.78E 00	5.4E-01
22.5	1.23E 00	8.6E-02
28.1	6.50E-01	4.4E-02
33.7	7.29E-01	4.8E-02
39.2	9.77E-01	6.1E-02
44.8	1.08E 00	6.6E-02
50.2	9.83E-01	6.1E-02
55.7	7.71E-01	5.1E-02
61.1	5.98E-01	4.2E-02
66.4	3.96E-01	3.1E-02
71.7	3.49E-01	2.9E-02
77.0	3.32E-01	2.8E-02
82.2	3.62E-01	3.0E-02
87.3	4.12E-01	3.3E-02
92.4	4.34E-01	3.5E-02
97.4	4.78E-01	3.7E-02
102.4	4.69E-01	3.7E-02
107.3	4.17E-01	3.4E-02
112.2	3.99E-01	3.3E-02
117.0	3.31E-01	2.9E-02
121.7	3.92E-01	3.3E-02
126.4	4.10E-01	3.5E-02
131.1	5.87E-01	4.1E-02
135.7	5.20E-01	3.7E-02
140.2	6.52E-01	4.9E-02
144.8	7.60E-01	5.5E-02
149.2	7.01E-01	5.2E-02
153.7	5.53E-01	4.4E-02

TABLE B47

12C(3HE,P)14N
BEAM ENERGY = 15.0 MEV
EX. ENERGY = 3.945 MEV

ANGLE C.M.	dσ/dω (MB/ST)	ERROR (MB/ST)
6.8	5.77E 00	1.7E 00
11.3	3.27E 00	6.4E-01
16.9	2.17E 00	4.3E-01
22.5	1.01E 00	6.0E-02
28.1	7.40E-01	2.8E-02
33.7	8.52E-01	3.1E-02
39.3	1.06E 00	3.6E-02
44.8	9.54E-01	3.4E-02
50.2	8.29E-01	3.1E-02
55.7	6.74E-01	2.8E-02
61.1	4.05E-01	2.1E-02
66.4	2.98E-01	1.7E-02
71.7	2.75E-01	1.7E-02
77.0	2.84E-01	1.7E-02
82.2	3.50E-01	1.9E-02
92.4	3.99E-01	2.1E-02
87.3	3.62E-01	1.9E-02
97.4	3.68E-01	2.0E-02
102.4	3.09E-01	1.8E-02
107.3	2.50E-01	1.6E-02
112.2	1.92E-01	1.4E-02
117.0	1.97E-01	1.5E-02
121.7	2.52E-01	1.7E-02
126.4	3.42E-01	2.0E-02
131.1	4.55E-01	2.4E-02
135.7	5.90E-01	2.8E-02
140.2	6.43E-01	3.0E-02
144.8	7.94E-01	3.5E-02
149.3	8.28E-01	3.6E-02
153.7	7.21E-01	3.3E-02

TABLE B48

12C(3HE,P)14N
BEAM ENERGY = 15.5 MEV
EX. ENERGY = 3.945 MEV

ANGLE C.M.	dσ/dω (MB/ST)	ERROR (MB/ST)
6.8	5.05E 00	1.5E 00
11.3	3.75E 00	7.5E-01
16.9	1.98E 00	4.0E-01
22.5	9.87E-01	6.1E-02
28.1	9.80E-01	6.3E-02
33.7	1.18E 00	3.9E-02
39.3	1.26E 00	4.1E-02
44.8	1.28E 00	4.1E-02
50.2	9.45E-01	3.4E-02
55.7	6.15E-01	2.7E-02
61.1	4.02E-01	2.1E-02
66.4	3.19E-01	1.8E-02
71.7	3.20E-01	1.9E-02
77.0	3.48E-01	2.0E-02
82.2	4.22E-01	2.3E-02
87.3	5.11E-01	2.3E-02
92.4	4.83E-01	2.2E-02
97.4	4.54E-01	2.2E-02
102.4	3.64E-01	1.9E-02
107.3	2.62E-01	1.6E-02
112.2	2.99E-01	1.7E-02
117.0	2.34E-01	1.5E-02
121.7	2.64E-01	1.7E-02
126.4	3.39E-01	1.9E-02
131.1	4.65E-01	2.3E-02
135.7	5.68E-01	2.6E-02
140.2	6.32E-01	2.8E-02
144.8	7.61E-01	3.2E-02
149.3	7.51E-01	3.1E-02
153.7	7.21E-01	3.1E-02

TABLE B49

12C(3HE,P)14N
BEAM ENERGY = 16.0 MEV
EX. ENERGY = 3.945 MEV

ANGLE C.M.	dσ/dω (MB/ST)	ERROR (MB/ST)
11.3	2.95E 00	5.9E-01
16.9	1.70E 00	3.4E-01
22.5	7.64E 00	4.9E-02
28.1	7.58E-01	5.1E-02
33.7	9.84E-01	6.5E-02
39.3	1.01E 00	3.9E-02
44.8	1.05E 00	4.0E-02
50.3	7.90E-01	3.3E-02
55.7	5.46E-01	2.7E-02
61.1	4.84E-01	2.5E-02
66.4	4.43E-01	2.4E-02
71.7	4.46E-01	2.4E-02
77.0	4.67E-01	2.5E-02
82.2	4.40E-01	2.5E-02
87.3	4.97E-01	2.7E-02
92.4	3.79E-01	2.2E-02
97.4	3.15E-01	2.0E-02
102.4	2.87E-01	2.0E-02
107.3	2.28E-01	1.7E-02
112.2	2.37E-01	1.8E-02
117.0	1.79E-01	1.5E-02
121.7	2.15E-01	1.7E-02
126.4	2.04E-01	2.2E-02
131.1	2.30E-01	1.8E-02
135.7	2.91E-01	2.1E-02
140.3	2.98E-01	2.1E-02
144.8	2.98E-01	2.1E-02
149.3	2.96E-01	2.1E-02
153.7	2.69E-01	2.0E-02

TABLE B50

12C(3HE,P)14N
BEAM ENERGY = 16.5 MEV
EX. ENERGY = 3.945 MEV

ANGLE C.M.	dσ/dω (MB/ST)	ERROR (MB/ST)
6.8	4.29E 00	1.3E 00
11.3	1.97E 00	3.9E-01
14.1	1.68E 00	3.4E-01
16.9	1.00E 00	2.0E-01
22.5	5.98E-01	3.1E-02
28.1	6.60E-01	3.5E-02
33.7	8.75E-01	4.2E-02
39.3	1.05E 00	4.7E-02
44.8	9.98E-01	4.6E-02
50.3	7.80E-01	4.0E-02
55.7	4.89E-01	3.0E-02
61.1	3.97E-01	2.7E-02
66.4	3.43E-01	2.5E-02
71.7	3.29E-01	2.5E-02
77.0	4.10E-01	2.8E-02
82.2	5.00E-01	3.2E-02
87.3	4.92E-01	3.2E-02
92.4	4.41E-01	3.2E-02
97.4	3.24E-01	2.4E-02
102.4	2.99E-01	2.4E-02
107.3	2.33E-01	2.1E-02
112.2	2.21E-01	2.1E-02
117.0	1.48E-01	1.7E-02
121.7	1.70E-01	1.8E-02
126.4	1.97E-01	2.0E-02
131.1	2.28E-01	2.2E-02
135.7	2.56E-01	2.4E-02
140.3	3.11E-01	2.7E-02
144.8	3.22E-01	2.7E-02
149.3	3.28E-01	2.7E-02
153.7	2.90E-01	2.6E-02

TABLE B51

12C(3HE,P)14N
BEAM ENERGY = 17.0 MEV
EX. ENERGY = 3.945 MEV

ANGLE C.M.	dσ/dω (MB/ST)	ERROR (MB/ST)
6.8	3.30E 00	9.9E-01
11.3	2.12E 00	4.2E-01
16.9	1.32E 00	2.6E-01
22.5	5.08E-01	2.9E-02
28.1	5.03E-01	3.0E-02
33.7	7.69E-01	3.9E-02
39.3	1.09E 00	4.8E-02
44.8	1.00E 00	4.6E-02
50.3	6.79E-01	3.7E-02
55.7	5.91E-01	3.5E-02
61.1	4.60E-01	3.0E-02
66.5	4.58E-01	3.0E-02
71.8	4.11E-01	2.9E-02
77.0	3.80E-01	2.7E-02
82.2	4.39E-01	3.0E-02
87.3	3.73E-01	2.8E-02
92.4	3.47E-01	2.7E-02
97.5	2.85E-01	2.5E-02
102.4	2.48E-01	2.4E-02
107.3	1.57E-01	1.8E-02
112.2	2.01E-01	2.1E-02
117.0	1.96E-01	2.2E-02
121.8	1.78E-01	2.1E-02
126.5	2.23E-01	2.3E-02
131.1	2.43E-01	2.5E-02
135.7	2.92E-01	2.7E-02
140.3	2.99E-01	2.8E-02
144.8	2.49E-01	2.4E-02
149.3	2.41E-01	2.5E-02
153.7	2.36E-01	2.5E-02

TABLE B52

12C(3HE,P)14N
BEAM ENERGY = 17.5 MEV
EX. ENERGY = 3.945 MEV

ANGLE C.M.	dσ/dω (MB/ST)	ERROR (MB/ST)
6.8	3.52E 00	1.0E 00
11.3	2.23E 00	4.5E-01
16.9	1.25E 00	2.5E-01
22.5	6.15E-01	2.5E-02
28.1	5.22E-01	2.7E-02
33.7	7.92E-01	3.9E-02
39.3	8.52E-01	3.9E-02
44.8	7.94E-01	4.2E-02
50.3	6.37E-01	3.5E-02
55.7	4.96E-01	3.1E-02
61.1	4.87E-01	3.1E-02
66.5	4.57E-01	2.9E-02
71.8	4.35E-01	2.9E-02
77.0	4.15E-01	2.9E-02
82.2	3.92E-01	2.8E-02
87.3	3.69E-01	2.7E-02
92.4	2.58E-01	2.2E-02
97.5	3.01E-01	2.6E-02
102.4	2.01E-01	2.1E-02
107.3	2.31E-01	2.3E-02
112.2	2.41E-01	2.4E-02
117.0	2.64E-01	2.8E-02
121.8	2.76E-01	2.6E-02
126.5	2.35E-01	2.4E-02
131.1	2.81E-01	2.7E-02
135.7	2.59E-01	2.6E-02
140.3	3.06E-01	2.9E-02
144.8	2.46E-01	2.6E-02
149.3	2.02E-01	2.3E-02
153.7	1.99E-01	2.3E-02

TABLE B53

12C(3HE,P)14N
BEAM ENERGY = 18.0 MEV
EX. ENERGY = 3.945 MEV

ANGLE C.M.	dσ/dω (MB/ST)	ERROR (MB/ST)
6.8	3.75E 00	1.1E 00
11.3	2.09E 00	4.2E-01
16.9	1.02E 00	2.0E-01
22.5	5.24E-01	3.2E-02
28.1	4.80E-01	2.9E-02
33.7	6.92E-01	3.5E-02
39.3	7.30E-01	3.7E-02
44.8	7.05E-01	3.7E-02
50.3	5.29E-01	4.5E-02
55.7	4.56E-01	2.8E-02
61.1	4.18E-01	2.8E-02
66.5	4.60E-01	2.9E-02
71.8	4.24E-01	2.8E-02
77.0	4.12E-01	2.7E-02
82.2	3.35E-01	2.5E-02
87.4	3.18E-01	2.4E-02
92.4	2.82E-01	2.3E-02
97.5	2.36E-01	2.2E-02
102.4	2.53E-01	2.4E-02
107.4	2.46E-01	2.4E-02
112.2	2.35E-01	2.3E-02
117.0	2.28E-01	2.3E-02
121.8	2.62E-01	2.5E-02
126.5	2.55E-01	2.5E-02
131.1	2.54E-01	2.5E-02
135.7	2.65E-01	2.6E-02
140.3	2.88E-01	2.8E-02
144.8	2.32E-01	2.5E-02
149.3	2.22E-01	2.4E-02
153.7	2.36E-01	2.5E-02

TABLE B54

12C(3HE,P)14N
BEAM ENERGY = 12.0 MEV
EX. ENERGY = 4.91 MEV

ANGLE C.M.	dσ/dω (MB/ST)	ERROR (MB/ST)
11.3	8.02E-01	2.5E-01
17.0	1.65E 00	3.3E-01
22.6	2.53E 00	4.9E-02
28.3	2.25E 00	5.0E-02
33.9	1.98E 00	4.8E-02
39.4	1.65E 00	4.4E-02
45.0	1.34E 00	3.9E-02
50.5	1.21E 00	3.6E-02
55.9	9.96E-01	3.2E-02
61.3	7.51E-01	2.8E-02
66.7	5.79E-01	2.4E-02
72.0	4.62E-01	2.1E-02
77.3	4.13E-01	2.0E-02
82.5	3.97E-01	2.0E-02
87.6	4.06E-01	2.0E-02
92.7	4.54E-01	2.3E-02
97.7	5.12E-01	2.5E-02
102.7	5.54E-01	2.7E-02
107.6	5.10E-01	2.6E-02
112.5	4.84E-01	2.5E-02
117.3	4.06E-01	2.3E-02
122.0	3.61E-01	2.2E-02
126.7	3.05E-01	2.0E-02
131.3	3.22E-01	2.1E-02
135.9	2.99E-01	2.0E-02
140.5	3.37E-01	2.2E-02
145.0	3.46E-01	2.2E-02
149.4	3.57E-01	2.7E-02
153.9	3.26E-01	2.2E-02

TABLE B55

12C(3HE,P)14N
BEAM ENERGY = 12.5 MEV
EX. ENERGY = 4.91 MEV

ANGLE C.M.	dσ/dω (MB/ST)	ERROR (MB/ST)
11.3	1.02E 00	3.1E-01
17.0	1.69E 00	3.4E-01
22.6	2.47E 00	7.1E-02
28.3	2.28E 00	7.2E-02
33.9	1.92E 00	4.8E-02
39.4	1.64E 00	4.4E-02
45.0	1.31E 00	3.8E-02
50.5	1.14E 00	3.5E-02
55.9	8.73E-01	3.0E-02
61.3	7.24E-01	2.7E-02
66.7	4.82E-01	2.1E-02
72.0	4.17E-01	2.0E-02
77.3	3.56E-01	1.8E-02
82.5	3.36E-01	1.8E-02
87.6	3.92E-01	2.0E-02
92.7	4.23E-01	2.1E-02
97.7	4.86E-01	2.5E-02
102.7	4.83E-01	2.5E-02
107.6	5.09E-01	2.6E-02
112.5	4.75E-01	2.5E-02
117.3	4.30E-01	2.4E-02
122.0	3.80E-01	2.3E-02
126.7	3.36E-01	2.1E-02
131.3	3.33E-01	2.1E-02
135.9	3.07E-01	2.1E-02
140.5	2.99E-01	2.0E-02
145.0	2.89E-01	2.0E-02
149.4	2.85E-01	2.0E-02
153.9	2.79E-01	2.0E-02

TABLE B56

12C(3HE,P)14N
BEAM ENERGY = 13.0 MEV
EX. ENERGY = 4.91 MEV

ANGLE C.M.	dσ/dω (MB/ST)	ERROR (MB/ST)
11.3	1.45E 00	4.3E-01
17.0	2.42E 00	4.8E-01
22.6	2.71E 00	7.3E-02
28.3	2.02E 00	6.7E-02
33.9	1.89E 00	5.2E-02
39.4	1.26E 00	4.9E-02
45.0	1.12E 00	4.8E-02
50.5	8.88E-01	4.2E-02
55.9	7.75E-01	3.5E-02
61.3	6.17E-01	3.4E-02
66.7	5.09E-01	3.1E-02
72.0	3.78E-01	2.6E-02
77.3	3.25E-01	2.4E-02
82.5	2.99E-01	2.3E-02
87.6	3.02E-01	2.4E-02
92.7	3.23E-01	2.5E-02
97.7	3.31E-01	2.5E-02
102.7	3.58E-01	2.6E-02
107.6	3.48E-01	2.6E-02
112.5	3.88E-01	2.8E-02
117.3	3.40E-01	2.6E-02
122.0	3.10E-01	2.5E-02
126.7	2.85E-01	2.5E-02
131.3	2.81E-01	2.5E-02
135.9	2.84E-01	2.5E-02
140.5	2.42E-01	2.3E-02
145.0	2.69E-01	2.5E-02
149.4	3.12E-01	2.7E-02
153.9	2.46E-01	2.4E-02

TABLE B57

12C(3HE,P)14N
BEAM ENERGY = 13.5 MEV
EX. ENERGY = 4.91 MEV

ANGLE C.M.	dσ/dω (MB/ST)	ERROR (MB/ST)
11.3	1.65E 00	4.9E-01
17.0	2.03E 00	4.1E-01
22.6	1.87E 00	5.9E-02
28.3	1.75E 00	6.1E-02
33.9	1.30E 00	5.2E-02
39.4	9.71E-01	4.3E-02
45.0	7.30E-01	3.6E-02
50.5	6.49E-01	3.4E-02
55.9	5.41E-01	3.1E-02
61.3	3.98E-01	2.6E-02
66.7	3.09E-01	2.3E-02
72.0	2.36E-01	2.0E-02
77.3	1.88E-01	1.7E-02
82.5	1.73E-01	1.7E-02
87.6	1.59E-01	1.6E-02
92.7	1.93E-01	1.8E-02
97.7	2.46E-01	2.1E-02
102.7	2.91E-01	2.4E-02
107.6	2.80E-01	2.3E-02
112.5	3.05E-01	2.5E-02
117.3	3.20E-01	2.6E-02
122.0	2.82E-01	2.4E-02
126.7	2.40E-01	2.2E-02
131.3	2.05E-01	2.1E-02
135.9	1.93E-01	2.0E-02
140.5	1.43E-01	1.7E-02

TABLE B58

12C(3HE,P)14N
BEAM ENERGY = 14.0 MEV
EX. ENERGY = 4.91 MEV

ANGLE C.M.	dσ/dω (MB/ST)	ERROR (MB/ST)
11.3	1.12E 00	3.4E-01
17.0	1.23E 00	2.4E-01
22.6	1.73E 00	6.2E-02
28.3	1.32E 00	5.3E-02
33.9	9.90E-01	4.4E-02
39.4	6.93E-01	3.6E-02
45.0	5.29E-01	3.1E-02
50.5	5.00E-01	3.0E-02
55.9	4.05E-01	2.6E-02
61.3	3.52E-01	2.4E-02
66.7	2.13E-01	1.9E-02
72.0	1.67E-01	1.6E-02
77.3	1.59E-01	1.6E-02
82.5	1.66E-01	1.7E-02
87.6	1.95E-01	1.8E-02
92.7	1.78E-01	1.7E-02
97.7	1.61E-01	1.7E-02
102.7	1.80E-01	1.8E-02
107.6	1.99E-01	2.0E-02
112.5	1.25E-01	1.5E-02
117.3	1.12E-01	1.5E-02
122.0	1.12E-01	1.5E-02
126.7	1.23E-01	1.6E-02
131.3	8.61E-02	1.3E-02
135.9	8.52E-02	1.3E-02
140.5	7.95E-02	1.2E-02
145.0	1.17E-01	1.6E-02
149.4	1.65E-01	1.9E-02
153.9	1.91E-01	2.9E-02

TABLE B59

12C(3HE,P)14N
BEAM ENERGY = 14.5 MEV
EX. ENERGY = 4.91 MEV

ANGLE C.M.	dσ/dω (MB/ST)	ERROR (MB/ST)
11.2	6.19E-01	1.9E-01
16.8	7.25E-01	1.4E-01
22.6	8.45E-01	5.4E-02
28.3	9.26E-01	5.8E-02
33.9	7.20E-01	4.8E-02
39.4	6.28E-01	4.3E-02
45.0	4.87E-01	3.6E-02
50.5	4.91E-01	3.6E-02
55.9	4.02E-01	3.1E-02
61.3	3.19E-01	2.7E-02
66.7	2.65E-01	2.4E-02
72.0	2.19E-01	2.1E-02
77.3	1.72E-01	1.8E-02
82.5	1.69E-01	1.8E-02
87.6	1.66E-01	1.8E-02
92.7	1.45E-01	1.6E-02
97.7	1.25E-01	1.5E-02
102.7	1.03E-01	1.3E-02
107.6	6.48E-02	1.0E-02
112.5	4.21E-02	7.8E-03
117.3	3.06E-02	6.5E-03
122.0	3.33E-02	6.9E-03
126.7	4.70E-02	8.5E-03
131.3	5.13E-02	9.3E-03
135.9	8.51E-02	1.1E-03
140.5	1.20E-01	1.5E-02
145.0	1.36E-01	1.7E-02
149.4	1.79E-01	2.0E-02
153.9	2.15E-01	2.3E-02

TABLE B60

12C(3HE,P)14N
BEAM ENERGY = 15.0 MEV
EX. ENERGY = 4.91 MEV

ANGLE C.M.	dσ/dω (MB/ST)	ERROR (MB/ST)
11.3	8.20E-01	2.5E-01
17.0	8.05E-01	1.6E-01
22.6	8.57E-01	5.4E-02
28.3	7.13E-01	4.8E-02
33.9	6.10E-01	2.5E-02
39.4	5.80E-01	2.5E-02
45.0	5.59E-01	2.4E-02
50.5	5.02E-01	2.3E-02
55.9	4.60E-01	2.2E-02
61.3	3.47E-01	1.9E-02
66.7	2.56E-01	1.6E-02
72.0	1.94E-01	1.4E-02
77.3	1.66E-01	1.2E-02
82.5	1.79E-01	2.4E-02
87.6	1.32E-01	1.1E-02
92.7	1.19E-01	1.0E-02
97.7	8.54E-02	8.9E-03
102.7	8.43E-02	8.9E-03
107.6	6.23E-02	7.6E-03
112.5	3.41E-02	5.5E-03
117.3	3.90E-02	6.1E-03
122.0	3.80E-02	6.0E-03
126.7	4.68E-02	6.8E-03
131.3	8.90E-02	9.8E-03
135.9	1.10E-01	1.1E-02
140.5	1.42E-01	1.3E-02
145.0	1.73E-01	1.4E-02
149.4	1.77E-01	1.5E-02
153.9	2.09E-01	1.6E-02

TABLE B61

12C(3HE,P)14N
BEAM ENERGY = 15.5 MEV
EX. ENERGY = 4.91 MEV

ANGLE C.M.	dσ/dω (MB/ST)	ERROR (MB/ST)
11.3	8.95E-01	2.7E-01
17.0	9.13E-01	1.8E-01
22.6	9.46E-01	5.9E-02
28.3	1.03E 00	6.3E-02
33.9	8.04E-01	3.1E-02
39.4	7.06E-01	2.8E-02
45.0	5.64E-01	2.5E-02
50.5	5.58E-01	2.5E-02
55.9	4.56E-01	2.2E-02
61.3	3.76E-01	2.0E-02
66.7	2.19E-01	1.5E-02
72.0	1.83E-01	1.4E-02
77.3	1.88E-01	1.4E-02
82.5	1.60E-01	1.3E-02
87.6	1.57E-01	2.1E-02
92.7	1.39E-01	1.1E-02
97.7	1.09E-01	9.7E-03
102.7	1.19E-01	1.0E-02
107.6	6.92E-02	7.7E-03
112.5	5.26E-02	6.6E-03
117.3	4.66E-02	6.3E-03
122.0	7.88E-02	9.2E-03
126.7	6.97E-02	8.0E-03
131.3	1.21E-01	1.1E-02
135.9	1.59E-01	1.3E-02
140.5	1.91E-01	1.4E-02
145.0	1.93E-01	1.5E-02
149.4	2.22E-01	1.6E-02
153.9	2.02E-01	1.5E-02

TABLE B62

12C(3HE,P)14N
BEAM ENERGY = 16.0 MEV
EX. ENERGY = 4.91 MEV

ANGLE C.M.	dσ/dω (MB/ST)	ERROR (MB/ST)
11.3	8.79E-01	2.7E-01
17.0	1.10E 00	2.2E-01
22.6	1.17E 00	6.7E-02
28.3	9.37E-01	5.8E-02
33.9	7.10E-01	5.0E-02
39.4	6.81E-01	3.0E-02
45.0	6.23E-01	2.9E-02
50.4	5.13E-01	2.6E-02
55.9	3.42E-01	2.0E-02
61.3	2.71E-01	1.8E-02
66.7	1.75E-01	1.4E-02
72.0	1.84E-01	1.5E-02
77.3	1.41E-01	1.3E-02
82.5	1.30E-01	1.2E-02
87.6	1.34E-01	1.3E-02
92.7	7.07E-02	8.8E-03
97.7	5.03E-02	7.4E-03
102.7	5.14E-02	7.6E-03
107.6	2.11E-02	4.8E-03
112.5	2.25E-02	5.0E-03
117.3	3.14E-02	6.0E-03
122.0	3.04E-02	5.9E-03
126.7	4.29E-02	7.3E-03
131.3	7.64E-02	9.9E-03
135.9	8.42E-02	1.1E-02
140.4	1.21E-01	1.3E-02
145.0	1.52E-01	1.5E-02
149.4	1.58E-01	1.5E-02
153.9	1.93E-01	1.7E-02

TABLE B63

12C(3HE,P)14N
BEAM ENERGY = 16.5 MEV
EX. ENERGY = 4.91 MEV

ANGLE C.M.	dσ/dω (MB/ST)	ERROR (MB/ST)
11.3	1.20E 00	3.3E-01
14.2	1.10E 00	2.0E-01
17.0	1.14E 00	2.2E-01
22.6	1.07E 00	4.5E-02
28.3	9.60E-01	4.3E-02
33.8	7.44E-01	3.7E-02
39.4	7.02E-01	3.5E-02
45.0	5.92E-01	3.4E-02
50.4	5.16E-01	3.1E-02
55.9	3.92E-01	2.7E-02
61.3	3.16E-01	2.4E-02
66.7	1.97E-01	1.8E-02
72.0	1.65E-01	1.7E-02
77.3	1.23E-01	1.4E-02
82.5	1.07E-01	1.4E-02
87.6	9.55E-02	1.3E-02
92.7	1.06E-01	1.5E-02
97.7	7.20E-02	1.2E-02
102.7	6.27E-02	1.0E-02
107.6	4.36E-02	8.6E-03
112.5	3.50E-02	7.7E-03
117.3	3.34E-02	7.5E-03
122.0	3.96E-02	8.4E-03
126.7	5.89E-02	1.1E-02
131.3	6.76E-02	1.1E-02
135.9	9.93E-02	1.4E-02
140.4	1.18E-01	1.6E-02
145.0	1.28E-01	1.7E-02
149.4	2.18E-01	2.2E-02
153.8	2.45E-01	2.4E-02

TABLE B64

12C(3HE,P)14N
BEAM ENERGY = 17.0 MEV
EX. ENERGY = 4.91 MEV

ANGLE C.M.	dσ/dω (MB/ST)	ERROR (MB/ST)
11.3	7.15E-01	2.2E-01
17.0	8.45E-01	1.7E-01
22.6	9.74E-01	4.3E-02
28.3	8.40E-01	4.1E-02
33.8	7.39E-01	3.8E-02
39.4	6.27E-01	3.5E-02
45.0	6.53E-01	3.6E-02
50.4	5.52E-01	3.3E-02
55.9	3.80E-01	2.7E-02
61.3	2.95E-01	2.3E-02
66.7	1.68E-01	1.7E-02
72.0	1.70E-01	1.8E-02
77.2	1.28E-01	1.5E-02
82.5	1.53E-01	1.7E-02
87.6	1.43E-01	1.7E-02
92.7	1.01E-01	1.4E-02
97.7	6.85E-02	1.2E-02
102.7	5.70E-02	1.1E-02
107.6	4.44E-02	9.5E-03
112.5	2.85E-02	7.6E-03
117.2	2.39E-02	7.1E-03
122.0	2.85E-02	7.9E-03
126.7	3.91E-02	9.3E-03
131.3	4.36E-02	9.9E-03
135.9	1.06E-01	1.7E-02
140.4	1.14E-01	1.7E-02
145.0	1.41E-01	1.9E-02
149.4	1.74E-01	2.1E-02
153.8	1.93E-01	2.3E-02

TABLE B65

12C(3HE,P)14N
BEAM ENERGY = 17.5 MEV
EX. ENERGY = 4.91 MEV

ANGLE C.M.	dσ/dω (MB/ST)	ERROR (MB/ST)
11.3	6.15E-01	1.9E-01
17.0	8.12E-01	1.6E-01
22.6	8.90E-01	3.2E-02
28.3	7.82E-01	3.4E-02
33.8	7.75E-01	3.7E-02
39.4	6.45E-01	3.8E-02
45.0	6.60E-01	3.5E-02
50.4	5.05E-01	3.0E-02
55.9	3.89E-01	2.6E-02
61.3	3.15E-01	2.4E-02
66.7	2.14E-01	1.9E-02
72.0	1.75E-01	1.7E-02
77.2	1.22E-01	1.5E-02
82.5	1.34E-01	1.5E-02
87.6	1.38E-01	1.6E-02
92.7	9.73E-02	1.3E-02
97.7	7.47E-02	1.2E-02
102.7	4.51E-02	9.6E-03
107.6	3.01E-02	7.8E-03
112.5	3.48E-02	8.5E-03
117.2	2.41E-02	7.2E-03
122.0	2.47E-02	7.4E-03
126.7	1.45E-02	5.6E-03
131.3	4.68E-02	1.0E-02
135.9	7.05E-02	1.3E-02
140.4	7.15E-02	1.3E-02
145.0	8.04E-02	1.4E-02
149.4	8.93E-02	1.5E-02
153.8	1.29E-01	1.8E-02

TABLE B 66

12C(3HE,P)14N
BEAM ENERGY = 18.0 MEV
EX. ENERGY = 4.91 MEV

ANGLE C.M.	dσ/dω (MB/ST)	ERROR (MB/ST)
11.3	7.35E-01	2.2E-01
17.0	7.65E-01	1.5E-01
22.6	8.26E-01	4.5E-02
28.3	7.94E-01	3.9E-02
33.8	7.13E-01	3.6E-02
39.4	6.96E-01	3.9E-02
44.9	6.30E-01	3.4E-02
50.4	5.15E-01	3.0E-02
55.9	4.19E-01	2.8E-02
61.3	2.96E-01	2.2E-02
66.7	1.87E-01	1.8E-02
72.0	1.24E-01	1.5E-02
77.2	1.03E-01	1.3E-02
82.4	9.71E-02	1.3E-02
87.6	9.19E-02	1.2E-02
92.7	6.62E-02	9.7E-03
97.7	8.53E-02	1.2E-02
102.7	6.70E-02	1.2E-02
107.6	6.96E-02	1.2E-02
112.4	3.02E-02	7.8E-03
117.2	5.09E-02	1.0E-02
122.0	2.92E-02	7.8E-03
126.7	3.84E-02	9.2E-03
131.3	2.49E-02	7.4E-03
135.9	3.84E-02	9.4E-03
140.4	5.45E-02	1.1E-02
144.9	5.03E-02	1.1E-02
149.4	8.52E-02	1.5E-02
153.8	7.03E-02	1.3E-02

TABLE B67

12C(3HE,P)14N
BEAM ENERGY = 12.0 MEV
EX. ENERGY = 5.11 MEV

ANGLE C.M.	dσ/dω (MB/ST)	ERROR (MB/ST)
6.8	9.91E 00	2.8E 00
11.4	1.06E 01	2.1E 00
17.0	9.35E 00	1.9E 00
22.7	6.90E 00	9.5E-02
28.3	5.50E 00	9.1E-02
33.9	4.24E 00	7.9E-02
39.5	3.25E 00	6.7E-02
45.0	2.67E 00	5.9E-02
50.5	2.36E 00	5.5E-02
56.0	2.09E 00	5.1E-02
61.4	2.00E 00	5.0E-02
66.8	1.98E 00	5.0E-02
72.1	1.83E 00	4.8E-02
77.3	1.60E 00	4.5E-02
82.5	1.35E 00	4.1E-02
87.7	1.22E 00	3.8E-02
92.8	1.08E 00	3.9E-02
97.8	1.03E 00	3.8E-02
102.8	1.02E 00	3.8E-02
107.7	1.11E 00	4.1E-02
112.5	1.25E 00	4.4E-02
117.3	1.33E 00	4.4E-02
122.1	1.56E 00	5.1E-02
126.8	1.69E 00	5.5E-02
131.4	1.78E 00	5.7E-02
136.0	1.82E 00	5.8E-02
140.5	1.82E 00	5.9E-02
145.0	1.72E 00	5.7E-02
149.5	1.61E 00	5.5E-02
153.9	1.40E 00	5.1E-02

TABLE B68

12C(3HE,P)14N
BEAM ENERGY = 12.5 MEV
EX. ENERGY = 5.11 MEV

ANGLE C.M.	dσ/dω (MB/ST)	ERROR (MB/ST)
11.4	8.32E 00	1.7E 00
17.0	7.16E 00	1.4E 00
22.7	5.50E 00	1.2E-01
28.3	3.95E 00	1.0E-01
33.9	2.45E 00	5.6E-02
39.5	2.45E 00	5.7E-02
45.0	1.94E 00	4.9E-02
50.5	1.78E 00	4.6E-02
56.0	1.75E 00	4.6E-02
61.4	1.54E 00	4.3E-02
66.8	1.31E 00	3.9E-02
72.1	1.20E 00	3.7E-02
77.3	1.04E 00	3.4E-02
82.5	7.52E-01	2.8E-02
87.7	7.76E-01	2.9E-02
92.8	7.23E-01	2.8E-02
97.8	7.96E-01	3.3E-02
102.8	8.99E-01	3.6E-02
107.7	1.03E 00	3.9E-02
112.5	1.17E 00	4.3E-02
117.3	1.34E 00	4.7E-02
122.1	1.48E 00	5.0E-02
126.8	1.56E 00	5.2E-02
131.4	1.69E 00	5.5E-02
136.0	1.55E 00	5.3E-02
140.5	1.59E 00	5.4E-02
145.0	1.35E 00	4.9E-02
149.5	1.11E 00	4.4E-02
153.9	9.70E-01	4.1E-02

TABLE B69

12C(3HE,P)14N
BEAM ENERGY = 13.0 MEV
EX. ENERGY = 5.11 MEV

ANGLE C.M.	dσ/dω (MB/ST)	ERROR (MB/ST)
11.4	8.55E 00	1.7E 00
17.0	7.50E 00	1.5E 00
22.7	5.13E 00	1.1E-01
28.3	3.46E 00	9.4E-02
33.9	3.05E 00	9.0E-02
39.5	2.31E 00	7.5E-02
45.0	2.15E 00	7.2E-02
50.5	2.24E 00	7.5E-02
56.0	1.91E 00	6.8E-02
61.4	1.79E 00	6.6E-02
66.8	1.62E 00	6.2E-02
72.1	1.32E 00	5.5E-02
77.3	1.04E 00	4.8E-02
82.5	9.63E-01	4.6E-02
87.7	8.51E-01	4.3E-02
92.8	8.45E-01	4.5E-02
97.8	9.55E-01	4.6E-02
102.8	1.10E 00	5.1E-02
107.7	1.29E 00	5.7E-02
112.5	1.60E 00	6.6E-02
117.3	1.66E 00	6.7E-02
122.1	1.81E 00	7.2E-02
126.8	1.89E 00	7.5E-02
131.4	1.90E 00	7.6E-02
136.0	1.65E 00	7.0E-02
140.5	1.50E 00	6.7E-02
145.0	1.51E 00	6.8E-02
149.5	1.21E 00	5.9E-02
153.9	9.52E-01	5.2E-02

TABLE B70

12C(3HE,P)14N
BEAM ENERGY = 13.5 MEV
EX. ENERGY = 5.11 MEV

ANGLE C.M.	dσ/dω (MB/ST)	ERROR (MB/ST)
6.8	1.12E 01	3.4E 00
11.3	8.72E 00	1.7E 00
17.0	7.19E 00	1.4E 00
22.7	5.28E 00	1.2E-01
28.3	3.98E 00	1.0E-01
33.9	2.55E 00	8.0E-02
39.5	1.97E 00	6.8E-02
45.0	1.83E 00	6.4E-02
50.5	1.87E 00	6.5E-02
56.0	1.76E 00	6.3E-02
61.4	1.64E 00	6.1E-02
66.7	1.45E 00	5.7E-02
72.1	1.23E 00	5.2E-02
77.3	8.90E-01	4.2E-02
82.5	6.73E-01	3.6E-02
87.7	5.75E-01	3.3E-02
92.8	6.19E-01	3.6E-02
97.8	7.60E-01	4.0E-02
102.8	9.69E-01	4.8E-02
107.7	1.18E 00	5.4E-02
112.5	1.42E 00	6.2E-02
117.3	1.53E 00	6.5E-02
122.1	1.68E 00	6.9E-02
126.7	1.74E 00	7.2E-02
131.4	1.65E 00	7.0E-02
136.0	1.68E 00	7.2E-02
140.5	1.51E 00	6.7E-02

TABLE B71

12C(3HE,P)14N
BEAM ENERGY = 14.0 MEV
EX. ENERGY = 5.11 MEV

ANGLE C.M.	dσ/dω (MB/ST)	ERROR (MB/ST)
11.3	6.56E 00	1.3E 00
17.0	5.91E 00	1.2E 00
22.7	3.96E 00	1.1E-01
28.3	2.58E 00	8.1E-02
33.9	2.14E 00	9.4E-02
39.5	1.68E 00	6.3E-02
45.0	1.66E 00	6.2E-02
50.5	1.77E 00	6.5E-02
56.0	1.63E 00	6.2E-02
61.4	1.51E 00	5.9E-02
66.7	1.37E 00	5.6E-02
72.1	1.09E 00	4.9E-02
77.3	8.26E-01	4.2E-02
82.5	6.17E-01	3.5E-02
87.7	5.44E-01	3.3E-02
92.8	5.34E-01	3.3E-02
97.8	6.55E-01	3.8E-02
102.8	8.01E-01	4.3E-02
107.7	9.98E-01	5.0E-02
112.5	1.03E 00	5.0E-02
117.3	1.28E 00	5.9E-02
122.1	1.35E 00	6.1E-02
126.7	1.56E 00	7.0E-02
131.4	1.51E 00	6.7E-02
136.0	1.42E 00	6.5E-02
140.5	1.28E 00	6.0E-02
145.0	1.15E 00	5.7E-02
149.5	1.09E 00	5.6E-02
153.9	4.15E-01	4.5E-02

TABLE B72

12C(3HE,P)14N
BEAM ENERGY = 14.5 MEV
EX. ENERGY = 5.11 MEV

ANGLE C.M.	dσ/dω (MB/ST)	ERROR (MB/ST)
11.2	4.83E 00	9.7E-01
16.8	3.95E 00	7.9E-01
22.7	2.75E 00	1.4E-01
28.3	2.19E 00	1.2E-01
33.9	1.83E 00	1.0E-01
39.5	1.64E 00	9.2E-02
45.0	1.73E 00	9.6E-02
50.5	1.98E 00	1.1E-01
56.0	2.02E 00	1.1E-01
61.4	1.83E 00	1.0E-01
66.7	1.60E 00	9.2E-02
72.1	1.27E 00	7.6E-02
77.3	9.30E-01	6.0E-02
82.5	6.85E-01	4.8E-02
87.7	5.77E-01	4.2E-02
92.8	5.10E-01	3.9E-02
97.8	6.20E-01	4.5E-02
102.8	7.28E-01	5.1E-02
107.7	9.50E-01	6.3E-02
112.5	1.09E 00	7.0E-02
117.3	1.27E 00	8.0E-02
122.1	1.41E 00	8.7E-02
126.7	1.39E 00	8.7E-02
131.4	1.40E 00	8.6E-02
136.0	1.41E 00	8.7E-02
140.5	1.18E 00	7.7E-02
145.0	1.06E 00	7.1E-02
149.5	9.42E-01	6.5E-02
153.9	7.07E-01	5.3E-02

TABLE B73

12C(3HE,P)14N
BEAM ENERGY = 15.0 MEV
EX. ENERGY = 5.11 MEV

ANGLE C.M.	dσ/dω (MB/ST)	ERROR (MB/ST)
11.3	4.26E-01	8.3E-01
17.0	4.08E 00	8.2E-01
22.7	3.22E 00	1.3E-01
28.3	2.16E 00	9.7E-02
33.9	1.87E 00	5.1E-02
39.5	1.68E 00	4.8E-02
45.0	1.78E 00	5.0E-02
50.5	1.91E 00	5.3E-02
56.0	1.85E 00	5.2E-02
61.4	1.65E 00	4.8E-02
66.7	1.34E 00	4.3E-02
72.1	9.97E-01	3.6E-02
77.3	7.78E-01	3.1E-02
82.5	5.71E-01	2.6E-02
87.7	4.47E-01	2.2E-02
92.8	3.96E-01	2.1E-02
97.8	5.01E-01	2.4E-02
102.8	6.22E-01	2.7E-02
107.7	7.38E-01	3.1E-02
112.5	8.31E-01	3.3E-02
117.3	9.44E-01	3.6E-02
122.1	9.24E-01	3.6E-02
126.7	9.38E-01	3.7E-02
131.4	9.37E-01	3.7E-02
136.0	8.65E-01	3.5E-02
140.5	7.20E-01	3.2E-02
145.0	6.73E-01	3.1E-02
149.5	5.78E-01	2.9E-02
153.9	4.81E-01	2.6E-02

TABLE B74

12C(3HE,P)14N
BEAM ENERGY = 15.5 MEV
EX. ENERGY = 5.11 MEV

ANGLE C.M.	dσ/dω (MB/ST)	ERROR (MB/ST)
6.8	5.85E 00	1.8E 00
11.3	4.89E 00	9.8E-01
17.0	4.48E 00	9.0E-01
22.7	3.44E 00	1.4E-01
28.3	2.67E 00	1.2E-01
33.9	2.30E 00	5.9E-02
39.5	2.23E 00	5.9E-02
45.0	2.29E 00	6.0E-02
50.5	2.26E 00	5.9E-02
56.0	2.01E 00	5.6E-02
61.4	1.69E 00	4.9E-02
66.7	1.47E 00	4.6E-02
72.0	1.07E 00	3.8E-02
77.3	7.66E-01	3.1E-02
82.5	5.79E-01	2.7E-02
87.7	5.21E-01	2.3E-02
92.8	5.15E-01	2.3E-02
97.8	5.68E-01	2.5E-02
102.8	6.33E-01	2.6E-02
107.7	7.01E-01	2.8E-02
112.5	7.51E-01	2.9E-02
117.3	7.57E-01	3.0E-02
122.0	7.97E-01	3.1E-02
126.7	7.41E-01	3.0E-02
131.4	6.65E-01	2.9E-02
136.0	6.49E-01	2.8E-02
140.5	6.02E-01	2.7E-02
145.0	5.20E-01	2.6E-02
149.5	4.93E-01	2.5E-02
153.9	4.80E-01	2.5E-02

TABLE B75

12C(3HE,P)14N
BEAM ENERGY = 16.0 MEV
EX. ENERGY = 5.11 MEV

ANGLE C.M.	dσ/dω (MB/ST)	ERROR (MB/ST)
11.3	4.02E 00	8.0E-01
17.0	3.46E 00	6.9E-01
22.7	2.75E 00	1.2E-01
28.3	2.41E 00	1.1E-01
33.9	2.23E 00	1.0E-01
39.5	2.37E 00	6.7E-02
45.0	2.44E 00	6.9E-02
50.5	2.34E 00	6.7E-02
56.0	2.16E 00	6.4E-02
61.4	1.67E 00	5.4E-02
66.7	1.20E 00	4.4E-02
72.0	9.55E-01	3.9E-02
77.3	7.65E-01	3.4E-02
82.5	5.96E-01	2.9E-02
87.7	6.20E-01	3.0E-02
92.7	5.41E-01	2.7E-02
97.8	5.87E-01	2.9E-02
102.7	6.11E-01	3.0E-02
107.7	6.20E-01	3.1E-02
112.5	5.64E-01	2.9E-02
117.3	5.59E-01	2.9E-02
122.0	5.17E-01	2.8E-02
126.7	4.93E-01	2.8E-02
131.4	5.59E-01	3.0E-02
136.0	6.59E-01	3.3E-02
140.5	6.36E-01	3.3E-02
145.0	6.22E-01	3.3E-02
149.5	6.21E-01	3.3E-02
153.9	5.52E-01	5.0E-02

TABLE B76

12C(3HE,P)14N
BEAM ENERGY = 16.5 MEV
EX. ENERGY = 5.11 MEV

ANGLE C.M.	dσ/dω (MB/ST)	ERROR (MB/ST)
11.3	3.49E 00	7.6E-01
17.0	3.02E 00	6.0E-01
22.7	2.61E 00	7.8E-02
28.3	2.51E 00	7.8E-02
33.9	2.30E 00	7.5E-02
39.4	2.34E 00	7.6E-02
45.0	2.37E 00	7.7E-02
50.5	2.28E 00	7.6E-02
55.9	1.96E 00	6.9E-02
61.4	1.63E 00	6.2E-02
66.7	1.20E 00	5.1E-02
72.0	9.17E-01	4.5E-02
77.3	6.76E-01	3.7E-02
82.5	6.39E-01	3.7E-02
87.7	4.76E-01	3.1E-02
92.7	5.00E-01	3.5E-02
97.8	5.51E-01	3.5E-02
102.7	5.54E-01	3.4E-02
107.7	5.96E-01	3.6E-02
112.5	5.85E-01	3.6E-02
117.3	5.48E-01	3.5E-02
122.0	5.53E-01	3.5E-02
126.7	5.47E-01	3.6E-02
131.4	5.20E-01	3.5E-02
135.9	5.40E-01	3.6E-02
140.5	5.50E-01	3.7E-02
145.0	6.01E-01	3.9E-02
149.4	4.84E-01	3.4E-02
153.9	6.09E-01	3.9E-02

TABLE B77

12C(3HE,P)14N
BEAM ENERGY = 17.0 MEV
EX. ENERGY = 5.11 MEV

ANGLE C.M.	dσ/dω (MB/ST)	ERROR (MB/ST)
6.8	3.57E 00	1.1E 00
11.3	2.91E 00	5.9E-01
17.0	2.81E 00	5.6E-01
22.7	2.42E 00	1.0E-01
28.3	2.08E 00	7.1E-02
33.9	2.06E 00	7.1E-02
39.4	2.20E 00	7.4E-02
45.0	2.31E 00	7.7E-02
50.5	2.25E 00	7.7E-02
55.9	1.80E 00	6.7E-02
61.4	1.48E 00	6.0E-02
66.7	1.11E 00	5.1E-02
72.0	9.13E-01	4.6E-02
77.3	6.30E-01	3.7E-02
82.5	5.64E-01	3.5E-02
87.7	5.44E-01	3.5E-02
92.7	5.06E-01	3.4E-02
97.8	5.79E-01	3.8E-02
102.7	5.30E-01	3.6E-02
107.7	5.22E-01	3.6E-02
112.5	5.25E-01	3.6E-02
117.3	5.02E-01	3.6E-02
122.0	4.95E-01	3.6E-02
126.7	4.93E-01	3.6E-02
131.4	5.65E-01	4.0E-02
135.9	5.56E-01	4.0E-02
140.5	5.79E-01	4.1E-02
145.0	6.02E-01	4.2E-02
149.4	5.67E-01	4.1E-02
153.9	5.65E-01	4.1E-02

TABLE B78

12C(3HE,P)14N
BEAM ENERGY = 17.5 MEV
EX. ENERGY = 5.11 MEV

ANGLE C.M.	dσ/dω (MB/ST)	ERROR (MB/ST)
6.8	2.96E 00	8.9E-01
11.3	2.80E 00	5.6E-01
17.0	2.19E 00	4.4E-01
22.6	1.99E 00	5.0E-02
28.3	1.78E 00	5.7E-02
33.9	1.93E 00	6.7E-02
39.4	2.02E 00	6.4E-02
45.0	2.12E 00	7.1E-02
50.5	1.93E 00	6.8E-02
55.9	1.64E 00	6.3E-02
61.4	1.44E 00	5.8E-02
66.7	9.76E-01	4.6E-02
72.0	7.56E-01	4.0E-02
77.3	6.60E-01	3.7E-02
82.5	5.40E-01	3.3E-02
87.7	5.15E-01	3.3E-02
92.7	4.46E-01	3.0E-02
97.8	4.39E-01	3.3E-02
102.7	4.29E-01	3.3E-02
107.7	4.50E-01	3.3E-02
112.5	4.87E-01	3.5E-02
117.3	4.72E-01	3.5E-02
122.0	4.77E-01	3.6E-02
126.7	4.76E-01	3.6E-02
131.4	5.14E-01	3.8E-02
135.9	5.20E-01	3.8E-02
140.5	6.23E-01	4.3E-02
145.0	5.39E-01	4.0E-02
149.4	5.18E-01	3.8E-02
153.9	4.69E-01	3.7E-02

TABLE B79

12C(3HE,P)14N
BEAM ENERGY = 18.0 MEV
EX. ENERGY = 5.11 MEV

ANGLE C.M.	dσ/dω (MB/ST)	ERROR (MB/ST)
6.8	3.19E 00	9.6E-01
11.3	2.62E 00	5.2E-01
17.0	2.40E 00	4.8E-01
22.6	1.78E 00	1.0E-01
28.3	1.58E 00	5.9E-02
33.9	1.64E 00	6.0E-02
39.4	1.62E 00	6.0E-02
45.0	1.66E 00	6.1E-02
50.5	1.51E 00	5.8E-02
55.9	1.41E 00	5.5E-02
61.4	1.12E 00	4.8E-02
66.7	8.26E-01	4.1E-02
72.0	7.56E-01	3.9E-02
77.3	5.52E-01	3.3E-02
82.5	5.36E-01	3.3E-02
87.6	3.85E-01	2.7E-02
92.7	3.36E-01	2.8E-02
97.8	3.67E-01	3.0E-02
102.7	4.02E-01	3.1E-02
107.6	4.03E-01	3.2E-02
112.5	4.49E-01	3.3E-02
117.3	4.41E-01	3.4E-02
122.0	4.64E-01	3.4E-02
126.7	4.39E-01	3.4E-02
131.4	4.44E-01	3.5E-02
135.9	5.00E-01	3.7E-02
140.5	5.46E-01	4.0E-02
145.0	4.38E-01	3.5E-02
149.4	4.80E-01	3.7E-02
153.9	4.05E-01	3.4E-02

TABLE B80

12C(3HE,P)14N
BEAM ENERGY = 12.0 MEV
EX. ENERGY = 5.69 MEV

ANGLE C.M.	dσ/dω (MB/ST)	ERROR (MB/ST)
11.4	1.15E 00	2.3E-01
17.1	1.43E 00	2.9E-01
22.8	1.59E 00	3.6E-02
28.4	1.84E 00	4.4E-02
34.0	1.73E 00	4.7E-02
39.6	1.77E 00	4.4E-02
45.2	1.73E 00	4.4E-02
50.7	1.52E 00	4.1E-02
56.2	1.39E 00	4.0E-02
61.6	1.17E 00	3.6E-02
67.0	1.04E 00	3.4E-02
72.3	8.88E-01	3.1E-02
77.6	7.71E-01	2.9E-02
82.8	7.50E-01	2.8E-02
88.0	7.01E-01	2.7E-02
93.0	7.64E-01	3.2E-02
98.1	7.98E-01	3.3E-02
103.0	8.99E-01	3.6E-02
108.0	8.75E-01	4.0E-02
112.8	9.23E-01	3.7E-02
117.6	9.51E-01	3.8E-02
122.3	9.71E-01	3.9E-02
127.0	1.02E 00	4.0E-02
131.6	9.94E-01	4.0E-02
136.2	1.01E 00	4.1E-02
140.7	1.23E 00	4.6E-02
145.2	1.38E 00	5.0E-02
149.6	1.58E 00	5.5E-02
154.0	1.82E 00	6.0E-02

TABLE B81

12C(3HE,P)14N
BEAM ENERGY = 12.5 MEV
EX. ENERGY = 5.69 MEV

ANGLE C.M.	dσ/dω (MB/ST)	ERROR (MB/ST)
11.4	1.13E 00	2.3E-01
17.1	1.52E 00	3.0E-01
22.7	1.98E 00	6.1E-02
28.4	2.14E 00	6.9E-02
34.0	2.14E 00	5.6E-02
39.6	2.05E 00	5.0E-02
45.2	1.73E 00	4.5E-02
50.7	1.36E 00	3.9E-02
56.2	1.21E 00	3.7E-02
61.6	8.94E-01	3.1E-02
67.0	7.05E-01	2.6E-02
72.3	6.07E-01	2.4E-02
77.6	5.70E-01	2.4E-02
82.8	4.89E-01	2.2E-02
87.9	5.60E-01	2.4E-02
93.0	5.66E-01	2.4E-02
98.1	5.14E-01	2.6E-02
103.0	6.36E-01	2.9E-02
107.9	5.93E-01	2.8E-02
112.8	5.97E-01	2.9E-02
117.6	5.59E-01	2.8E-02
122.3	5.85E-01	2.9E-02
127.0	5.42E-01	2.8E-02
131.6	5.60E-01	2.9E-02
136.2	5.97E-01	3.0E-02
140.7	6.32E-01	3.1E-02
145.2	7.33E-01	3.4E-02
149.6	8.75E-01	3.8E-02
154.0	9.85E-01	4.1E-02

TABLE B82

12C(3HE,P)14N
BEAM ENERGY = 13.0 MEV
EX. ENERGY = 5.69 MEV

ANGLE C.M.	dσ/dω (MB/ST)	ERROR (MB/ST)
11.4	2.26E 00	3.7E-01
17.1	2.82E 00	5.6E-01
22.7	2.49E 00	6.9E-02
28.4	2.16E 00	6.9E-02
34.0	2.01E 00	6.7E-02
39.6	1.78E 00	6.3E-02
45.2	1.69E 00	6.1E-02
50.7	1.30E 00	5.3E-02
56.2	1.03E 00	4.6E-02
61.6	8.53E-01	4.1E-02
67.0	6.00E-01	3.4E-02
72.3	4.64E-01	2.9E-02
77.6	4.83E-01	3.0E-02
82.8	4.92E-01	3.1E-02
87.9	4.24E-01	2.9E-02
93.0	4.47E-01	3.0E-02
98.0	3.88E-01	2.7E-02
103.0	4.30E-01	2.9E-02
107.9	3.73E-01	2.7E-02
112.8	3.83E-01	2.8E-02
117.6	3.17E-01	2.5E-02
122.3	2.16E-01	2.1E-02
127.0	2.18E-01	2.1E-02
131.6	2.40E-01	2.3E-02
136.2	2.53E-01	2.3E-02
140.7	2.98E-01	2.6E-02
145.2	3.52E-01	2.9E-02
149.6	4.25E-01	3.2E-02
154.0	4.47E-01	3.4E-02

TABLE B83

12C(3HE,P)14N
BEAM ENERGY = 13.5 MEV
EX. ENERGY = 5.69 MEV

ANGLE C.M.	dσ/dω (MB/ST)	ERROR (MB/ST)
11.4	1.57E 00	3.0E-01
17.1	1.94E 00	3.9E-01
22.7	2.19E 00	1.0E-01
28.4	2.30E 00	7.1E-02
34.0	2.15E 00	7.1E-02
39.6	1.85E 00	6.5E-02
45.1	1.51E 00	5.7E-02
50.7	1.14E 00	4.8E-02
56.1	8.79E-01	4.1E-02
61.6	6.73E-01	3.5E-02
66.9	6.02E-01	3.3E-02
72.3	5.12E-01	3.1E-02
77.5	5.04E-01	3.0E-02
82.8	5.26E-01	3.3E-02
87.9	5.21E-01	3.1E-02
93.0	5.53E-01	3.3E-02
98.0	5.61E-01	3.3E-02
103.0	4.69E-01	3.1E-02
107.9	4.18E-01	2.9E-02
112.8	3.41E-01	2.7E-02
117.5	2.64E-01	2.3E-02
122.3	2.67E-01	2.4E-02
126.9	2.05E-01	2.1E-02
131.6	2.12E-01	2.1E-02
136.1	2.08E-01	2.1E-02
140.7	2.81E-01	2.5E-02

TABLE B84

12C(3HE,P)14N
BEAM ENERGY = 14.0 MEV
EX. ENERGY = 5.69 MEV

ANGLE C.M.	dσ/dω (MB/ST)	ERROR (MB/ST)
11.4	1.25E 00	2.5E-01
17.1	3.16E 00	6.3E-01
22.7	2.11E 00	7.0E-02
28.4	2.09E 00	7.1E-02
34.0	1.75E 00	6.4E-02
39.6	1.63E 00	6.1E-02
45.1	1.33E 00	5.4E-02
50.7	1.09E 00	4.8E-02
56.1	9.33E-01	4.3E-02
61.6	8.46E-01	4.1E-02
66.9	7.33E-01	3.8E-02
72.3	7.28E-01	3.8E-02
77.5	7.20E-01	3.8E-02
82.7	6.46E-01	3.6E-02
87.9	6.15E-01	3.6E-02
93.0	5.27E-01	3.2E-02
98.0	5.09E-01	3.2E-02
103.0	4.55E-01	3.1E-02
107.9	4.24E-01	3.2E-02
112.7	3.50E-01	2.7E-02
117.5	3.17E-01	2.6E-02
122.3	3.65E-01	2.8E-02
126.9	3.90E-01	3.1E-02
131.6	3.81E-01	3.0E-02
136.1	4.31E-01	3.2E-02
140.7	4.39E-01	3.2E-02
145.1	5.44E-01	3.7E-02
149.6	5.59E-01	3.8E-02
154.0	5.19E-01	5.1E-02

TABLE B85

12C(3HE,P)14N
BEAM ENERGY = 14.5 MEV
EX. ENERGY = 5.69 MEV

ANGLE C.M.	dσ/dω (MB/ST)	ERROR (MB/ST)
11.4	1.61E 00	3.2E-01
16.8	1.55E 00	3.1E-01
22.7	1.26E 00	7.3E-02
28.4	1.24E 00	7.3E-02
34.0	1.05E 00	7.2E-02
39.6	1.04E 00	7.0E-02
45.1	1.03E 00	6.3E-02
50.6	1.05E 00	6.4E-02
56.1	9.88E-01	6.2E-02
61.5	1.13E 00	6.9E-02
66.9	9.02E-01	5.8E-02
72.2	8.06E-01	5.3E-02
77.5	7.82E-01	5.3E-02
82.7	6.84E-01	4.8E-02
87.9	6.44E-01	4.6E-02
93.0	5.37E-01	4.0E-02
98.0	4.67E-01	3.7E-02
103.0	3.98E-01	3.3E-02
107.9	3.98E-01	3.3E-02
112.7	3.23E-01	2.9E-02
117.5	3.71E-01	3.2E-02
122.2	4.59E-01	3.7E-02
126.9	4.33E-01	3.6E-02
131.6	4.87E-01	3.9E-02
136.1	4.12E-01	3.5E-02
140.6	4.97E-01	4.1E-02
145.1	4.84E-01	4.0E-02
149.6	4.69E-01	3.9E-02
154.0	4.60E-01	3.9E-02

TABLE B86

12C(3HE,P)14N
BEAM ENERGY = 15.0 MEV
EX. ENERGY = 5.69 MEV

ANGLE C.M.	dσ/dω (MB/ST)	ERROR (MB/ST)
11.4	2.01E 00	4.0E-01
17.1	1.65E 00	3.3E-01
22.7	1.18E 00	6.6E-02
28.4	1.11E 00	6.5E-02
34.0	9.76E-01	3.4E-02
39.6	8.98E-01	3.2E-02
45.1	1.02E 00	3.5E-02
50.6	8.56E-01	3.2E-02
56.1	9.42E-01	3.4E-02
61.5	9.03E-01	3.3E-02
66.9	7.66E-01	3.0E-02
72.2	6.91E-01	2.8E-02
77.5	6.31E-01	2.7E-02
82.7	5.29E-01	2.4E-02
87.9	4.81E-01	2.2E-02
93.0	4.13E-01	2.1E-02
98.0	3.63E-01	2.0E-02
103.0	3.63E-01	2.0E-02
107.9	3.38E-01	1.9E-02
112.7	2.78E-01	1.7E-02
117.5	2.94E-01	1.8E-02
122.2	3.29E-01	2.0E-02
126.9	3.79E-01	2.2E-02
131.5	3.67E-01	2.1E-02
136.1	4.37E-01	2.4E-02
140.6	3.61E-01	2.2E-02
145.1	4.24E-01	2.4E-02
149.6	3.80E-01	2.3E-02
154.0	2.68E-01	1.9E-02

TABLE B87

12C(3HE,P)14N
BEAM ENERGY = 15.5 MEV
EX. ENERGY = 5.69 MEV

ANGLE C.M.	dσ/dω (MB/ST)	ERROR (MB/ST)
11.4	2.22E 00	4.4E-01
17.1	1.82E 00	3.6E-01
22.7	9.19E-01	5.8E-02
28.4	8.85E-01	5.7E-02
34.0	7.04E-01	2.8E-02
39.6	6.87E-01	2.8E-02
45.1	7.77E-01	3.0E-02
50.6	8.90E-01	3.3E-02
56.1	7.63E-01	3.0E-02
61.5	8.16E-01	3.1E-02
66.9	7.05E-01	2.9E-02
72.2	5.42E-01	2.5E-02
77.5	5.64E-01	2.6E-02
82.7	5.30E-01	2.5E-02
87.9	3.20E-01	2.1E-02
92.9	2.58E-01	1.5E-02
98.0	2.01E-01	1.3E-02
102.9	2.21E-01	1.4E-02
107.9	2.90E-01	1.7E-02
112.7	2.96E-01	1.7E-02
117.5	3.70E-01	2.0E-02
122.2	4.12E-01	2.1E-02
126.9	4.15E-01	2.2E-02
131.5	4.39E-01	2.3E-02
136.1	4.14E-01	2.2E-02
140.6	4.08E-01	2.2E-02
145.1	4.22E-01	2.3E-02
149.6	3.98E-01	2.2E-02
154.0	3.34E-01	2.0E-02

TABLE B88

12C(3HE,P)14N
BEAM ENERGY = 16.0 MEV
EX. ENERGY = 5.69 MEV

ANGLE C.M.	dσ/dω (MB/ST)	ERROR (MB/ST)
11.3	1.78E 00	3.6E-01
17.1	1.51E 00	3.0E-01
22.7	9.36E-01	5.5E-02
28.4	5.75E-01	4.3E-02
34.0	5.45E-01	4.2E-02
39.6	7.50E-01	3.2E-02
45.1	7.94E-01	3.3E-02
50.6	8.53E-01	3.5E-02
56.1	7.86E-01	3.3E-02
61.5	6.42E-01	3.0E-02
66.9	6.40E-01	3.0E-02
72.2	4.47E-01	2.4E-02
77.5	3.65E-01	2.2E-02
82.7	3.00E-01	2.0E-02
87.8	2.98E-01	2.0E-02
92.9	9.86E-02	1.0E-02
98.0	2.53E-01	1.8E-02
102.9	3.27E-01	2.1E-02
107.8	3.19E-01	2.1E-02
112.7	3.63E-01	2.3E-02
117.5	3.27E-01	2.2E-02
122.2	3.94E-01	2.4E-02
126.9	3.80E-01	2.4E-02
131.5	3.94E-01	2.5E-02
136.1	2.95E-01	2.1E-02
140.6	3.41E-01	2.3E-02
145.1	4.81E-01	2.8E-02
149.6	3.61E-01	2.4E-02
154.0	4.24E-01	2.9E-02

TABLE B89

12C(3HE,P)14N
BEAM ENERGY = 16.5 MEV
EX. ENERGY = 5.69 MEV

ANGLE C.M.	dσ/dω (MB/ST)	ERROR (MB/ST)
11.3	1.66E 00	3.3E-01
17.1	1.15E 00	2.3E-01
22.7	9.10E-01	3.9E-02
28.4	5.28E-01	3.0E-02
34.0	6.20E-01	3.4E-02
39.6	6.80E-01	3.6E-02
45.1	7.99E-01	4.0E-02
50.6	8.48E-01	4.2E-02
56.1	8.67E-01	4.2E-02
61.5	7.35E-01	3.9E-02
66.9	5.88E-01	3.4E-02
72.2	5.63E-01	3.4E-02
77.5	4.29E-01	2.9E-02
82.7	3.49E-01	2.6E-02
87.8	3.34E-01	2.5E-02
92.9	2.95E-01	2.6E-02
98.0	3.28E-01	2.8E-02
102.9	2.48E-01	2.2E-02
107.8	2.72E-01	2.3E-02
112.7	3.41E-01	2.7E-02
117.5	3.43E-01	2.7E-02
122.2	4.17E-01	3.0E-02
126.9	4.06E-01	3.0E-02
131.5	3.38E-01	2.7E-02
136.1	4.00E-01	3.0E-02
140.6	4.10E-01	3.1E-02
145.1	4.31E-01	3.2E-02
149.6	3.77E-01	3.0E-02
154.0	4.22E-01	3.2E-02

TABLE B90

12C(3HE,P)14N
BEAM ENERGY = 17.0 MEV
EX. ENERGY = 5.69 MEV

ANGLE C.M.	dσ/dω (MB/ST)	ERROR (MB/ST)
11.4	1.14E 00	2.2E-01
17.1	1.04E 00	2.1E-01
22.7	8.96E-01	4.1E-02
28.4	5.85E-01	3.3E-02
34.0	6.01E-01	3.3E-02
39.6	6.72E-01	3.6E-02
45.1	7.28E-01	3.8E-02
50.6	8.22E-01	4.1E-02
56.1	7.28E-01	3.9E-02
61.5	6.97E-01	3.8E-02
66.9	5.12E-01	3.2E-02
72.2	4.47E-01	3.0E-02
77.5	3.78E-01	2.7E-02
82.7	3.46E-01	2.7E-02
87.8	3.11E-01	2.5E-02
92.9	2.52E-01	2.3E-02
98.0	2.81E-01	2.5E-02
102.9	2.65E-01	2.5E-02
107.8	3.34E-01	2.8E-02
112.7	3.31E-01	2.8E-02
117.5	3.56E-01	3.0E-02
122.2	4.15E-01	3.3E-02
126.9	4.05E-01	3.3E-02
131.5	3.78E-01	3.2E-02
136.1	3.73E-01	3.3E-02
140.6	3.29E-01	3.0E-02
145.1	3.41E-01	3.2E-02
149.6	3.84E-01	3.3E-02
154.0	3.24E-01	3.0E-02

TABLE B91

12C(3HE,P)14N
BEAM ENERGY = 17.5 MEV
EX. ENERGY = 5.69 MEV

ANGLE C.M.	dσ/dω (MB/ST)	ERROR (MB/ST)
11.4	1.43E 00	2.9E-01
17.0	1.08E 00	2.2E-01
22.7	8.85E-01	3.5E-02
28.3	6.95E-01	3.2E-02
34.0	6.52E-01	3.5E-02
39.5	6.27E-01	3.4E-02
45.1	6.38E-01	3.5E-02
50.6	6.68E-01	3.6E-02
56.1	6.45E-01	3.6E-02
61.5	5.18E-01	3.2E-02
66.9	4.13E-01	2.8E-02
72.2	3.99E-01	2.7E-02
77.5	3.36E-01	2.5E-02
82.7	2.60E-01	2.2E-02
87.8	2.76E-01	2.2E-02
92.9	2.06E-01	2.0E-02
97.9	2.19E-01	2.1E-02
102.9	2.22E-01	2.3E-02
107.8	2.47E-01	2.4E-02
112.7	3.25E-01	2.8E-02
117.5	3.72E-01	3.1E-02
122.2	3.14E-01	2.5E-02
126.9	3.42E-01	3.0E-02
131.5	3.32E-01	3.0E-02
136.1	3.35E-01	3.0E-02
140.6	3.29E-01	3.0E-02
145.1	3.19E-01	3.0E-02
149.5	3.32E-01	3.1E-02
154.0	2.88E-01	2.9E-02

TABLE B92

12C(3HE,P)14N
BEAM ENERGY = 18.0 MEV
EX. ENERGY = 5.69 MEV

ANGLE C.M.	dσ/dω (MB/ST)	ERROR (MB/ST)
11.4	1.43E 00	2.9E-01
17.0	1.35E 00	2.7E-01
22.7	1.01E-01	4.6E-02
28.3	7.30E-01	3.6E-02
34.0	6.00E-01	3.2E-02
39.5	6.49E-01	3.4E-02
45.1	6.44E-01	3.4E-02
50.6	5.38E-01	2.9E-02
56.1	5.73E-01	3.2E-02
61.5	4.23E-01	2.7E-02
66.9	4.60E-01	2.8E-02
72.2	3.72E-01	2.6E-02
77.5	2.77E-01	2.3E-02
82.7	2.45E-01	1.9E-02
87.8	2.67E-01	2.2E-02
92.9	2.46E-01	2.1E-02
97.9	1.99E-01	1.9E-02
102.9	2.05E-01	2.1E-02
107.8	2.22E-01	3.2E-02
112.7	2.35E-01	2.3E-02
117.5	2.08E-01	2.2E-02
122.2	2.60E-01	2.5E-02
126.9	2.88E-01	2.7E-02
131.5	3.29E-01	2.9E-02
136.1	2.45E-01	2.5E-02
140.6	1.84E-01	2.1E-02
145.1	2.18E-01	2.9E-02
149.5	2.30E-01	2.5E-02
154.0	2.08E-01	2.4E-02

TABLE B93

12C(3HE,P)14N
BEAM ENERGY = 12.0 MEV
EX. ENERGY = 5.83 MEV

ANGLE C.M.	dσ/dω (MB/ST)	ERROR (MB/ST)
11.4	1.51E 00	3.0E-01
17.1	1.43E 00	2.9E-01
22.8	1.43E 00	3.4E-02
28.4	1.44E 00	3.8E-02
34.1	1.69E 00	5.3E-02
39.7	1.86E 00	4.7E-02
45.2	2.05E 00	4.9E-02
50.7	2.12E 00	5.1E-02
56.2	2.14E 00	5.2E-02
61.7	1.92E 00	4.9E-02
67.0	1.88E 00	4.9E-02
72.4	1.65E 00	4.5E-02
77.6	1.49E 00	4.3E-02
82.9	1.39E 00	4.1E-02
88.0	1.36E 00	4.1E-02
93.1	1.28E 00	4.3E-02
98.1	1.26E 00	4.3E-02
103.1	1.17E 00	4.2E-02
108.0	1.24E 00	4.4E-02
112.9	1.06E 00	4.0E-02
117.6	1.09E 00	4.1E-02
122.4	1.05E 00	4.1E-02
127.0	1.03E 00	4.1E-02
131.7	1.05E 00	4.1E-02
136.2	1.13E 00	4.3E-02
140.7	1.26E 00	4.7E-02
145.2	1.46E 00	5.2E-02
149.7	1.66E 00	5.6E-02
154.1	1.81E 00	6.0E-02

TABLE B94

12C(3HE,P)14N
BEAM ENERGY = 12.5 MEV
EX. ENERGY = 5.83 MEV

ANGLE C.M.	dσ/dω (MB/ST)	ERROR (MB/ST)
11.4	1.38E 00	2.8E-01
17.1	1.51E 00	3.0E-01
22.8	1.58E 00	5.3E-02
28.4	1.59E 00	5.7E-02
34.0	1.94E 00	5.2E-02
39.6	2.02E 00	5.0E-02
45.2	2.02E 00	4.9E-02
50.7	2.17E 00	5.2E-02
56.2	1.97E 00	5.0E-02
61.6	1.90E 00	4.9E-02
67.0	1.78E 00	4.7E-02
72.4	1.60E 00	4.4E-02
77.6	1.49E 00	4.3E-02
82.8	1.36E 00	4.0E-02
88.0	1.35E 00	4.1E-02
93.1	1.35E 00	4.1E-02
98.1	1.34E 00	4.5E-02
103.1	1.16E 00	4.2E-02
108.0	1.09E 00	4.1E-02
112.8	1.03E 00	3.9E-02
117.6	1.00E 00	4.0E-02
122.4	8.99E-01	3.7E-02
127.0	8.10E-01	3.5E-02
131.6	7.95E-01	3.5E-02
136.2	7.88E-01	3.5E-02
140.7	8.59E-01	3.7E-02
145.2	9.45E-01	4.0E-02
149.6	1.15E 00	4.5E-02
154.0	1.29E 00	4.9E-02

TABLE B95

12C(3HE,P)14N
BEAM ENERGY = 13.0 MEV
EX. ENERGY = 5.83 MEV

ANGLE C.M.	dσ/dω (MB/ST)	ERROR (MB/ST)
11.4	2.01E 00	4.0E-01
17.1	2.19E 00	4.4E-01
22.8	2.50E 00	6.2E-02
28.4	2.18E 00	6.6E-02
34.0	1.85E 00	6.4E-02
39.6	2.01E 00	6.8E-02
45.2	2.00E 00	6.9E-02
50.7	1.91E 00	6.7E-02
56.2	1.75E 00	6.4E-02
61.6	1.78E 00	6.5E-02
67.0	1.54E 00	6.0E-02
72.3	1.45E 00	5.8E-02
77.6	1.38E 00	5.7E-02
82.8	1.45E 00	6.0E-02
88.0	1.46E 00	6.0E-02
93.1	1.44E 00	6.0E-02
98.1	1.51E 00	6.1E-02
103.1	1.52E 00	6.2E-02
108.0	1.52E 00	6.3E-02
112.8	1.34E 00	5.9E-02
117.6	1.29E 00	5.7E-02
122.3	1.23E 00	5.7E-02
127.0	9.74E-01	5.0E-02
131.6	8.99E-01	4.8E-02
136.2	7.19E-01	4.3E-02
140.7	7.50E-01	4.4E-02
145.2	7.45E-01	4.4E-02
149.6	6.78E-01	4.2E-02
154.0	8.13E-01	4.7E-02

TABLE B96

12C(3HE,P)14N
BEAM ENERGY = 13.5 MEV
EX. ENERGY = 5.83 MEV

ANGLE C.M.	dσ/dω (MB/ST)	ERROR (MB/ST)
11.4	1.96E 00	3.9E-01
17.1	2.26E 00	4.5E-01
22.8	2.02E 00	6.2E-02
28.4	2.08E 00	6.6E-02
34.0	2.11E 00	7.0E-02
39.6	2.28E 00	7.4E-02
45.2	2.17E 00	7.2E-02
50.7	2.14E 00	7.1E-02
56.2	1.91E 00	6.7E-02
61.6	1.89E 00	6.7E-02
67.0	1.83E 00	6.6E-02
72.3	1.78E 00	6.5E-02
77.6	1.79E 00	6.5E-02
82.8	1.94E 00	7.0E-02
88.0	2.09E 00	7.3E-02
93.1	2.29E 00	7.9E-02
98.1	2.14E 00	7.6E-02
103.1	2.18E 00	7.9E-02
108.0	1.91E 00	7.3E-02
112.8	1.69E 00	6.9E-02
117.6	1.57E 00	6.6E-02
122.3	1.41E 00	6.2E-02
127.0	1.26E 00	5.9E-02
131.6	1.09E 00	5.4E-02
136.2	1.11E 00	5.6E-02
140.7	1.02E 00	5.3E-02

TABLE B97

12C(3HE,P)14N
BEAM ENERGY = 14.0 MEV
EX. ENERGY = 5.83 MEV

ANGLE C.M.	dσ/dω (MB/ST)	ERROR (MB/ST)
11.4	1.89E 00	3.8E-01
17.1	1.80E 00	3.6E-01
22.8	1.86E 00	6.4E-02
28.4	1.83E 00	6.5E-02
34.0	1.92E 00	6.7E-02
39.6	1.81E 00	6.6E-02
45.2	1.78E 00	6.5E-02
50.7	1.76E 00	6.5E-02
56.2	1.77E 00	6.5E-02
61.6	1.70E 00	6.3E-02
67.0	1.83E 00	6.7E-02
72.3	1.96E 00	7.1E-02
77.6	2.00E 00	7.2E-02
82.8	2.10E 00	7.5E-02
87.9	2.08E 00	7.5E-02
93.0	1.92E 00	7.1E-02
98.1	1.95E 00	7.6E-02
103.0	1.88E 00	7.4E-02
107.9	1.62E 00	6.8E-02
112.8	1.50E 00	6.4E-02
117.6	1.46E 00	6.4E-02
122.3	1.37E 00	6.2E-02
127.0	1.59E 00	7.1E-02
131.6	1.44E 00	6.5E-02
136.2	1.49E 00	6.7E-02
140.7	1.49E 00	6.6E-02
145.2	1.40E 00	6.4E-02
149.6	1.51E 00	6.9E-02
154.0	1.41E 00	9.3E-02

TABLE B98

12C(3HE,P)14N
BEAM ENERGY = 14.5 MEV
EX. ENERGY = 5.83 MEV

ANGLE C.M.	dσ/dω (MB/ST)	ERROR (MB/ST)
11.4	1.41E 00	2.8E-01
17.1	1.40E 00	2.8E-01
22.7	1.35E 00	1.2E-01
28.4	1.49E 00	8.4E-02
34.0	1.55E 00	8.8E-02
39.6	1.61E 00	9.0E-02
45.2	1.59E 00	9.0E-02
50.7	1.62E 00	9.1E-02
56.2	1.47E 00	8.5E-02
61.6	1.45E 00	8.4E-02
67.0	1.59E 00	9.1E-02
72.3	1.60E 00	9.2E-02
77.6	1.69E 00	9.6E-02
82.8	1.84E 00	1.0E-01
87.9	1.79E 00	1.0E-01
93.0	1.81E 00	1.0E-01
98.1	1.77E 00	1.0E-01
103.0	1.75E 00	1.0E-01
107.9	1.54E 00	9.2E-02
112.8	1.42E 00	8.7E-02
117.6	1.29E 00	8.1E-02
122.3	1.27E 00	8.0E-02
127.0	1.25E 00	8.0E-02
131.6	1.32E 00	8.3E-02
136.2	1.45E 00	8.9E-02
140.7	1.40E 00	8.8E-02
145.2	1.45E 00	9.1E-02
149.6	1.41E 00	8.9E-02
154.0	1.28E 00	8.3E-02

TABLE B99

12C(3HE,P)14N
BEAM ENERGY = 15.0 MEV
EX. ENERGY = 5.83 MEV

ANGLE C.M.	dσ/dω (MB/ST)	ERROR (MB/ST)
11.4	1.03E 00	2.1E-01
17.1	1.20E 00	2.4E-01
22.7	1.25E 00	6.9E-02
28.4	1.18E 00	3.7E-02
34.0	1.17E 00	3.8E-02
39.6	1.12E 00	3.7E-02
45.2	1.12E 00	3.7E-02
50.7	1.06E 00	3.6E-02
56.2	1.03E 00	3.6E-02
61.6	8.91E-01	3.3E-02
67.0	8.56E-01	3.2E-02
72.3	8.93E-01	3.3E-02
77.6	1.07E 00	3.7E-02
82.8	1.23E 00	4.1E-02
87.9	1.29E 00	4.1E-02
93.0	1.35E 00	4.4E-02
98.0	1.41E 00	4.5E-02
103.0	1.33E 00	4.3E-02
107.9	1.33E 00	4.4E-02
112.8	1.28E 00	4.3E-02
117.6	1.20E 00	4.2E-02
122.3	1.15E 00	4.1E-02
127.0	1.07E 00	4.0E-02
131.6	1.06E 00	4.0E-02
136.2	1.04E 00	4.0E-02
140.7	1.04E 00	4.1E-02
145.2	1.12E 00	4.3E-02
149.6	1.13E 00	4.4E-02
154.0	1.19E 00	4.5E-02

TABLE B100

12C(3HE,P)14N
BEAM ENERGY = 15.5 MEV
EX. ENERGY = 5.83 MEV

ANGLE C.M.	dσ/dω (MB/ST)	ERROR (MB/ST)
11.4	1.72E 00	3.4E-01
17.1	1.69E 00	3.4E-01
22.7	2.01E 00	9.5E-02
28.4	1.74E 00	8.7E-02
34.0	1.85E 00	5.1E-02
39.6	1.81E 00	5.1E-02
45.2	1.63E 00	4.8E-02
50.7	1.25E 00	4.0E-02
56.1	1.00E 00	3.6E-02
61.6	9.39E-01	3.4E-02
66.9	8.55E-01	3.3E-02
72.3	9.88E-01	3.6E-02
77.5	1.01E 00	3.7E-02
82.8	1.07E 00	3.9E-02
87.9	1.13E 00	4.2E-02
93.0	1.54E 00	4.4E-02
98.0	1.51E 00	4.5E-02
103.0	1.57E 00	4.6E-02
107.9	1.39E 00	4.3E-02
112.8	1.20E 00	3.9E-02
117.5	1.10E 00	3.8E-02
122.3	1.05E 00	3.7E-02
126.9	1.11E 00	3.9E-02
131.6	1.10E 00	3.9E-02
136.1	1.10E 00	3.9E-02
140.7	1.09E 00	3.9E-02
145.2	1.15E 00	4.1E-02
149.6	1.09E 00	4.0E-02
154.0	1.12E 00	4.1E-02

TABLE B101

12C(3HE,P)14N
BEAM ENERGY = 16.0 MEV
EX. ENERGY = 5.83 MEV

ANGLE C.M.	dσ/dω (MB/ST)	ERROR (MB/ST)
11.4	1.03E 00	2.1E-01
17.1	1.50E 00	3.0E-01
22.7	1.48E 00	7.4E-02
28.4	1.50E 00	7.8E-02
34.0	1.53E 00	7.9E-02
39.6	1.02E 00	3.9E-02
45.1	9.12E-01	3.6E-02
50.7	8.05E-01	3.4E-02
56.1	7.45E-01	3.2E-02
61.6	7.02E-01	3.1E-02
66.9	6.17E-01	2.9E-02
72.3	7.17E-01	3.2E-02
77.5	8.08E-01	3.5E-02
82.7	7.61E-01	3.5E-02
87.9	7.46E-01	3.4E-02
93.0	6.95E-01	3.2E-02
98.0	5.37E-01	2.8E-02
103.0	3.58E-01	2.2E-02
107.9	3.04E-01	2.0E-02
112.7	3.30E-01	2.1E-02
117.5	3.27E-01	2.2E-02
122.3	3.49E-01	2.2E-02
126.9	4.86E-01	2.8E-02
131.6	6.42E-01	3.3E-02
136.1	6.89E-01	3.4E-02
140.7	7.19E-01	3.5E-02
145.1	6.07E-01	3.2E-02
149.6	7.43E-01	3.7E-02
154.0	6.72E-01	5.9E-02

TABLE B102

12C(3HE,P)14N
BEAM ENERGY = 16.5 MEV
EX. ENERGY = 5.83 MEV

ANGLE C.M.	dσ/dω (MB/ST)	ERROR (MB/ST)
11.3	1.26E 00	2.7E-01
17.1	1.28E 00	2.6E-01
22.7	1.35E 00	5.1E-02
28.4	1.43E 00	5.5E-02
34.0	1.33E 00	5.3E-02
39.6	1.19E 00	5.0E-02
45.1	9.98E-01	4.5E-02
50.7	8.79E-01	4.3E-02
56.1	6.94E-01	3.7E-02
61.6	6.52E-01	3.6E-02
66.9	6.39E-01	3.5E-02
72.3	6.93E-01	3.8E-02
77.5	7.62E-01	4.0E-02
82.7	7.54E-01	4.1E-02
87.9	6.72E-01	3.8E-02
93.0	6.24E-01	3.9E-02
98.0	5.75E-01	3.5E-02
103.0	5.14E-01	3.3E-02
107.9	4.06E-01	2.9E-02
112.7	3.98E-01	2.9E-02
117.5	4.17E-01	3.0E-02
122.3	4.52E-01	3.2E-02
126.9	5.48E-01	3.6E-02
131.6	6.61E-01	4.0E-02
136.1	7.12E-01	4.2E-02
140.7	6.63E-01	4.1E-02
145.1	6.89E-01	4.2E-02
149.6	6.63E-01	4.1E-02
154.0	5.61E-01	3.8E-02

TABLE B103

12C(3HE,P)14N
BEAM ENERGY = 17.0 MEV
EX. ENERGY = 5.83 MEV

ANGLE C.M.	dσ/dω (MB/ST)	ERROR (MB/ST)
11.4	1.14E 00	2.3E-01
17.1	1.30E 00	2.6E-01
22.7	1.24E 00	5.0E-02
28.4	1.02E 00	4.6E-02
34.0	9.49E-01	4.2E-02
39.6	8.92E-01	4.2E-02
45.1	7.85E-01	4.0E-02
50.6	6.53E-01	3.6E-02
56.1	6.02E-01	3.5E-02
61.5	5.65E-01	3.4E-02
66.9	5.83E-01	3.5E-02
72.2	6.81E-01	3.8E-02
77.5	7.36E-01	4.0E-02
82.7	6.79E-01	3.9E-02
87.9	5.39E-01	3.5E-02
93.0	5.13E-01	3.4E-02
98.0	4.44E-01	3.2E-02
103.0	3.06E-01	2.7E-02
107.9	2.87E-01	2.6E-02
112.7	2.39E-01	2.3E-02
117.5	2.64E-01	2.5E-02
122.2	3.15E-01	2.8E-02
126.9	4.14E-01	3.3E-02
131.5	4.51E-01	3.5E-02
136.1	5.61E-01	4.0E-02
140.6	6.22E-01	4.3E-02
145.1	5.60E-01	4.1E-02
149.6	5.71E-01	4.1E-02
154.0	4.97E-01	3.8E-02

TABLE B104

12C(3HE,P)14N
BEAM ENERGY = 17.5 MEV
EX. ENERGY = 5.83 MEV

ANGLE C.M.	dσ/dω (MB/ST)	ERROR (MB/ST)
11.4	1.00E 00	2.0E-01
17.1	1.31E 00	2.6E-01
22.7	1.04E 00	3.3E-02
28.4	1.13E 00	4.3E-02
34.0	1.08E 00	4.6E-02
39.6	9.54E-01	4.7E-02
45.1	8.59E-01	4.4E-02
50.6	7.48E-01	3.8E-02
56.1	6.98E-01	3.7E-02
61.5	6.77E-01	3.7E-02
66.9	7.11E-01	3.8E-02
72.2	6.85E-01	3.7E-02
77.5	7.11E-01	3.9E-02
82.7	6.72E-01	3.8E-02
87.9	6.15E-01	3.7E-02
93.0	5.33E-01	3.5E-02
98.0	4.64E-01	3.4E-02
103.0	2.79E-01	2.6E-02
107.9	2.74E-01	2.5E-02
112.7	2.25E-01	2.3E-02
117.5	2.09E-01	2.2E-02
122.2	2.36E-01	2.7E-02
126.9	3.67E-01	3.1E-02
131.5	4.14E-01	3.4E-02
136.1	4.39E-01	3.5E-02
140.6	5.05E-01	3.9E-02
145.1	5.23E-01	3.9E-02
149.6	4.27E-01	3.6E-02
154.0	4.26E-01	3.4E-02

TABLE B105

12C(3HE,P)14N
BEAM ENERGY = 18.0 MEV
EX. ENERGY = 5.83 MEV

ANGLE C.M.	dσ/dω (MB/ST)	ERROR (MB/ST)
11.4	1.82E 00	3.6E-01
17.1	1.55E 00	3.1E-01
22.7	1.48E 00	5.6E-02
28.4	1.24E 00	4.9E-02
34.0	1.10E 00	4.6E-02
39.6	9.79E-01	4.3E-02
45.1	8.06E-01	3.8E-02
50.6	7.06E-01	3.4E-02
56.1	6.41E-01	3.4E-02
61.5	6.38E-01	3.4E-02
66.9	6.42E-01	3.5E-02
72.2	6.82E-01	3.6E-02
77.5	6.26E-01	3.5E-02
82.7	6.94E-01	3.9E-02
87.9	5.21E-01	3.2E-02
92.9	4.86E-01	3.0E-02
98.0	3.88E-01	3.0E-02
102.9	3.03E-01	2.6E-02
107.9	2.68E-01	2.5E-02
112.7	2.78E-01	2.6E-02
117.5	2.34E-01	2.4E-02
122.2	2.25E-01	2.3E-02
126.9	2.64E-01	2.6E-02
131.5	3.19E-01	2.9E-02
136.1	4.10E-01	3.4E-02
140.6	4.28E-01	3.5E-02
145.1	4.02E-01	3.4E-02
149.6	3.82E-01	3.3E-02
154.0	3.41E-01	3.1E-02

REFERENCES

Ade 67 E. G. Adelberger, California Institute of Technology Thesis, (unpublished) 1967.

Ajz 70 F. Ajzenberg-Selove, Nucl. Phys. A152, 1 (1970).

Aus 65 N. Austern, Phys. Rev. 137, B752 (1965).

ADHS 64 N. Austern, R. M. Drisko, E. C. Halbert, and G. R. Satchler, Phys. Rev. 133, B3 (1964).

AM 70 E. G. Adelberger and A. B. McDonald, Nucl. Phys. A145, 497 (1970).

Bar 69 C. A. Barnes, in Nuclear Isospin edited by J. D. Anderson, S. D. Bloom, J. Cerny and W. W. True. (Academic Press, New York 1969) p. 179.

Bas 66 R. H. Bassel, Phys. Rev. 149, 791 (1966).

Bay 71 B. F. Bayman, Nucl. Phys. 168, 1 (1971).

BZ 66 Gy. Bencze and J. Zimanyi, Nucl. Phys. 81, 76 (1966).

BDS 67 R. H. Bassel, R. M. Drisko and G. R. Satchler. Memorandum to the user of the code 'JULIE'. Oakridge National Laboratory, June, 1966, (unpublished).

BPRS 67 D. J. Baugh, G. J. B. Pyle, P. M. Rolph and S. M. Scarrott, Nucl. Phys. A95, 115 (1967).

BR 67 R. A. Broglia and C. Riedel, Nucl. Phys. A92, 145 (1967).

CK 65 S. Cohen and D. Kurath, Nucl. Phys. 73, 1 (1965).

CK 70 S. Cohen and D. Kurath, Nucl. Phys. A141,145 (1970).

CM 70 N. S. Chant and N. F. Mangelson, Nucl. Phys. A140, 81 (1970).

DDPS 65 J. K. Dickens, R. M. Drisko, F. G. Perey and G. R. Satchler, Phys. Letters 15, 337 (1965).

DMT 70 O. Dragún, E. Maqueda and J. Testoni, Comisión Nacional de Energía Atómica Argentina, private communication.

DR 66 R. M. Drisko and F. Rybicki, Phys. Rev. Letters 16, 275 (1966).

For 71 T. De Forest, Nucl. Phys. A163, 237 (1971).

FCG 68 D. G. Fleming, J. Cerny and N. K. Glendenning, Phys. Rev. 165, 1153 (1968).

FDS 71 J. L. Foster Jr., O. Dietzsch and D. Spalding, Nucl. Phys. A169, 187 (1971).

FGTF 68 H. T. Fortune, T. J. Gray, W. Frost and N. R. Fletcher, Phys. Rev. 173, 1002 (1968).

Gle 65 N. K. Glendenning, Phys. Rev. 137, B102 (1965).

GFGH 66 S. Gorodetsky, R. M. Freeman, A. Gallmann, and F. Haas, Phys. Rev. 149, 801 (1966).

GRKG 67 E. F. Gibson, B. W. Ridley, J. J. Kraushaar, M. E. Rickey and R. H. Bassel, Phys. Rev. 155, 1194 (1967).

Hen 69 D. C. Hensley, California Institute of Technology Thesis, (unpublished) 1969.

Hod 68 P. E. Hodgson, Adv. in Phys. 17, 563 (1968).

Hus 71 D. Hussain, Nucl. Phys. A166, 667 (1971).

HM 60 S. Hinds and R. Middleton, Proc. Phys. Soc. (London) 75, 745 (1960).

HMBP 66 C. H. Holbrow, R. Middleton, J. Parks, and J. Bishop, in Nuclear Spin-Parity Assignments. Edited by R. B. Grove and R. L. Robinson (Academic Press, New York, 1966). p. 354.

HNB 67 J. C. Hiebert, E. Newman and R. H. Bassel, Phys. Rev. 154, 898 (1967).

KBDF 64 C. C. Kim, M. Bunch, D. W. Devins and H. H. Forster, Nucl. Phys. 58, 32 (1964).

Man 67 N. F. Mangelson, U. C. Berkeley Thesis (1967) (unpublished).

Mos 59 M. Moshinsky, Nucl. Phys. 13, 104 (1959).

MR 67 U. S. Mathur and J. R. Rook, Nucl. Phys. A91, 305 (1967).

Par 68 J. Y. Park, Nucl. Phys. A111, 433 (1968).

PB 63 F. Percy and B. Buck, Nucl. Phys. 32, 353 (1963).

PS 64 F. G. Perey and D. S. Saxon, Phys. Letters 10, 107 (1964).

PTB 60 J. R. Priest, D. J. Tendam and E. Bleuler, Phys. Rev. 119, 1295 (1960).

Roo 67 J. R. Rook, Nucl. Phys. A97, 217 (1967).

RBS 71 A. A. Rush, E. J. Burge and D. A. Smith, Nucl. Phys. A166, 378 (1971).

RK 71 E. Rost and P. D. Kunz, Nucl. Phys. A162, 376 (1971).

Sat 66 G. R. Satchler, Nucl. Phys. 85, 273 (1966).

Sin 70 J. Singh, Nucl. Phys. A155, 443 (1970).

SSG 70 G. Scheklinski, U. Strohbusch and B. Goel, Nucl. Phys. A153, 97 (1970).

Tru 63 W. W. True, Phys. Rev. 130, 1530 (1963).

TU 60 I. Talmi and I. Unna, Ann. Rev. Nucl. Sci. 10, 353 (1960).

WBBB 68 S. I. Warshaw, A. J. Bauffa, J. B. Barengoltz, and M. K. Brussel, Nucl. Phys. A121, 350 (1968).

WC 71 H. Wilsch and G. Clausnitzer, Nucl. Phys. A160, 609 (1971).

WP 60 E. K. Warburton and W. T. Pinkston, Phys. Rev. 118, 733 (1960).

ZF 69 R. W. Zurmühle and C. M. Fou, Nucl. Phys. A129, 502 (1969).

Table 1

Optical Parameters for $^{12}C(^{3}He,^{3}He)^{12}C$ elastic scattering

The elastic scattering was analysed using the optical potential

$$U(r) = Vf_r(r) + iWf_w(r) + V_c(r) \quad ,$$

where

$$f_r = \left\{1 + \exp[(r - R_r)/A_r]\right\}^{-1} \quad ,$$

$$f_w = \left\{1 + \exp[(r - R_w)/A_w]\right\}^{-1} \quad ,$$

$$V_c(r) = \frac{Z_1 Z_2 e^2}{2R_c}\left\{3 - \frac{r^2}{R_c^2}\right\} \qquad r \leqslant R_c \ ,$$

$$= \frac{Z_1 Z_2 e^2}{r} \qquad r \geqslant R_c \ ,$$

$$R_c = 3.2 \text{ fm.}$$

E Mev	V Mev	R_r fm	A_r fm	W Mev	R_w fm	A_w fm
12.0	-163.8	2.9	0.798	-7.34	4.96	0.80
12.5	-165.5	"	"	-9.33	"	"
13.0	-165.1	"	"	-8.48	"	"
13.5	-165.0	"	"	-8.32	"	"
14.0	-165.1	"	"	-9.96	"	"
14.5	-165.1	"	"	-9.96	"	"
15.0	-165.1	"	"	-9.96	"	"
15.5	-164.6	"	"	-8.16	"	"
16.0	-164.9	"	"	-9.00	"	"
16.5	-163.6	"	"	-7.26	"	"
17.0	-165.0	"	"	-9.96	"	"
17.5	-164.9	"	"	-9.73	"	"
18.0	-164.0	"	"	-7.41	"	"

Table 2

Structure factor $G_{NLSJT\gamma}$ for the $^{12}C(^{3}He,p)^{14}N$ reaction, based on True's (Tru 63) and Cohen and Kurath's (CK 65) wave functions, taken from Mangelson (Man 67). A similar calculation was done by Dragún (DMT 70) using only the Cohen and Kurath wave functions, and it produced very similar results.

LEVEL				True (Tru 63)				Cohen & Kurath (CK 65)	
E_x Mev	J^π	T	L	N = 1	N = 2	N = 3	N = 4	N = 1	N = 2
0.0	1^+	0	0	0.02	0.11	-0.11		-0.01	-0.09
			2	-0.56	0.12			0.42	
2.311	0^+	1	0	-0.05	-0.35	0.19	-0.01	0.08	0.54
3.945	1^+	0	0					0.06	0.41
			2					0.02	
4.91	0^-		1	-0.02	0.639				
5.10	2^-	0	1	0.07	0.64	-0.08			
			3	0.22					
5.69	1^-	0	1	-0.01	0.54	-0.02			
5.83	3^-	0	3	0.56	-0.05				

Table 3

The optical-model parameters for $^{14}N(p,p)^{14}N$ elastic scattering obtained by fitting the data of Kim et. al. (KBDF 64) at 30.1 Mev and Rush et. al. (RBS 71) at 49.4 Mev. The optical-model parameters for the present DWBA calculation have been extrapolated from these, assuming that the depth of the real potential has a linear dependence on energy. The optical potential has the form

$$U(r) = Vf_r(r) + iWf_w(r) + V_c(r)$$

where $$f_r = \left\{1 + \exp[(r - R_r)/A_r]\right\}^{-1}$$

$$f_w = \exp - \left\{(r - R_w)/A_w\right\}^2$$

$$V_c(r) = \frac{Z_1 Z_2 e^2}{2R_c}\left\{3 - \frac{r^2}{R_c^2}\right\} \qquad r \leqslant R_c$$

$$= Z_1 Z_2 \frac{e^2}{r} \qquad r \geqslant R_c$$

$$R_c = 2.86 \text{ fm.}$$

E Mev	V Mev	R_r fm	A_r fm	W Mev	R_w fm	A_w fm
49.4	32.4	2.86	0.65	-6	2.86	0.65
30.1	42.0	2.86	0.65	-6	2.86	0.65

Figure 1

Schematic Diagram of Scattering Chamber

The scattering chamber is made of aluminium. The Faraday cup consists of a small magnet which is biased at -300 volt, and a tantalum cup which is biased at +300 volt. Both the magnet and the tantalum cup are insulated from ground by a layer of nylon lining.

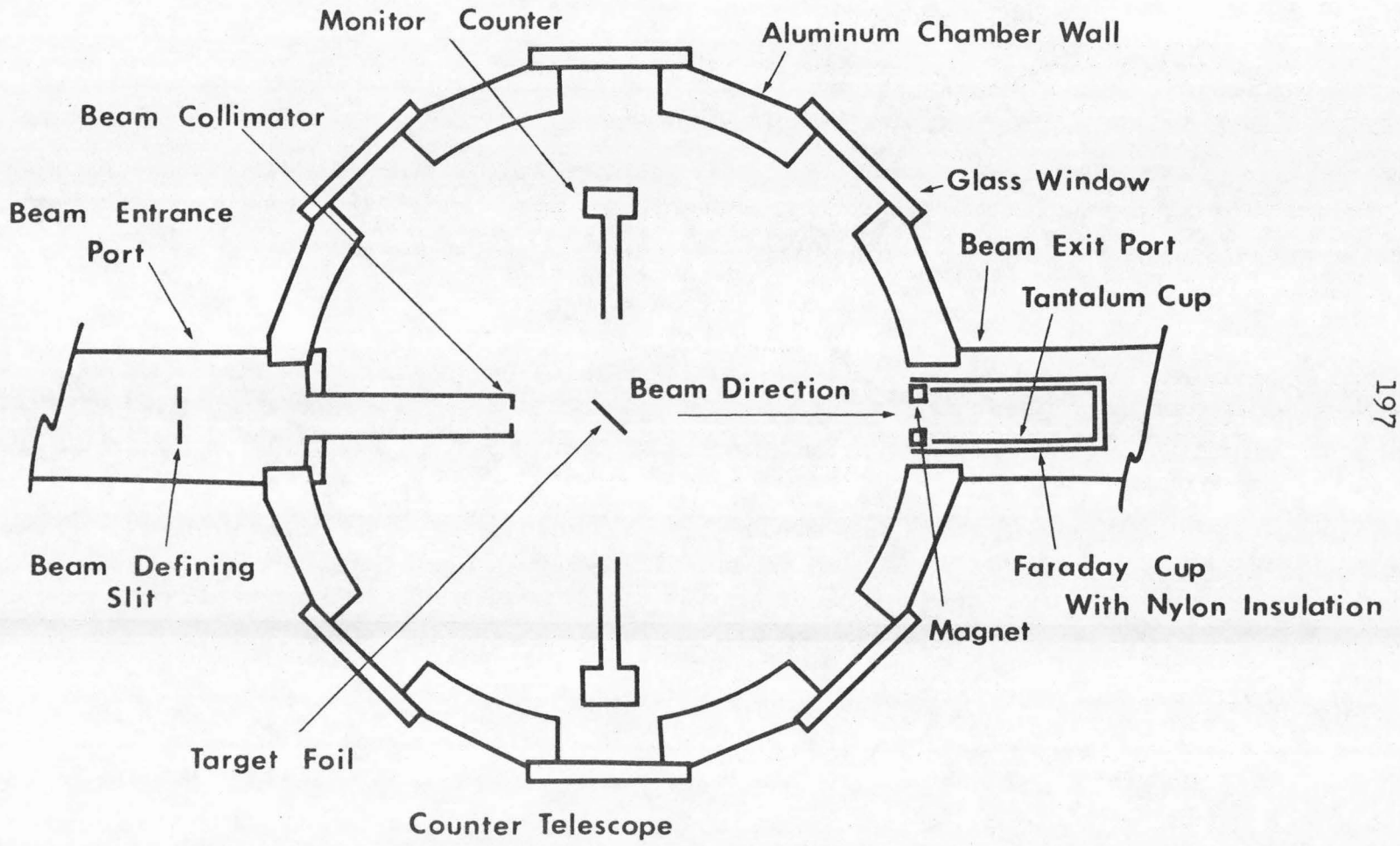
Monitor Counter
Aluminum Chamber Wall
Beam Collimator
Glass Window
Beam Entrance Port
Beam Exit Port
Tantalum Cup
Beam Direction
Beam Defining Slit
Faraday Cup With Nylon Insulation
Magnet
Target Foil
Counter Telescope

Figure 2

Block Diagram of the Electronic Circuits

Most of the electronic components used in this experiment are commercially available, and they are

A. ΔE detector - 200μ Si transmission counter (ORTEC),
B. E detector - 3mm Si(Li) counter (Kevex),
C. Monitor detector - 2mm Si(Li) counter (Kevex),
D. Pre-amp - Tennelec model 100A pre-amplifier,
E. Attenuator - ORTEC dual decade attenuator,
F. Amp 1-ORTEC model 410 amplifier,
G. Amp 2 - Tennelec model TC200 amplifier
H. SCA - ORTEC model 420 single channel analyser,
I. Summing amp - Summing amplifier developed in Kellogg Radiation Laboratory,
J. Stretcher - Logic pulse stretcher developed in Kellogg Radiation Laboratory,
K. Slow Coinc Gate - ORTEC model 409 slow coincidence and linear gate,
L. Amp 3 - CI model 1416 amplifier,
M. Nuclear Data Analyser - Nuclear Data Model 2200-028 A 4096-channel analyser,
N. RIDL Analyser 1 - RIDL model 34-27 400-channel analyser, and
O. RIDL Analyser 2 - RIDL model 34-12 400-channel analyser.

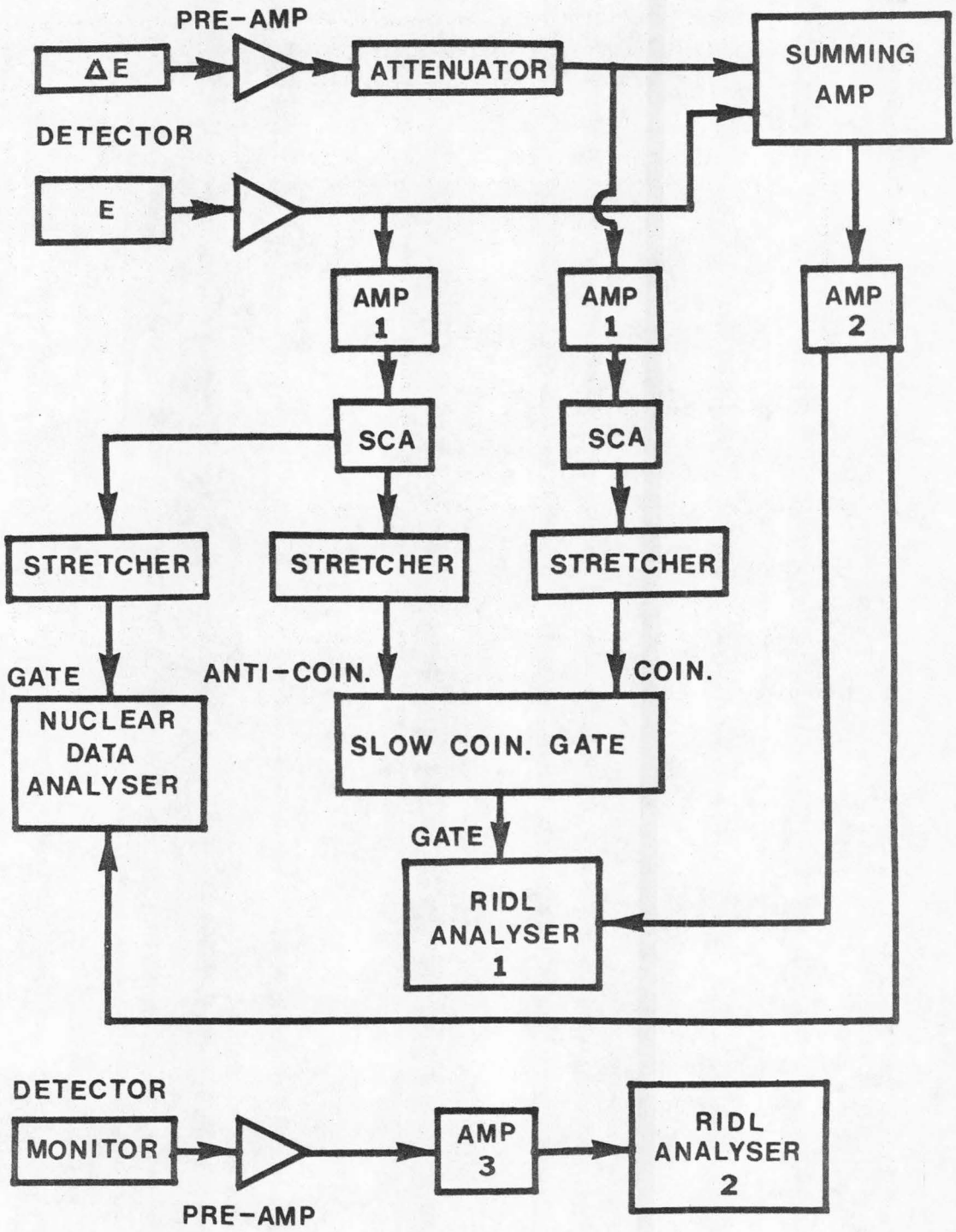
PRE-AMP
ΔE
ATTENUATOR
SUMMING AMP
DETECTOR
E
AMP 1
AMP 1
AMP 2
SCA
SCA
STRETCHER
STRETCHER
STRETCHER
GATE
ANTI-COIN.
COIN.
NUCLEAR DATA ANALYSER
SLOW COIN. GATE
GATE
RIDL ANALYSER 1
DETECTOR
MONITOR
PRE-AMP
AMP 3
RIDL ANALYSER 2

Figure 3

Particle Spectra obtained at E_{lab} = 17.0 Mev with the counter telescope at $\theta_{lab} = 45^{o}$. Particle identification is described in the text. The proton groups from $^{12}C(^{3}He,p)^{14}N$ are labelled by the excitation energy in ^{14}N. The proton groups labelled $^{18}F(0.93,1.12)$ are from an oxygen contaminant in the target.

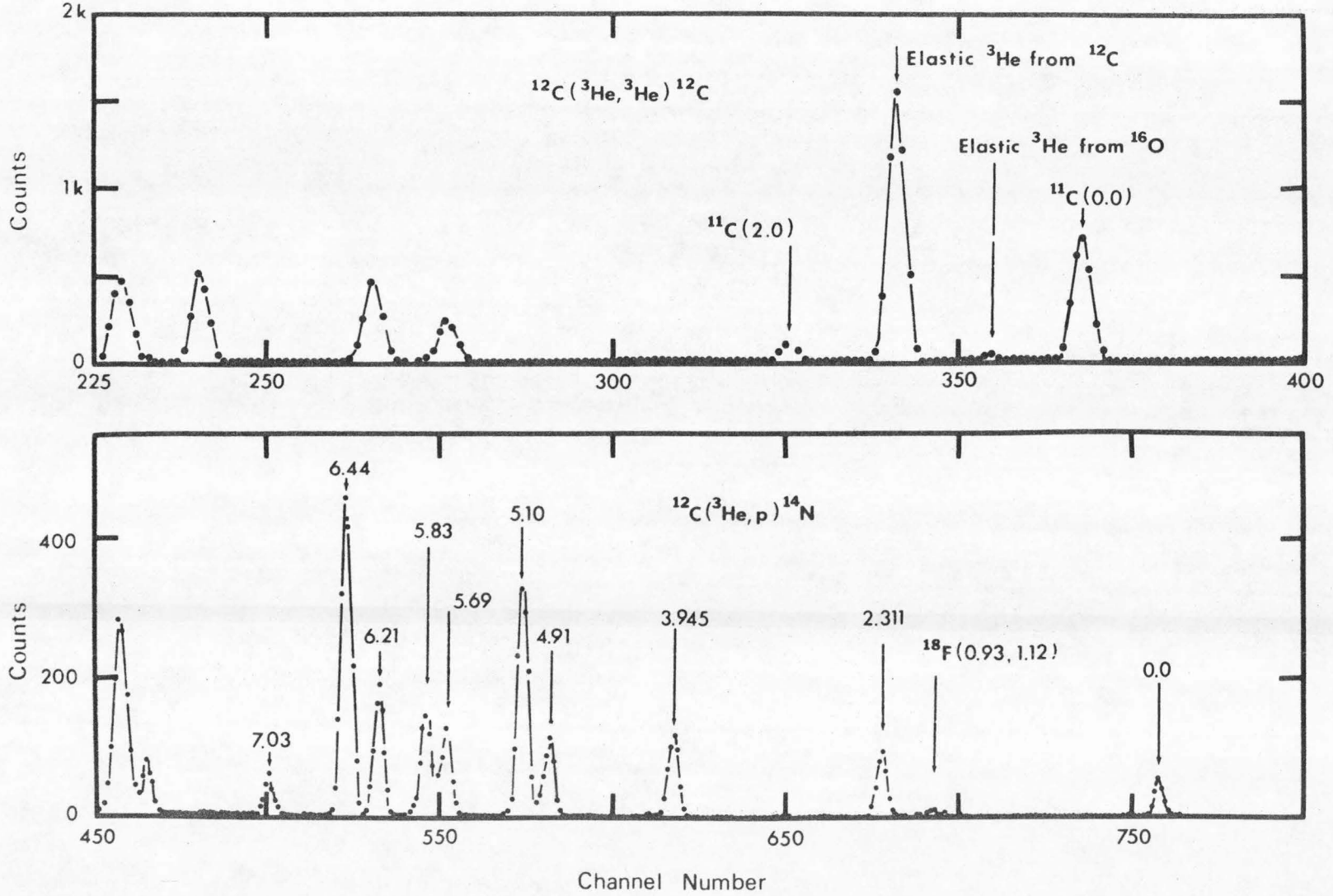
2k
1k
0
Counts
225
250
300
350
400
$^{12}C(^{3}He,^{3}He)^{12}C$
Elastic ^{3}He from ^{12}C
Elastic ^{3}He from ^{16}O
$^{11}C(0.0)$
$^{11}C(2.0)$
400
200
0
Counts
450
550
650
750
$^{12}C(^{3}He,p)^{14}N$
6.44
5.83
5.10
5.69
6.21
4.91
3.945
2.311
$^{18}F(0.93, 1.12)$
0.0
7.03
Channel Number

Figure 4

Excitation function for the $^{12}C(^{3}He,^{3}He)^{12}C$ reaction at $\theta_{lab} = 45^{o}$

The data points indicated by × were obtained in this experiment, using a 129 $\mu gm/cm^2$ thick carbon foil. The data points indicated by o were taken from Fortune et. al. (FGTF 68).

This curve was used to normalize the yields of the reactions $^{12}C(^{3}He,^{3}He)^{12}C$ and $^{12}C(^{3}He,p)^{14}N$. The resultant differential cross-sections are tabulated in Appendix B.

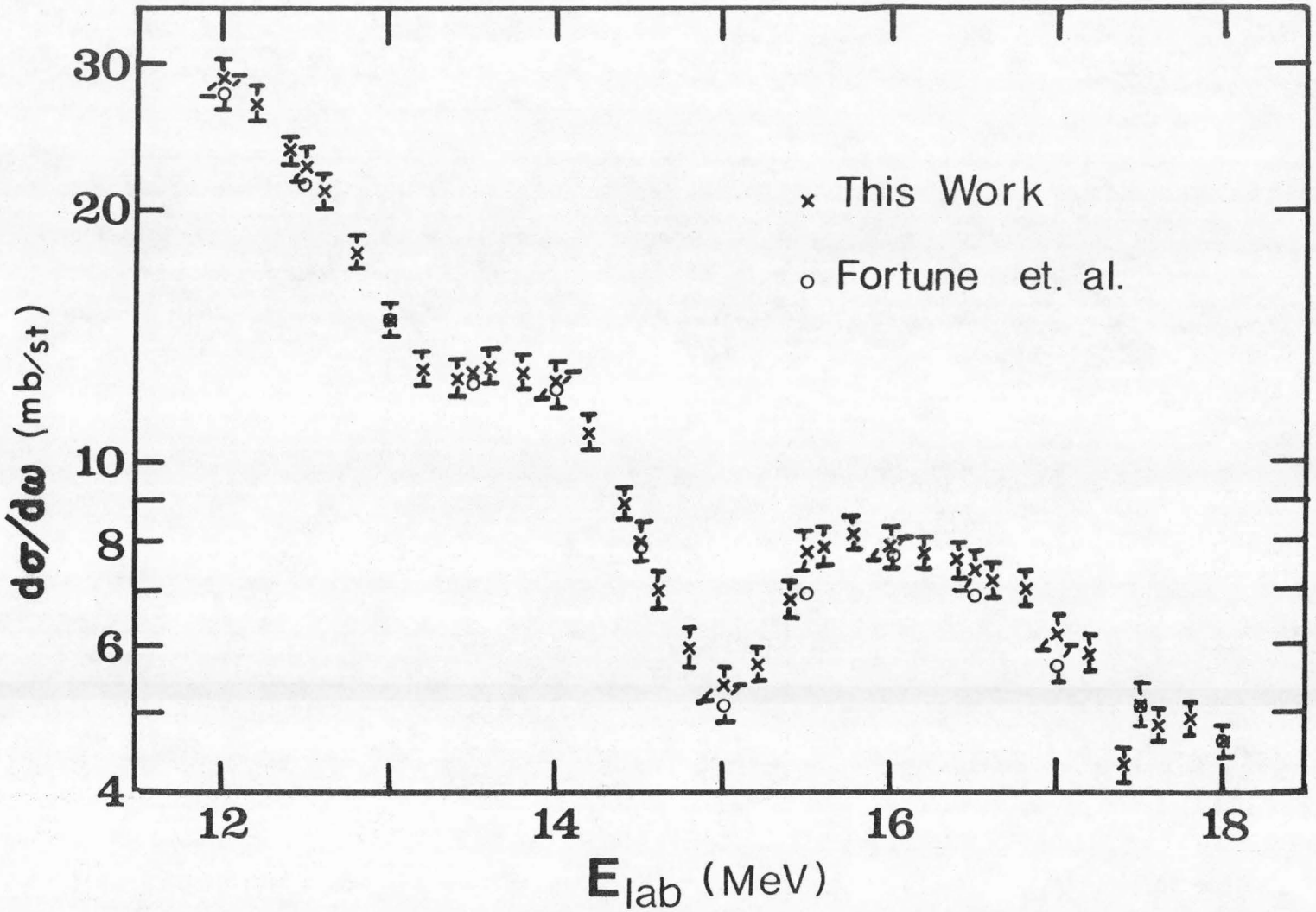
30
20
10
8
6
4
12
14
16
18
dσ/dω (mb/st)
E lab (MeV)
× This Work
o Fortune et. al.

Figure 5

Differential cross-section for the $^{12}C(^{3}He,^{3}He)^{12}C$ elastic scattering. The dashed curves are least squares fits to the data points, using Optical Model potentials. The optical parameters are listed in Table 1 and the differential cross-sections are tabulated in Appendix B.

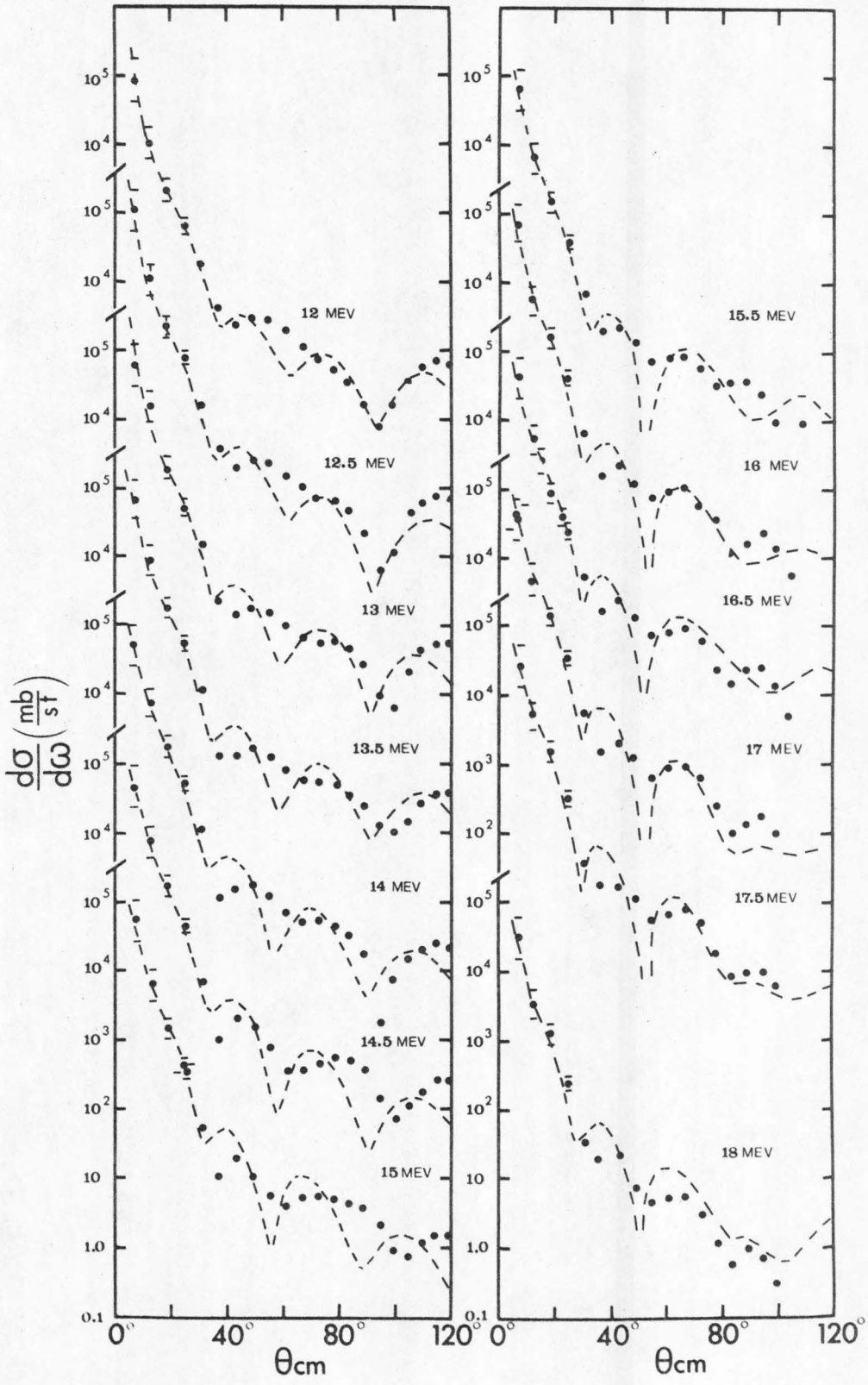
12 MEV
12.5 MEV
13 MEV
13.5 MEV
14 MEV
14.5 MEV
15 MEV
15.5 MEV
16 MEV
16.5 MEV
17 MEV
17.5 MEV
18 MEV
dσ/dω (mb/sr)
θcm
θcm
0°
40°
80°
120°

Figure 6

Energy level diagram of ^{14}N, taken from Ajzenberg-Selove (Ajz 70).

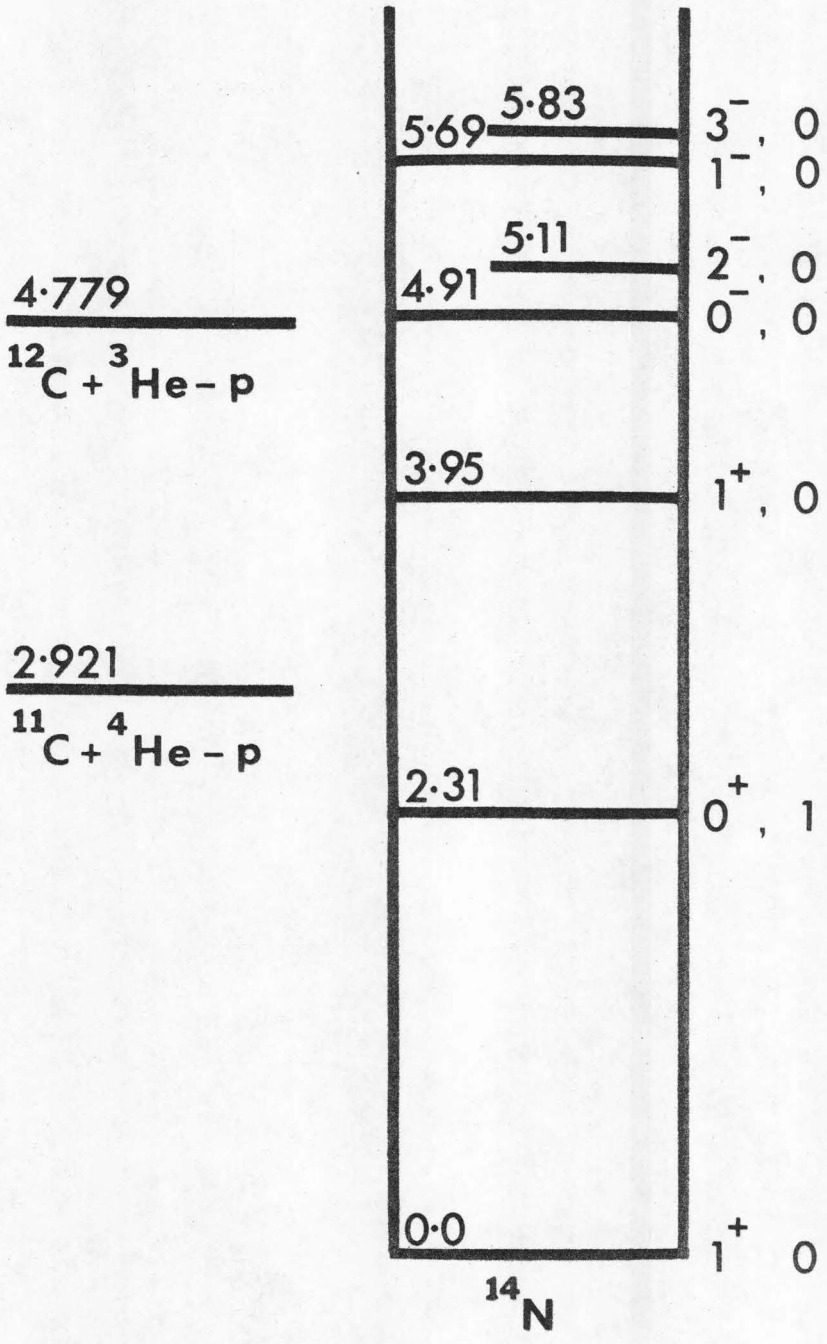
5·83
5·69
3⁻, 0
1⁻, 0
5·11
4·91
2⁻, 0
0⁻, 0
4·779
12C + 3He – p
3·95
1⁺, 0
2·921
11C + 4He – p
2·31
0⁺, 1
0·0
1⁺ 0
14N

Figure 7

Angular distributions of protons from the reaction $^{12}C(^{3}He,p)^{14}N$, leading to the ground state of ^{14}N. The differential cross-sections are tabulated in Appendix B.

The errors, if not indicated, are smaller than the size of the points.

The curves are DWBA calculations using zero-range, local potentials. The optical parameters are listed in tables 1 and 3. The transition shows an $L = 2$ character.

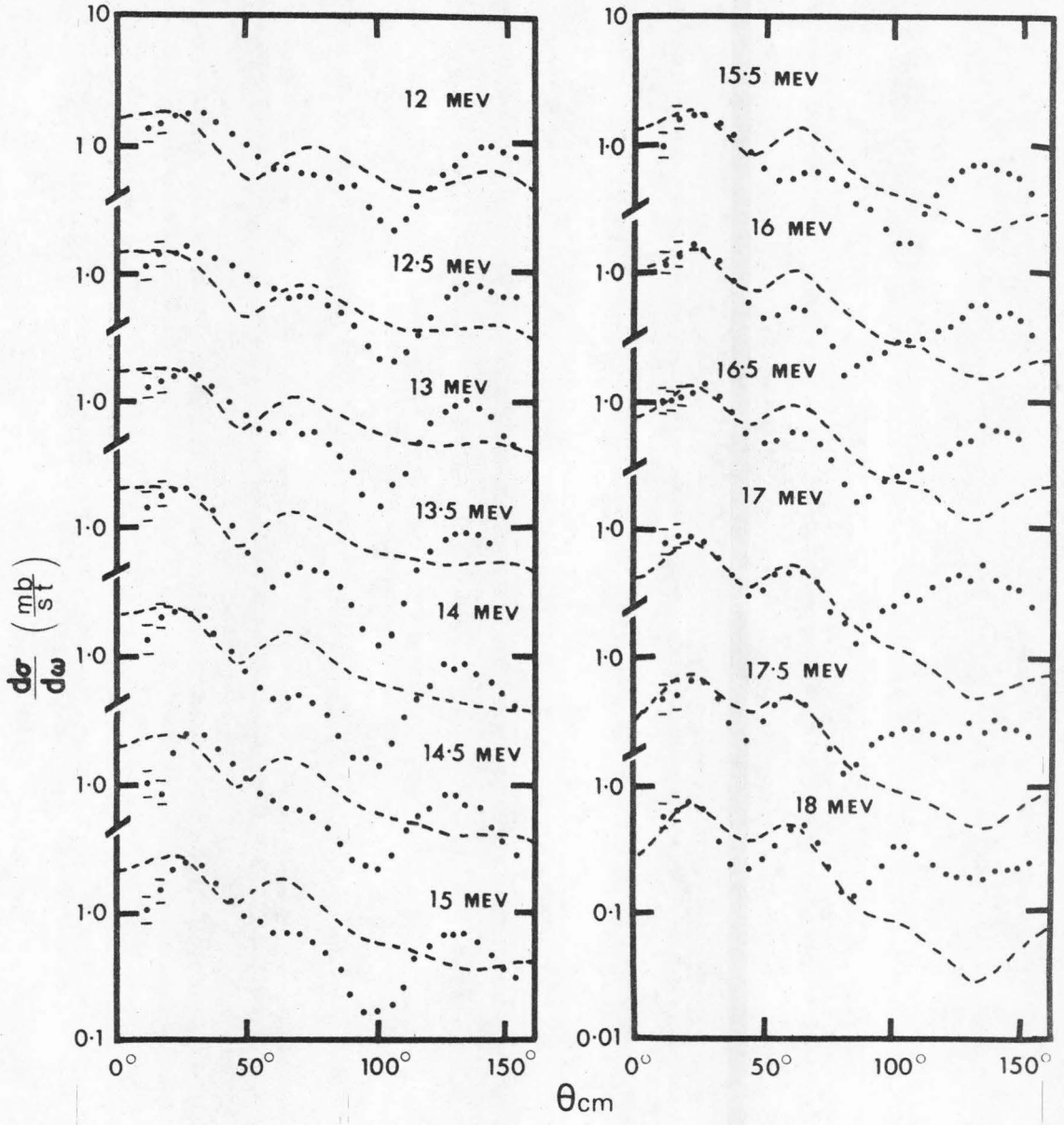
12 MEV
12·5 MEV
13 MEV
13·5 MEV
14 MEV
14·5 MEV
15 MEV
15·5 MEV
16 MEV
16·5 MEV
17 MEV
17·5 MEV
18 MEV
dσ/dω (mb/st)
θcm
0°
50°
100°
150°
10
1·0
0·1
0·01

Figure 8

Angular distributions of protons from the reaction $^{12}C(^{3}He,p)^{14}N$, leading to the 2.311 Mev state of ^{14}N.

The transition shows an $L = 0$ character.

Refer to Figure 7 for more description.

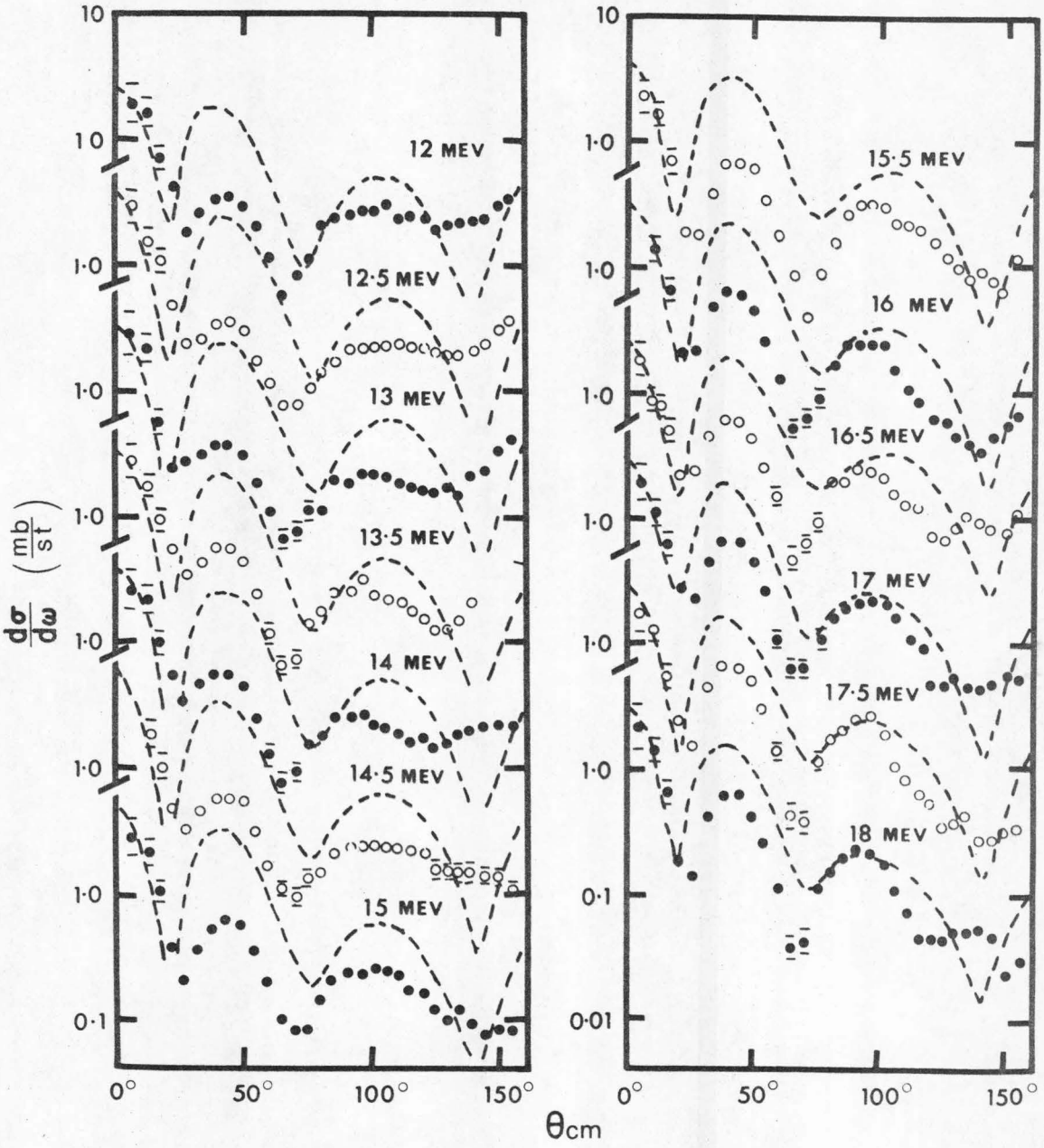
12 MEV
12·5 MEV
13 MEV
13·5 MEV
14 MEV
14·5 MEV
15 MEV
15·5 MEV
16 MEV
16·5 MEV
17 MEV
17·5 MEV
18 MEV
dσ/dω (mb/st)
θcm
0°
50°
100°
150°

Figure 9

Angular distributions of protons from the reaction $^{12}C(^{3}He,p)^{14}N$, leading to the 3.95-Mev state of ^{14}N. The transition shows an $L = 0$ character.

Refer to Figure 7 for more description.

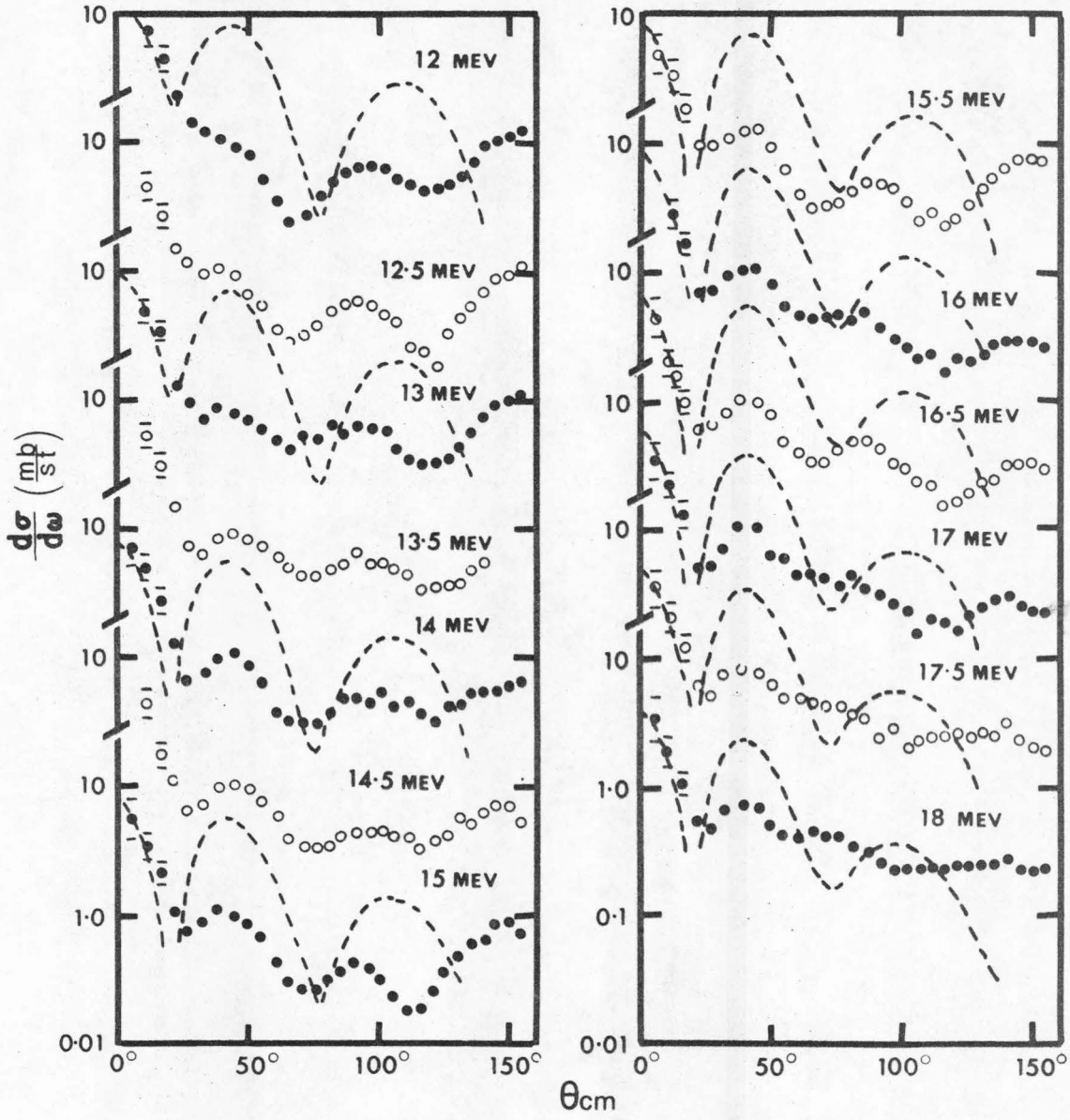
12 MEV
12·5 MEV
13 MEV
13·5 MEV
14 MEV
14·5 MEV
15 MEV
15·5 MEV
16 MEV
16·5 MEV
17 MEV
17·5 MEV
18 MEV
dσ/dω (mb/sr)
θcm
0°
50°
100°
150°
10
1·0
0·1
0·01

Figure 10

Angular distributions of protons from the reaction $^{12}C(^{3}He,p)^{14}N$, leading to the 4.91-Mev state in ^{14}N.

The transition shows an L = 1 character.

Refer to Figure 7 for more description.

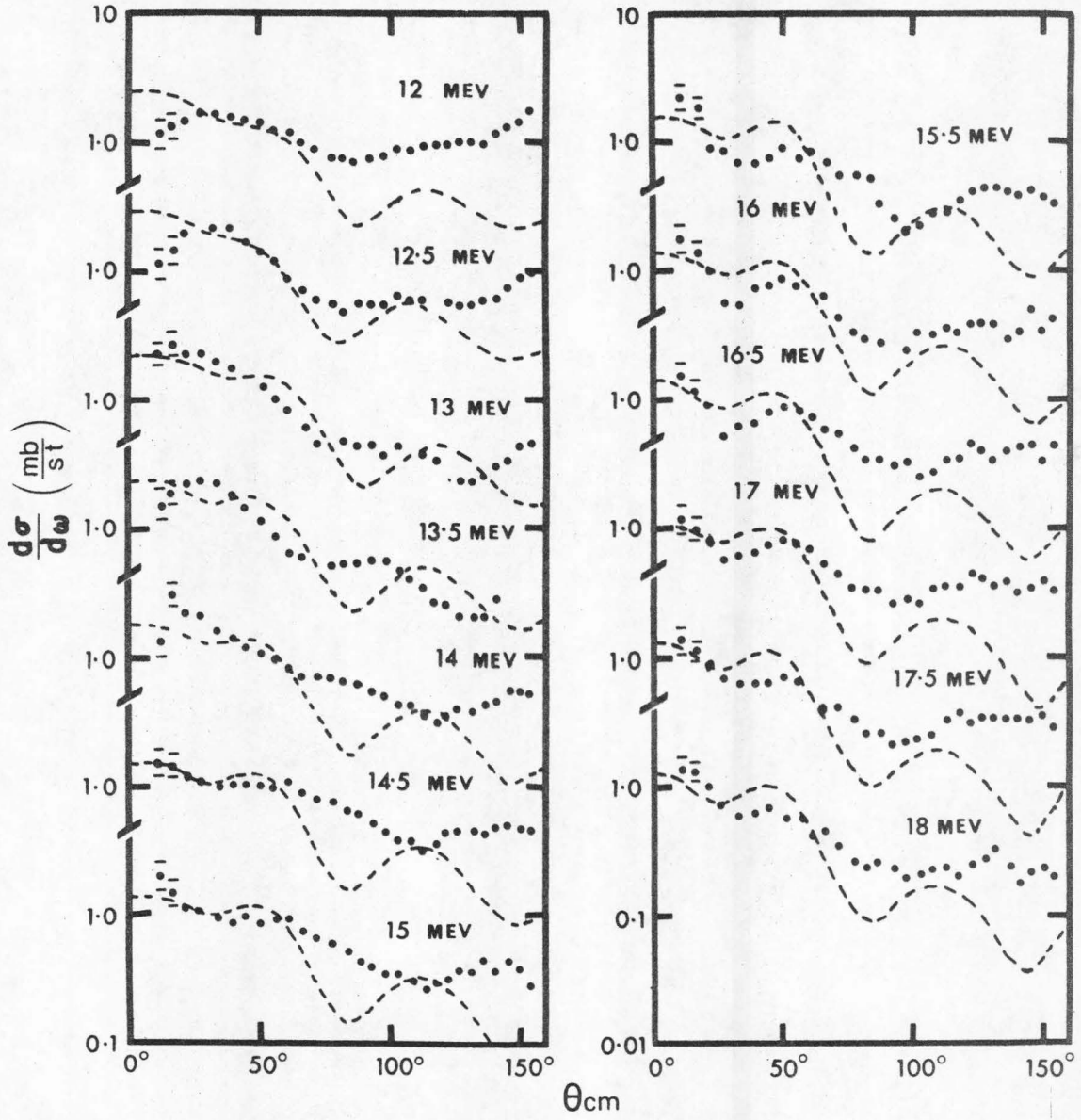
12 MEV
12·5 MEV
13 MEV
13·5 MEV
14 MEV
14·5 MEV
15 MEV
15·5 MEV
16 MEV
16·5 MEV
17 MEV
17·5 MEV
18 MEV
10
1·0
0·1
0·01
0°
50°
100°
150°
θcm
dσ/dω (mb/st)

Figure 11

Angular distributions of protons from the reaction $^{12}C(^{3}He,p)^{14}N$, leading to the 5.11-Mev state in ^{14}N.

The transition shows an L = 1 character.

Refer to Figure 7 for more description.

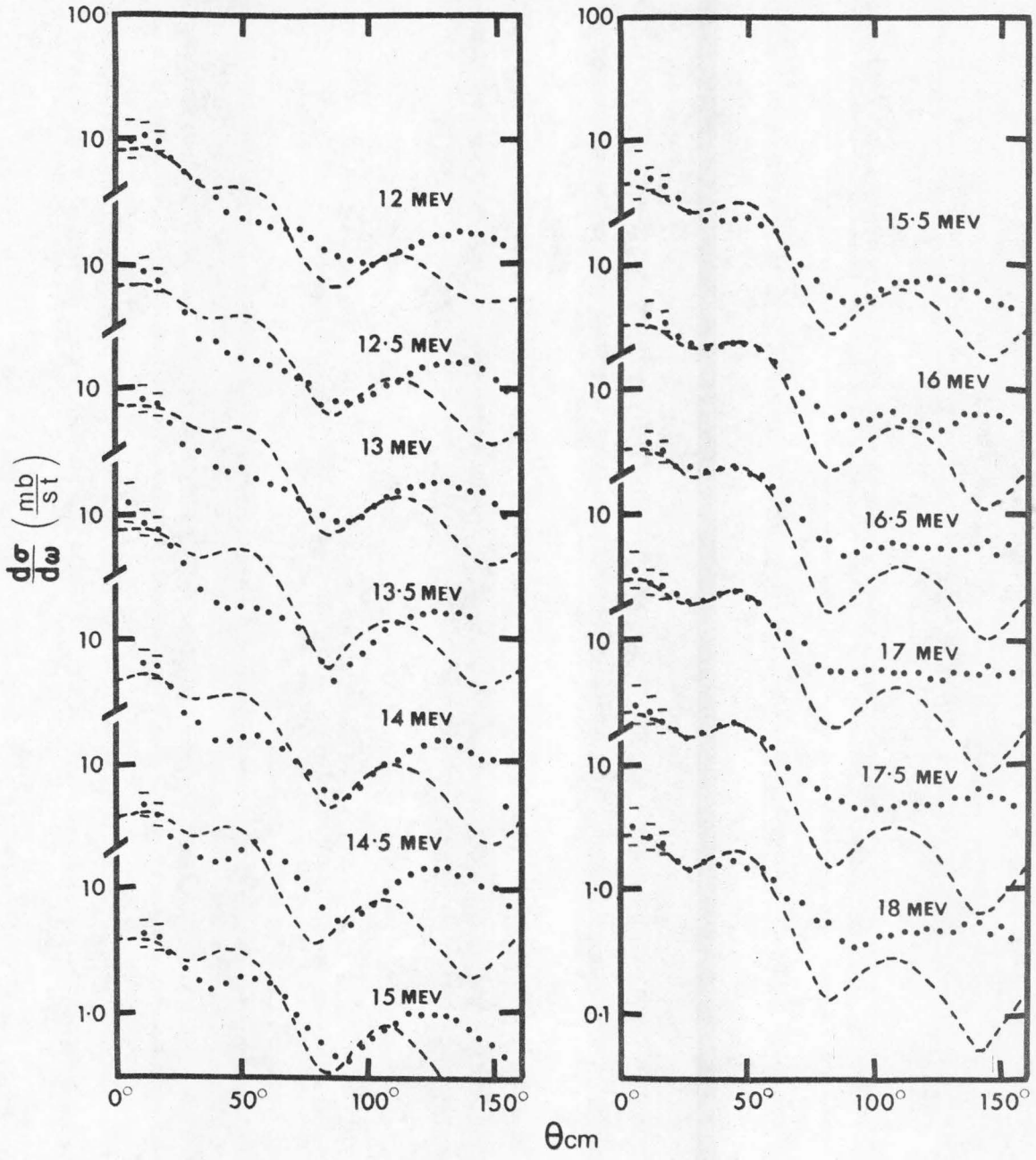
100
10
10
10
10
10
10
10
1·0
12 MEV
12·5 MEV
13 MEV
13·5 MEV
14 MEV
14·5 MEV
15 MEV
0°
50°
100°
150°
dσ/dω (mb/st)
100
10
10
10
10
10
10
1·0
0·1
15·5 MEV
16 MEV
16·5 MEV
17 MEV
17·5 MEV
18 MEV
0°
50°
100°
150°
θcm

Figure 12

Angular distributions of protons from the reaction $^{12}C(^{3}He,p)^{14}N$, leading to the 5.69-Mev state in ^{14}N.

The transition has an L = 1 character.

Refer to Figure 7 for more description.

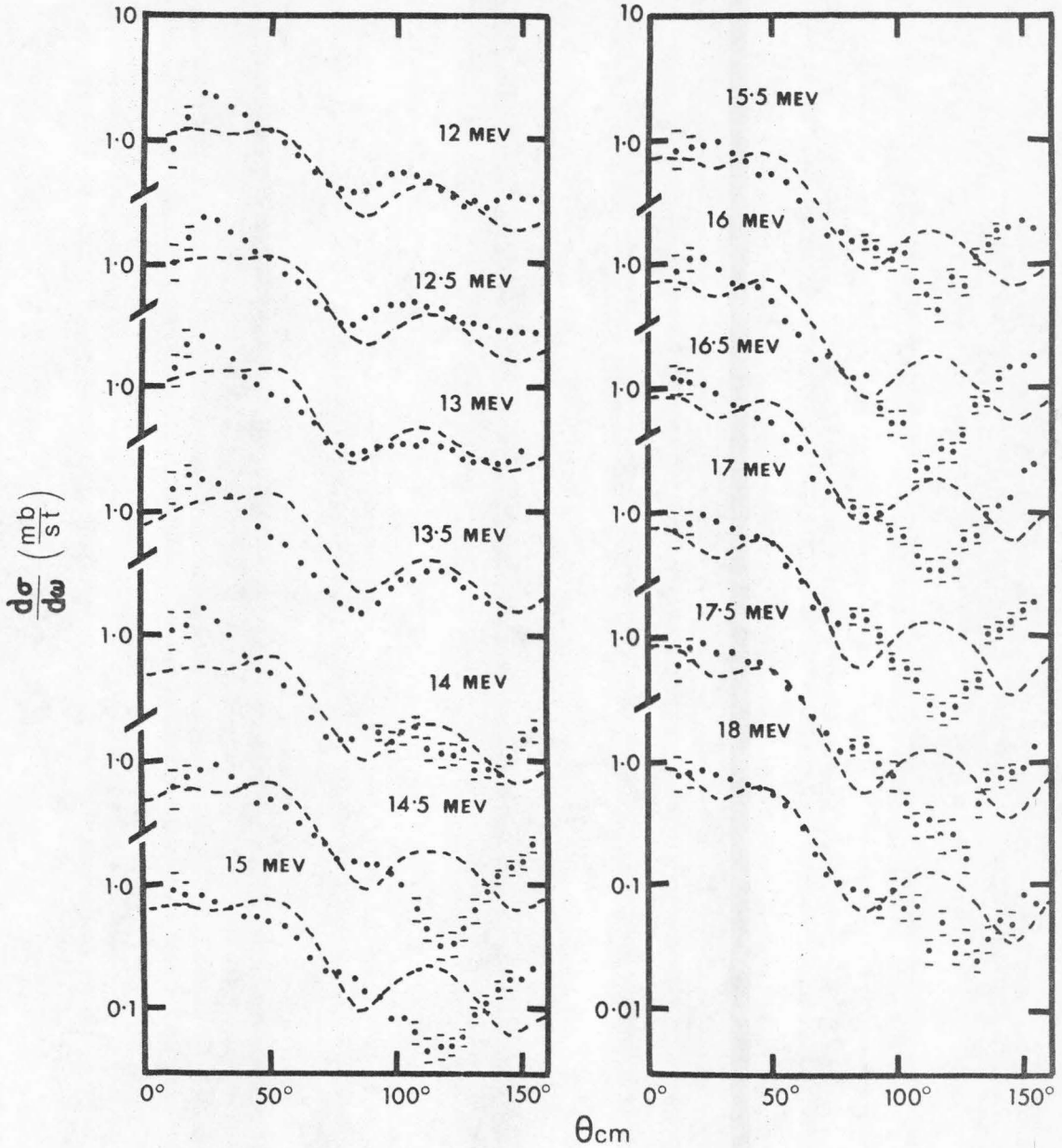
10
1·0
12 MEV
12·5 MEV
13 MEV
13·5 MEV
14 MEV
14·5 MEV
15 MEV
0·1
15·5 MEV
16 MEV
16·5 MEV
17 MEV
17·5 MEV
18 MEV
0·01
0°
50°
100°
150°
θcm
dσ/dω (mb/st)

Figure 13

Angular distributions of protons from the reaction $^{12}C(^{3}He,p)^{14}N$, leading to the 5.83-Mev state of ^{14}N.

The solid curves correspond to an L = 3 fit.

Refer to Figure 7 for more description.

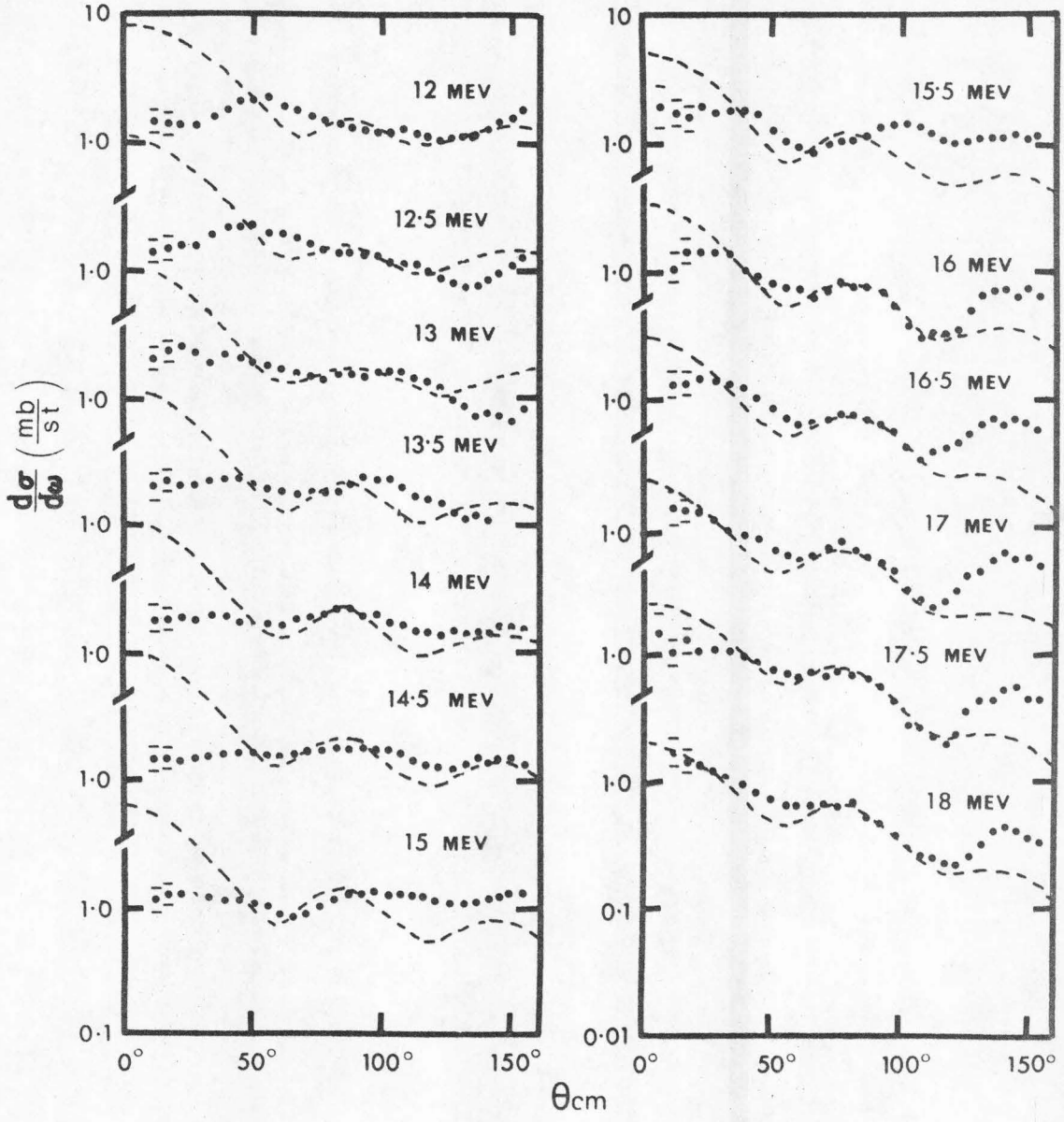
12 MEV
12·5 MEV
13 MEV
13·5 MEV
14 MEV
14·5 MEV
15 MEV
15·5 MEV
16 MEV
16·5 MEV
17 MEV
17·5 MEV
18 MEV
10
1·0
0·1
0·01
0°
50°
100°
150°
θcm
dσ/dω (mb/st)

Figure 14

DWBA calculations at 18 Mev using different sets of parameters.

curve	chan.	V_r Mev	R_r fm	A_r fm	function*	W Mev	R_w fm	A_w fm	function*	R_c fm
solid	$^3He + ^{12}C$	-164.0	2.9	o.798	WS	-7.41	4.96	0.80	WS	3.2
	$p + ^{14}N$	-46.7	2.86	0.65	WS	-6	2.86	0.65	G	2.86
	form factor		2.06	0.9	WS					2.97
dotted	$^3He + ^{12}C$	-164.0	2.9	0.798	WS	-7.41	4.96	0.80	WS	3.2
	$p + ^{14}N$	-46.7	2.86	0.65	WS	-6.0	2.86	0.65	G	2.86
	form factor		2.75	0.71	WS					3.2
dashed	$^3He + ^{12}C$	-176.0	2.81	0.683	WS	-28.0	2.74	0.70	WS	3.2
	$p + ^{14}N$	-48.0	2.86	0.65	WS	-6.0	2.86	0.65	G	
	form factor		2.75	0.71	WS					3.2

* WS = Woods-Saxon potential, $f = \left\{ 1 + \exp[(r - R)/A] \right\}^{-1}$.

G = Gaussian potential, $f = \exp - \left\{ (r - R)/A \right\}^2$.

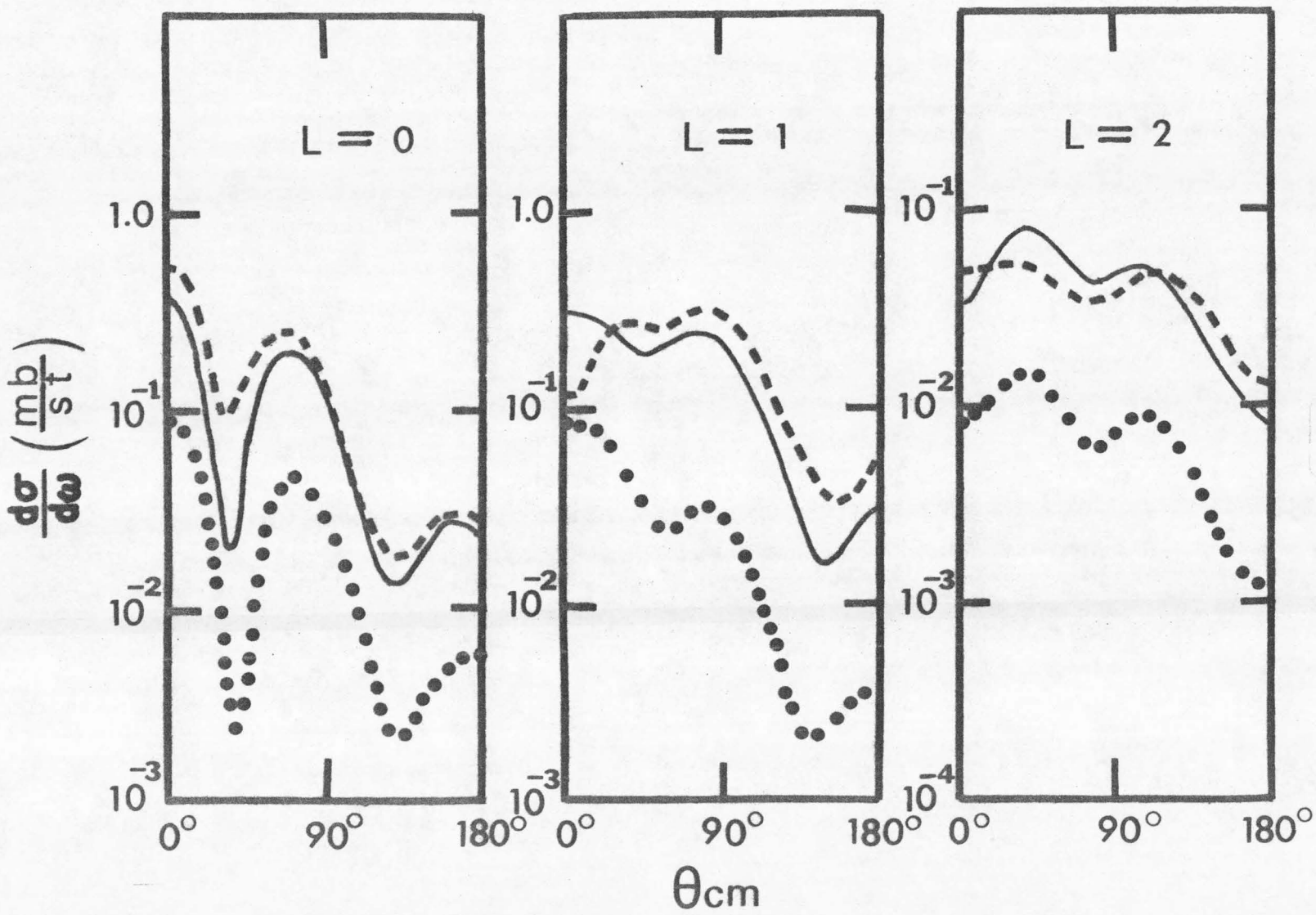
L = 0
L = 1
L = 2
1.0
10^{-1}
10^{-2}
10^{-3}
10^{-4}
0°
90°
180°
$\frac{d\sigma}{d\omega}\left(\frac{mb}{sr}\right)$
θ_{cm}

Figure 15

The spatial coordinates between the center-of-mass of particles in the $A(^3He,p)B$ reaction. p denotes the outgoing proton and (np), the transferred pair, A, the target nucleus and B, the product nuclei.

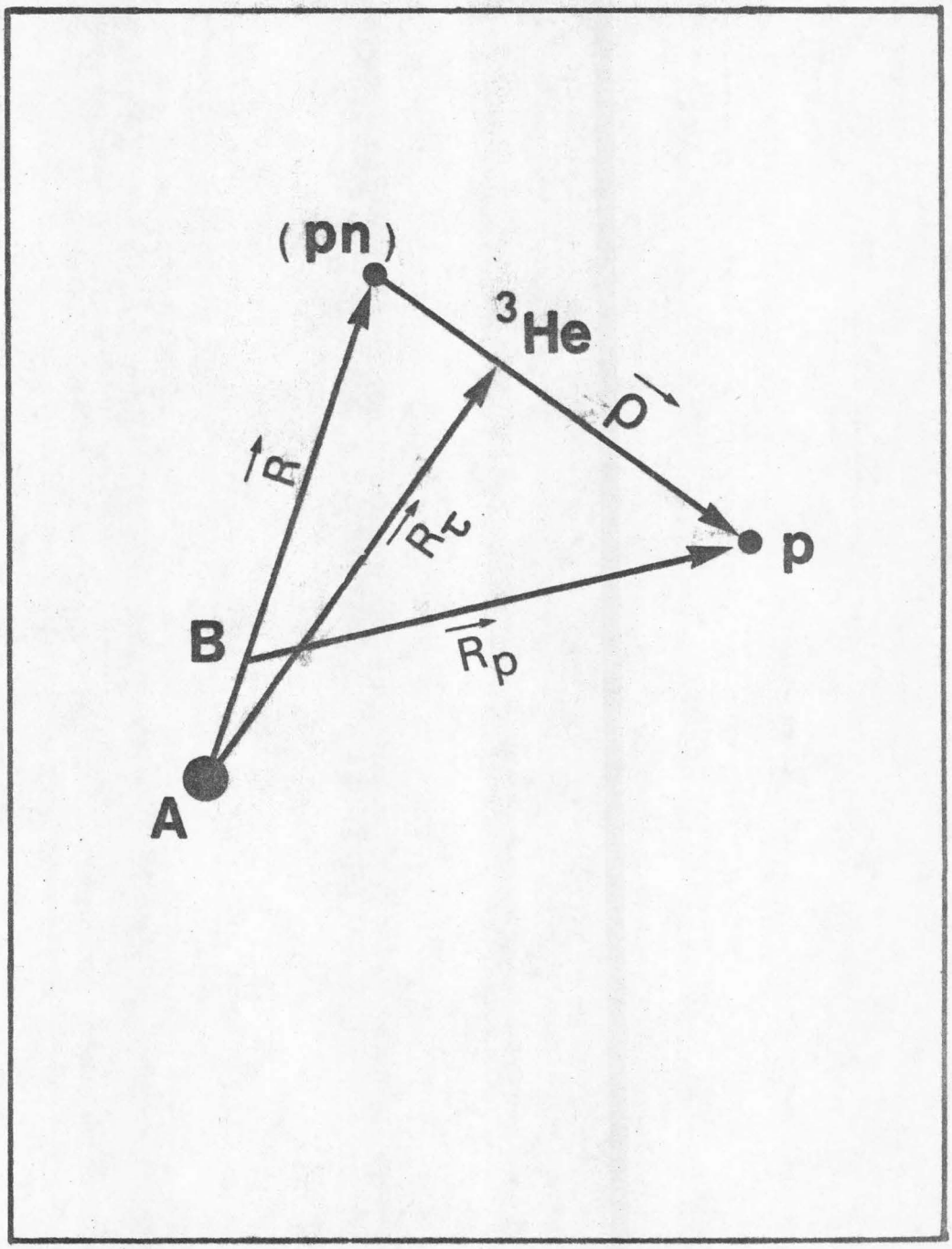
(pn)
^{3}He
$\vec{\rho}$
$\vec{R}$
$\vec{R}_\tau$
p
B
$\vec{R}_p$
A